

**NATURE AND ORIGIN OF SALT DEPOSITS AROUND THE CRATER OF
EREBUS VOLCANO, ANTARCTICA**

by

Melissa Maria Kammerer

Submitted in Partial Fulfillment
of the Requirements for the Degree of
Master of Science in Geochemistry

New Mexico Institute of Mining and Technology

October, 2011

To Tinka
She will never read this,
But she was the main outlet for stress relief during the process.

ABSTRACT

Salt deposits are widespread around the summit crater of the active 3794-meter high Erebus volcano in Antarctica. The distribution, composition and formation of the salts provide insight into the interaction of the gas plume with the snow and rocks around the summit crater. The greatest salt accumulations are located within 1 km of the active crater and are found under rocks and in crevices in the lava flows as white to yellow incrustations, massive deposits, efflorescences, and needles. Salt deposits are most abundant downwind of the crater where individual salt accumulations of 20 grams or more are common. The salts are not associated with fumaroles or fumarolic ice towers but form under the ambient -15 to -65 °C temperatures. XRD analyses of Erebus salts has led to the positive identification of alunite, calcite, gypsum, halite, khademite, mirabilite, ralstonite, sylvite, and thenardite, along with numerous tentatively identified phases. New salt phases identified in this study include rancieite, katoite, and potassian-halite. SEM observations indicate that the salts are well crystallized on a very fine scale, with crystal size ranging between 1 to 20 microns. One of the most common crystal habits consists of well-formed fibrous habit, although angular, cubic, hexagonal, needle, rectangular, spindle, stacked plate, and sub-angular habitss are also observed, along with cauliflower

and shark-tooth textures. Multiple salt morphologies are present in each sample. Qualitative electron microprobe chemical scans indicate that a wide range of elements is present in the salts. These include Al, Cl, F, Fe, K, Mg, Mn, Na, P, S, and Ti. The Erebus plume, snow, and ice samples around the summit region contain large quantities of Cl, F, and S, with lesser amounts of Al, Ca, Fe, K, Mg, Mn, and Na, some of which are major components of the salt deposits. The salts are rich in Al, K, Mn, and Mg, but these components are minor in the plume. This suggests that although some of the elements that form the salts are derived from the plume, interaction with rock fragments is an important component of the salt forming process, allowing for the scavenging of other elements. Salts from the summit crater form by weathering processes, which break up volcanic rocks, exposing fresh glass surfaces, which are then weathered / altered by reaction with the plume, liberating Al, Fe, Mn, Mg, and Ti. These liberated elements from the rock then combine with elements in the plume to form the well-crystallized salt deposits. The formation of the salts under such extreme temperatures conditions may have application to salt formation at other active planetary volcanoes.

Keywords: Salts; Erebus volcano; volcanic plume, Antarctica.

ACKNOWLEDGMENTS

I would like to thank my advisor Philip Kyle for allowing me to finally discover what that “stuff growing on volcanic rocks” was. His knowledge, help, guidance, patience, and support throughout this project were invaluable. I would also like to thank my committee members Andrew Campbell, Nelia Dunbar, and Virgil Lueth for their stimulating conversation and ideas regarding my research. This project would not have been possible without funding from the NSF and logistical support from RPSC. I would also like to thank Harry Keys for his assistance in the field and “passing down the salt sampling teaspoon”. Special thanks to Bill McIntosh, Aaron Curtis, Laura Jones, and all other team members from the 2009-2010 G-081 crew up on Erebus, your companionship and assistance made the trip one I will never forget.

My greatest thanks go out to my friends and family for their encouragement and support over the past two years. I would especially like to thank my parents Dave and Barb, and my Socorro friends Hunter and James Knox and Nels Iverson. You guys truly are the best friends anyone could ask for!

TABLE OF CONTENTS

	Page
Title Page	i
Dedication	ii
Abstract	iii
Acknowledgements	v
Table of Contents	vi
List of Tables	viii
List of Figures	ix
List of Abbreviations	xi
1. Introduction	1
2. Background	4
2.1 Cold Deserts Salts In The McMurdo Sound Region	4
2.2 Erebus Volcano	8
2.2.1 Previous Salt Studies	8
2.2.2 Plume Chemistry	10
2.2.2.1 Plume Gases	10
2.2.2.2 Plume Aerosols	11
2.2.3 Snow Chemistry	13
2.2.4 Rock Chemistry	13
3. Methods	16
3.1 Sampling	16
3.2 Salt Analysis	18
3.2.1 Electron Microprobe (EMP)	18
3.2.2 X-Ray Diffraction (XRD)	19
3.3 Snow Analysis	20
4. Results	21
4.1 Salt Samples	21
4.1.1 Field Characteristics	21
4.1.2 Electron Microprobe (EMP) Results	25

4.1.3 XRD Results	29
4.2 Snow Chemistry	36
5. Discussion	43
5.1 Plume Influence On Snow Chemistry	43
5.2 Snow Chemistry Ionic Balance	52
5.3 Summit Region Mineral Identifications	54
5.4 Salt Formation On Erebus	62
6. Conclusions	66
Appendix A: Detailed Methods and Materials	68
A.1 Sample Locations	68
A.2 Salt Sample Analysis	69
A.2.1 Electron Microprobe Methods	69
Appendix B: Electron Microprobe Data	70
B.1 SEM Images (DVD-Rom)	
B.2 BSE Images (DVD-Rom)	
B.3 Qualitative Scans (DVD-Rom)	
B.4 Normalized Qualitative Scan Data	70
Appendix C: XRD Patterns	77
C.1 XRD Spectra Pattern Images and With Pattern Tables (DVD-Rom)	
C.2 XRD Reference Codes	77
C.3 XRD Identifications	78
References	80

LIST OF TABLES

Table	Page
Table 1. Ten most widespread salt minerals identified in the McMurdo Sound region	5
Table 2. Positively and tentatively identified salt phases from the summit region of Erebus	10
Table 3. Average chemical composition of whole-rock phonolite lavas erupted over the past 17 ka	15
Table 4. Field characteristics of salt deposits with a visual estimate of deposit size, salt color, and location from which salt was sampled	24
Table 5. Basic elemental composition of salt samples measured via qualitative scans on an electron microprobe with the salt morphologies present as determined by SEM imaging	26
Table 6. XRD mineral identifications for all thirty-seven salt samples analyzed	31
Table 7. Mineral identifications of Erebus salt samples	34
Table 8. Raw snow chemistry data with measured cations and anions, pH, and conductivity, along with the calculated ionic balance	38
Table 9. Correlation coefficients for six prominent elements in Erebus summit snow chemistry	45
Table 10. Calculated hydrogen component of snow chemistry with measured pH	53
Table 11. Possible element sources for Erebus salts	64
Table A-1. Salt sample locations	68
Table B-1. Normalized probe data	71
Table C-1. XRD reference codes for all mineral phases identified	77
Table C-2. XRD identifications of Erebus salt deposits	78

LIST OF FIGURES

Figure	Page
Figure 1. Soil salts from Ross Island, which are constrained by the two isotopic mixing hyperbolas	7
Figure 2. Average concentration of the Erebus plume measured using filter packs in 1986-91	12
Figure 3. A. Map of Ross Island, Antarctica with Erebus volcano salt sampling region indicated by the box. B. Erebus volcano with salt sample locations ranging from summit to coast	17
Figure 4. Field characteristics of salt deposits with salt accumulations Indicated by the boxes	23
Figure 5. SEM images of habits present in salt samples showing distinct habits on a micron scale, with multiple habits present in samples on a micron scale	27
Figure 6. Example XRD pattern for Erebus salt sample ERE-09-001	30
Figure 7. XRD spectra for all 37 samples analyzed with major unidentified peak groupings indicated by the arrows	35
Figure 8. Fluctuations in the concentration of major elements found in Erebus snow samples	39
Figure 9a. Concentrations of major cation Al^{3+} and anion Cl^- in Erebus snow plotted individually against elevation	40
Figure 9b. Concentrations of major cation K^+ and anion F^- in Erebus snow plotted individually against elevation	41
Figure 9c. Concentrations of major cation Na^+ and anion S^{2-} in Erebus snow plotted individually against elevation	42
Figure 10a. Enrichment factors (EF) for Erebus snow samples Fe normalized relative to McMurdo Sound region snow.....	48
Figure 10b. Enrichment factors (EF) for Erebus snow samples Fe normalized relative to the Erebus plume	49

Figure 11. Measured pH for Erebus snow samples relative to the calculated concentration of H⁺54

Figure 12. Phase diagram for the solubility of kaolinite59

Figure 13. Possible formation pathways for Erebus salts, showing potential reactions between acidic plume gases, volcanic rocks, and solid aerosols63

Figure 14. Flow feature found in the summit region of Erebus65

Figure A-1. Electron microprobe sample plug69

LIST OF ABBREVIATIONS

VSD: Volcanogenic Salt Deposits

XRD: X-Ray Diffraction

EMP: Electron Microprobe

IC: Ion Chromatograph

ICP-OES: Inductively Coupled Plasma Optical Emission Spectroscopy

SEM: Scanning Electron Microscope

EF: Enrichment Factor

1. INTRODUCTION

Salt deposits are common in the bedrock areas in the McMurdo Sound region of Antarctica (Keys, 1980; Keys and Williams, 1981). A salt is any chemical compound formed from the reaction of an acid with a base, with all or part of the hydrogen of the acid replaced by a metal or other cation. The neutralization reaction between the acid and base forms an ionic compound composed of anions and cations. Salt deposits can be formed as a weathering product or as a direct fallout deposit (e.g. NaCl from sea spray) and can appear to be clear and transparent, opaque, or metallic and lustrous (Keys, 1980). Salts also occur in a range of colors including yellow, orange, black, red, blue, purple, green, white, and colorless.

A volcanogenic salt deposit (VSD) differs from other salt deposits in that they are formed from the condensation/sublimation of hot gases released from a volcanic vent (Bernard and Le Guern, 1986; Ferreira and Oskarsson, 1999; Hampton and Bailey, 1985; Kodosky and Keskinen, 1990; Naughton et al., 1976; Naughton et al., 1974; Óskarsson, 1981; Stoiber and Rose, 1974). VSDs typically occur as sublimates, incrustations, efflorescences, or needles on rock surfaces, and encircling fumarolic vents. An efflorescence is a thin coating of an alteration product on a rock surface that is the result of a reaction between a rock surface

and components in the air. The chemistry of VSDs can give qualitative information regarding the composition of the gas phase emitted by a volcano. This then could be used as a sensitive indicator of condensable trace compounds involved in the latest stages of magma degassing (Óskarsson, 1981).

Typical VSD studies have focused on the pattern of salts forming at various temperatures within and surrounding gas vents and fumaroles through the use of silica sampling tubes (Bernard and Le Guern, 1986). A distinct zonation of salt minerals forms incrustations at specific temperature ranges as the volcanic gas sublimates into a salt phase. This zonation can be highly irregular and erratic due to: irregularity of wall rock surfaces around the fumarole opening, variations in wind direction and velocity in the immediate area, and variation in the rate of gas venting from the fumarole. It is also important to note that the volume of incrustations depositing at high temperatures is far less than the volume of lower temperature incrustations (Stoiber and Rose, 1974).

Erebus volcano (3794m) is the world's southernmost active volcano and is known for its active, convecting, degassing phonolite lava lake. The distribution, composition and formation of the salts on Erebus volcano can provide insight into the degassing of the lava lake and the interaction of the gas plume with the snow and rocks around the summit crater. Salt deposits may form as a reaction product between the plume, rocks, and snow, as a weathering product, or as a direct sublimate depositing from the plume. Aerosol particles can form salt deposits in the summit region by direct fallout, or plume gases can aid in the weathering of rocks in combination with freeze-thaw breakup of rocks by snow. The plume gases and rocks provide elements not found in other areas of the

McMurdo Sound region, which accounts for the different nature of the Erebus salts compared to other salt deposits in the McMurdo Sound region.

This paper focuses on the nature and origin of salt deposits found in the summit region of Erebus volcano. Salt deposits on Erebus are not associated with fumarolic ice towers, which are frozen ice and snow towers formed by the freezing of meteoric and volcanic gases. Instead they are found under rocks, ejecta, and in crevices in the lava flows as white to yellow incrustations, massive deposits, efflorescences, and needles, forming under ambient air temperatures of -65 to -15°C . The identification of salt deposits using X-ray diffraction (XRD) and Electron Microprobe (EMP) qualitative data have helped to determine salt phases present and specific chemistry of previously unidentified phases.

In this study the chemistry of the salts is compared to plume, snow, and rock chemistry in order to determine salt forming processes operating in the summit region of Erebus volcano. Snow samples ranging from the coast to the summit will be used to determine if there is a marine influence on snow chemistry in the summit region. This study will help to clarify whether the salts form as sublimates, directly depositing from the plume, or if acidic gases in the plume interact with the snow and rocks to form the salts. Depending on the relationship between the salts and the plume, the salts may contain a good record of the gas emitted from the plume. Also, the snow chemistry preserves a record of the plume. The ultimate mechanism of salt formation operating in the summit region of Erebus will be determined as either marine, volcanic, a chemical weather product, or a combination of all these processes.

2. BACKGROUND

2.1 Cold Desert Salts In The McMurdo Sound Region

Antarctica is considered to be a cold desert and the presence of salt deposits is indicative of prevailing arid conditions (Keys and Williams, 1981). Salt deposits are widespread in the McMurdo Sound region and range in size from massive deposits (10^{10} kg in Hobbs Valley) down to small traces under rock and as loose deposits in the soil and snow (Bowser et al., 1970; Keys, 1980; Keys and Williams, 1981). The lack of flowing water and low humidity limits the dissolution of salt deposits, so deposits on the order of 10^{10} kg may form. The larger salt deposits in the region typically have a marine source, whereas smaller deposits form from chemical weathering processes (Keys, 1980).

The most common salt deposits are expressed as efflorescences and encrustations on rock surfaces and as accumulations under rocks and boulders and in cracks. Overall, more than 30 different salt phases have been identified by Keys and Williams (1981) in the McMurdo Sound region and the ten most common are listed in Table 1. Keys and Williams (1981) also noted that the wind is an important factor in salt distribution. Larger salt accumulations are present in the prevailing Erebus summit region wind direction and deposits can have an

asymmetry, depending on the wind conditions. Wind is also an important agent in rock weathering and scour, aiding in the release of material available for salt formation.

Table 1. Ten most widespread salt minerals identified in the McMurdo Sound region (from Keys and Williams, 1981)

Salt Mineral	Chemical Formula
Thenardite	Na_2SO_4
Gypsum	$\text{CaSO}_4\cdot 2\text{H}_2\text{O}$
Halite	NaCl
Calcite	CaCO_3
Darapskite	$\text{Na}_3\text{NO}_3\text{SO}_4\text{H}_2\text{O}$
Soda Nitre	NaNO_3
Mirabilite	$\text{Na}_2\text{SO}_4\cdot 10\text{H}_2\text{O}$
Bloedite	$\text{Na}_2\text{Mg}(\text{SO}_4)_2\cdot 4\text{H}_2\text{O}$
Epsomite	$\text{MgSO}_4\cdot 7\text{H}_2\text{O}$
Hexahydrate	$\text{MgSO}_4\cdot 6\text{H}_2\text{O}$

Salts in the McMurdo Sound region are thought to form from either a marine source, or as a result of chemical weathering of the rocks in the region. Chemical weathering changes the composition of rocks, usually aided by water, resulting in various chemical reactions. The mineralogy of the rock adjusts to the surface environment as new and secondary minerals are formed. Marine

derived salts most likely form as a result of direct deposition from sea spray, dry fallout, and influx of seawater (Keys and Williams, 1981). Mirabilite deposits associated with glaciers in Victoria Land, Antarctica have an ultimate marine source, but are mainly formed by freeze-concentration and evaporation of small saline glacial ponds (Bowser et al., 1970). This is evident from interstratified algae and sediments in the deposits. Evaporation at the surface and capillary draw of meltwater to glacial surfaces has resulted in the development of thenardite deposits in the Dry Valley regions.

The most common salt deposits found along the west coast of Ross Island include thenardite, mirabilite, halite, and minor Na and Ca carbonates (Faure and Jones, 1989). The $^{87}\text{Sr}/^{86}\text{Sr}$ ratios and $\delta^{34}\text{S}$ of salts was used to determine a marine or volcanic source for salt deposits in the McMurdo Sound region (Faure and Jones, 1989; Jones et al., 1983). Jones and Faure (1967) recorded strontium and sulfur values for the marine components as: $^{87}\text{Sr}/^{86}\text{Sr} = 0.7090$, $\delta^{34}\text{S} = +20\text{‰}$. The recorded strontium and sulfur values for the volcanic component are: $^{87}\text{Sr}/^{86}\text{Sr} = 0.7035$, $\delta^{34}\text{S} = 0.00\text{‰}$ (Faure and Jones, 1989). Figure 1 is a model developed by Faure and Jones (1989), which indicates that the marine component ranges from 1% at Fang Ridge (near the summit of Erebus) to 98% for salt along the beach at Cape Bird. The Sr found in coastal soil salts is of primary marine origin and the Sr found in the summit region of Erebus is mainly from chemical weathering of the volcanic rocks (Faure and Jones, 1989). This trend from coast to summit also indicates a mixing trend along the flanks of the volcano, with inputs from both the sea and volcano. Salts analyzed from the summit region of Erebus have $^{87}\text{Sr}/^{86}\text{Sr}$ values that range from 0.70330 ± 3 to 0.70449 ± 3 and $\delta^{34}\text{S}$

values that range from +1‰ to +3.1‰. In comparison, salts analyzed from the coast at Cape Bird have $^{87}\text{Sr}/^{86}\text{Sr}$ values that range from 0.70802 ± 3 to 0.70912 ± 3 and $\delta^{34}\text{S}$ values that range from +17.8‰ to +19.6‰. These salts are represented as dots in Figure 1.

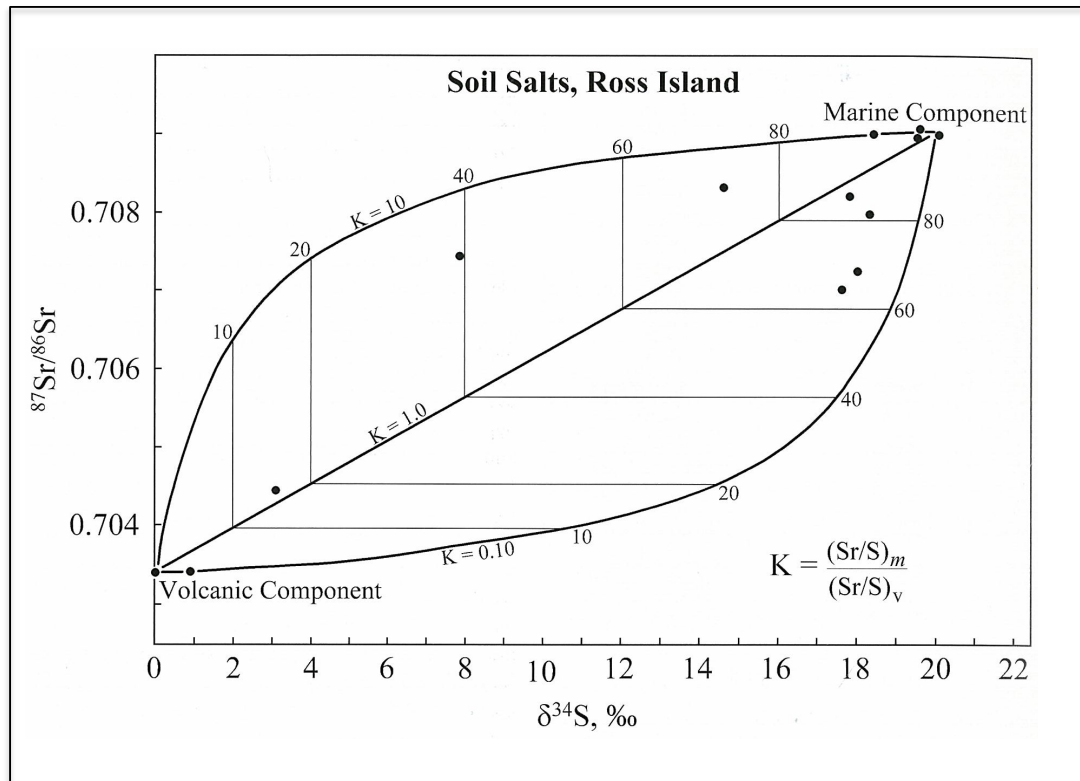


Figure 1. Soil salts from Ross Island (dots), which are constrained by the two isotopic mixing hyperbolas. The shape of the hyperbola was determined by the parameter K, which represents the assumed concentrations of strontium and sulfur from the marine component (m) and volcanic component (v). The salt samples plotted in this model represent volcanic and marine end members, along with samples showing mixing between the two components (Faure and Jones, 1989).

Chemical weathering of rock fragments, mobilization of ions, and the deposition of secondary minerals in the Dry Valleys of southern Victoria Land are all contributing factors to soil salt formation (Faure and Jones, 1989). It is important to note that accumulations of soil salts are typically located where they

form and reflect primary local conditions. Bockheim (2002) determined that the size and morphology of soil salt deposits in the McMurdo Dry Valleys is highly correlated with soil age. Overall, soils containing the largest salt concentrations occur on older surfaces (>1 Ma in age). Also, the distribution of anions in soil salts is an important indicator of air-mass movement in the McMurdo Sound region (Claridge and Campbell, 1977).

2.2 Erebus Volcano

2.2.1 Previous Salt Studies

The occurrence, nature, characterization, and identification of salt deposits from the summit region of Erebus volcano have been examined in several studies, yet many questions regarding these features remain unanswered. Keys and Williams (1981) noted that the composition of the Erebus salts differed from the other salts identified in the McMurdo Sound region. Keys (1980) determined that in general, the Erebus salts are free from large rock fragments, contained 10 percent sand, and many of the phases contained significant amounts of aluminum, silicon, fluorine, and some iron. Salts found in the summit region are mostly low temperature deposits (-15 to -65°C) and are not associated with the low temperature fumaroles (Zreda-Gostynska, 1995). Salt distribution, occurrence, and characteristics change with relation to their proximity to the main crater. Keys (1980) noted that the largest deposits are concentrated in the prevailing wind direction and salts at the summit tend to have a yellow color

which transitions to pale yellow and white the further away from the main crater.

XRD identifications of Erebus salts have been complicated due to peak overlap and post sampling alteration of the salts (Faure and Jones, 1989; Jones et al., 1983; Keys, 1980; Keys and Williams, 1981; Rosenberg, 1988; Zreda-Gostynska, 1995). Table 2 lists salt phases that have been previously identified in the summit region of Erebus. Of particular interest in previous studies has been the identification of a possible new salt mineral, tentatively named "Erebusite". This material is bright yellow in color, is located close to the main crater, and has a proposed formula of $\text{NaAl}_4\text{O}_4\text{Cl}_5$ (Zreda-Gostynska, 1995). This compound has not been found in nature, and is only known as a man-made inorganic product. Zreda-Gostynska (1995) postulated an amended chemical formula of $\text{Na}(\text{Al}, \text{Fe})_4\text{O}_4(\text{F}, \text{Cl})_5$, with Fe substituting for Al, and F for Cl. Despite the strong yellow color found in many of the summit salts, native sulfur has not been identified in any of the previous Erebus salt analysis, but has been identified in Erebus aerosols (Chuan, 1994; Jones et al., 1983). Aluminum fluoride hydrates ($\text{AlF}_3 \cdot n\text{H}_2\text{O}$) have also been tentatively identified on Erebus, but the presence of multiple phases made a positive identification impossible (Rosenberg, 1988). Aluminum trifluoride (AlF_3) is thought to be a high-temperature volcanogenic salt, forming incrustations from fractional condensation of volcanic gases, but it has not been identified as a natural mineral (Óskarsson, 1981).

Table 2. Positively and tentatively identified salt phases from the summit region of Erebus (Keys, 1980; Keys and Williams, 1981; Zreda-Gostynska, 1995)

Positively Identified	Chemical Formula
Alunite	$KAl_3(SO_4)_2(OH)_6$
Calcite	$CaCO_3$
Gypsum	$CaSO_4 \cdot 2H_2O$
Halite	$NaCl$
Khademite	$Al(SO_4)F \cdot 5(H_2O)$
Mirabilite	$Na_2SO_4 \cdot 10(H_2O)$
Sylvite	KCl
Thenardite	Na_2SO_4
Ralstonite	$Na_xMg_xAl_{2-x}(F,OH)_6 \cdot H_2O$
Tentatively Identified	Chemical Formula
Aluminum trifluoride	AlF_3
Alunogen	$Al_2(SO_4)_3 \cdot 18H_2O$
Chloraluminatite	$AlCl_3 \cdot 6H_2O$
Elpasolite	K_2NaAlF_6
Gibbsite	$Al(OH)_3$
Hieratite	K_2NaAlF_6
Hydromolysite	$FeCl_3 \cdot 6H_2O$
Illite	$(K, H_3O)(Al, Mg, Fe)_2(Si, Al)_4O_{10}[(OH)_2, (H_2O)]$
Iron chloride	$FeCl_2$
Jarosite	$(K, Na)(Fe, Al)(SO_4)_2(OH)_6$
Malladrite	Na_2SiF_6
Meta-autunite	$Ca(UO_2)(PO_4)_2 \cdot 6H_2O$
Montmorillonite	$(Na, Ca)_{0.33}(Al, Mg)_2(Si_4O_{10})(OH)_2 \cdot nH_2O$
Natroalunite	$NaAl_3(SO_4)_2(OH)_6$
Natrojarosite	$NaFe_3(SO_4)_2(OH)_6$
Tamarugite	$NaAl(SO_4)_2 \cdot 6H_2O$
Sodium aluminum oxychloride	$NaAl_4O_4Cl_5$
Sulphohalite	$Na_6ClF(SO_4)_2$

2.2.2 Plume Chemistry

2.2.2.1 Plume Gases

It has been postulated that the continuously emitted Erebus plume plays a role in salt formation in the summit region (Keys, 1980; Keys and Williams, 1981; Zreda-Gostynska, 1995). Therefore, an understanding of plume composition and dispersal is necessary in order to link the chemistry of the salts to the chemistry

of the plume. Zreda-Gostynska (1995) identified gas species CO, HCl, HF, CO₂, SO₂, H₂O, and others. The main gas composition of the plume is H₂O (57.88 mol percent), CO₂ (36.41 mol percent), CO (2.33 mol percent), and SO₂ (1.40 mol percent) and is distributed over the flanks of the volcano with the prevailing wind direction to the northeast and the strongest winds to the northwest (Oppenheimer and Kyle, 2008). In recent years plume chemistry has been determined by infrared spectrometer and an instrumented aircraft (Oppenheimer et al., 2010). Chemical species measured in the plume include HNO₃, HO₂NO₂, SO₂, COS, CO, O₃, CO₂, HCl, HF, OCS, and H₂O. The acidic species are of particular interest for salt formation by aiding in the alteration of exposed volcanic rocks in the summit region.

2.2.2.2 Aerosols

An aerosol is a suspension of fine solid particles or liquid droplets in a gas. Aerosols represents small particles (up to 20µm) contained in the Erebus plume, which are typically deposited within the summit region and may be represented as a direct fallout salt deposit. In 1983 it was estimated that the plume contributes upwards of 21 ± 3 metric tonnes/day of aerosol particles to the Antarctic upper troposphere (Chuan et al., 1986). Particle measurements were made using a quartz crystal microbalance (QCM) cascade impactor, which makes a real-time measurement of sample mass and size and separates samples into different size ranges (Chuan, 1994; Chuan et al., 1986; Ilyinskaya et al., 2010; Meeker et al., 1991). Halite, thenardite, sylvite, sulfuric acid, Fe-rich silica, Fe-Al

silicate, Al-sulfate, and Cl rich particles have been identified in the Erebus plume (Chuan et al., 1986). Soluble plume aerosol particles make up 30% of the total mass and are dominated by Cl bearing particles (Ilyinskaya et al., 2010). Overall, coarse particles are not abundant in the soluble aerosol fraction of the plume. Elevated concentrations of F⁻, Cl⁻, Br⁻, and SO₄²⁻ make up the 0.1-0.25µm fraction. Halide-alkali metal salts (Na,K)(Cl,F) are the most abundant species found in Erebus plume aerosol. The average concentration of elements from filter packs from 1986-91 indicates major concentrations of Cl, F, and S with minor amounts of Na, Al, K, and other species (Figure 2) (Zreda-Gostynska, 1995).

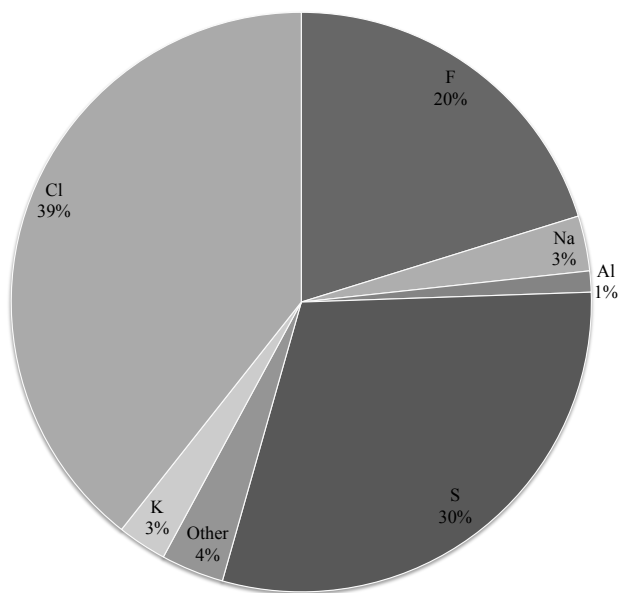


Figure 2. Average concentration of the Erebus plume measured using filter packs in 1986-91. Components are represented as the percent of total mass collected (Zreda-Gostynska, 1995).

Chuan (1994) suggested that there was a shift in aerosol composition between eruptive and non-eruptive stages. During stages with frequent Strombolian eruptions glass shards, elemental sulfur crystals, silica, and salts

(KCl, K₂S, NaCl) are the major aerosol particles. Some of the salt particles have sulfuric acid and oxides of iron and chromium attached as droplets. When the volcano is only fuming (non-eruptive periods) sulfuric acid or elemental sulfur is not present, but instead hydrated HCl is present (Chuan, 1994). SEM imaging found elemental gold particles in the Erebus plume (Meeker et al., 1991). The gold particles may be transported as a gold-chloride particle, or as AuS(g). Erebus is the first volcano where elemental gold has been identified in the plume, aerosols, ambient air, and in snow samples (Meeker et al., 1991).

2.2.3 Snow Chemistry

The chemistry of snow samples with relation to salt samples is important since the snow may be a good record of plume distribution. Ice serves as a weathering agent, aiding in breaking up volcanic rock through freeze thaw cycles. Ice formation is possible through the melting of snow and then refreezing into ice. Results of detailed snow chemistry have not been published to date, but unpublished results indicate high concentrations of S, F, Cl closest to the Main Crater, with values returning to background along the flanks of the volcano (Margolin, 2006).

2.2.4 Rock Chemistry

Erebus volcano has undergone three main cone building stages, with an evolution of material erupted over the past 1.3 Ma (Esser et al., 2004; Kelly et al., 2008). From 1.3 Ma to 1.0 Ma there was a transition from subaqueous to

subaerial eruptive material with the eruption of basanite during this proto-Erebus shield-building phase. From 1.0 Ma to 250 ka a more evolved phonotephrite lava, forming steeper slopes, was erupted during this proto-Erebus cone building phase, with a caldera collapse at ~75 ka. The third and current stage, beginning at 250 ka, is the modern-Erebus cone-building phase. This period has been a time of increased activity with the eruption of large volumes of anorthoclase-phyric tephriphonolite and phonolite lavas (Caldwell and Kyle, 1994; Kelly et al., 2008).

Current eruptive material has a phaneritic texture and contains ~30-40% anorthoclase feldspar crystals (Kelly et al., 2008). The phonolites are undersaturated in Si and have strong enrichments in alkali and incompatible elements, as well as being enriched in REEs. Table 3 lists that average chemical composition of whole-rock analysis of phonolite lavas erupted over the past 17 ka. When initially erupted, lava bombs have an iridescent luster which quickly alters to light grey from alteration by the acidic gases in the plume which results in the build-up of efflorescences on the surface (Caldwell and Kyle, 1994).

Table 3. Average chemical composition of whole-rock phonolite lavas erupted over the past 17 ka (from Kelly et al., 2008)

Chemical Species	Average Weight Percent
SiO ₂	56.39
TiO ₂	1.04
Al ₂ O ₃	19.80
Fe ₂ O ₃	5.55
MnO	0.23
MgO	0.94
CaO	2.84
Na ₂ O	8.17
K ₂ O	4.46
P ₂ O ₅	0.45
Total	99.85

3. METHODS

3.1 Sampling

Salt and snow samples were collected during the 2009 austral summer, primarily from the summit area of Erebus, but also on the flanks and one sample was from the coast (Figure 3). A field estimate of deposit size, along with GPS position, elevation, and sample characteristics were recorded at each sample collection site (Appendix A). Two main sample collection profiles were conducted, one from summit to coast, and another trending horizontally along the flank of the volcano, within the upper caldera. Salt samples were collected using a stainless steel teaspoon, placed into sample vials, and kept frozen at -20°C to avoid alteration (eg. dehydration and rehydration) until analyzed. The salt samples were first sub-sampled and brought to room temperature in order to determine which samples altered when thawed. Unstable salt samples dehydrated at room temperature and altered from a powder form to a more liquid form.

Fresh snow samples were collected as loose surface snow, compacted older snow, and firn ice layers. All snow samples were collected in plastic zip-loc bags, melted, and then transferred into nalgene bottles and sealed for

shipment. Snow samples were taken adjacent to salt samples in order to determine similar chemical compositions.

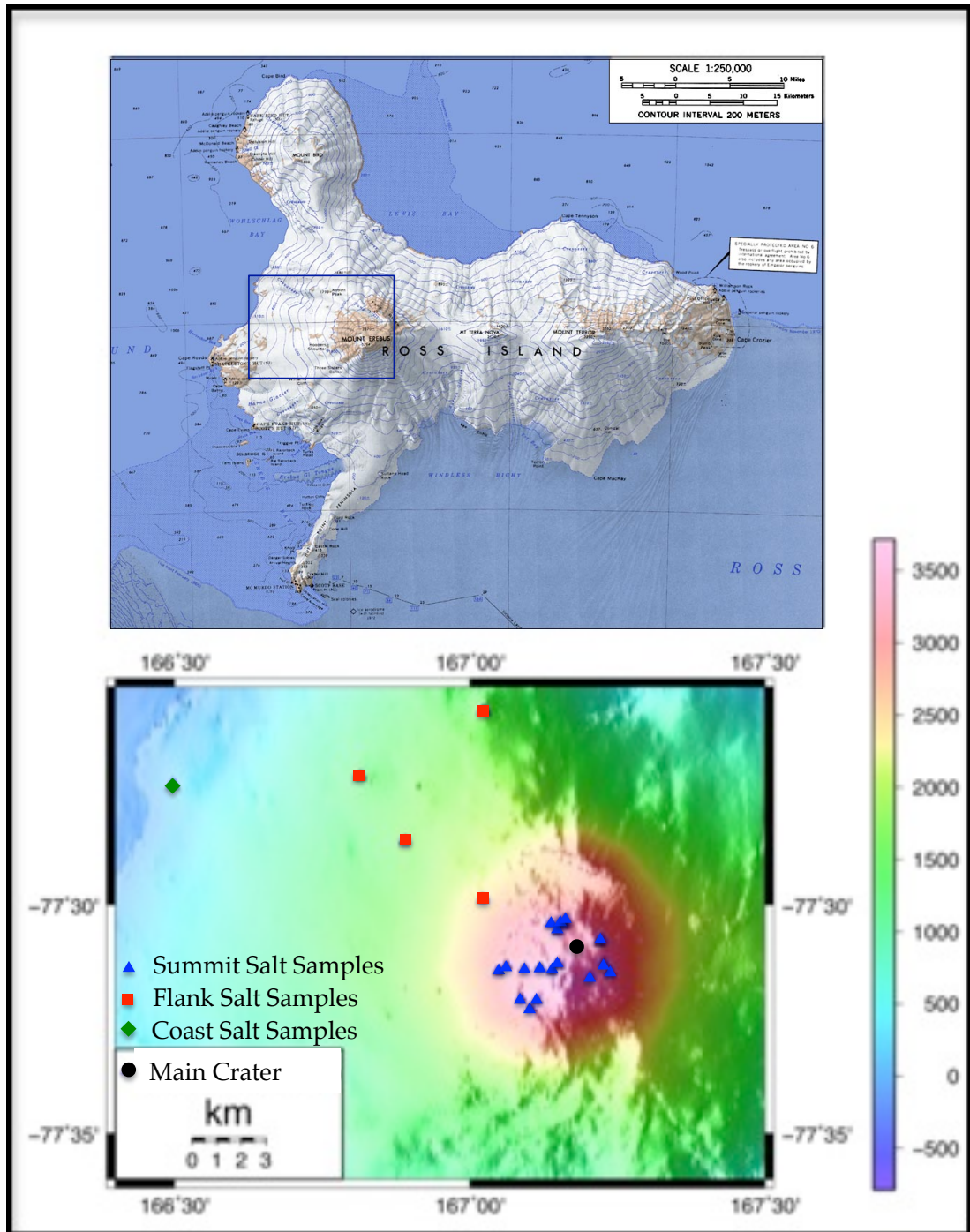


Figure 3. A. Map of Ross Island, Antarctica with Erebus volcano salt sampling region indicated by the box. B. Erebus volcano with salt sample locations ranging from summit to coast.

3.2 Salt Analysis

3.2.1 Electron Microprobe (EMP)

Salt samples that did not dehydrate or change form at room temperature were examined using a Cameca SX-100 three-spectrometer electron microprobe (EMP) at the New Mexico Bureau of Geology Microprobe Lab. The purpose of the EMP was to determine crystal morphology on the micron scale and basic qualitative geochemistry of the various habits present. Each stable salt sample was sub-sampled at least four times in order to have a full representation of all phases present in the sample. Samples were selected under a microscope to ensure the selection of homogeneous sub-samples, despite an overall heterogeneous bulk sample. Secondary Electron Imaging (SEM) was performed first to determine the ranges of crystal morphologies present in each salt. A beam current of 1nA was used with an initial frame time of 1.067 seconds and a resolution of 1024x768. Images were acquired at a frame time of 12.8 seconds and ranged in scale from 100 microns to 10 microns. Minimal sample charging and movement occurred; overall the samples were remarkably stable under the beam. Qualitative elemental scans were performed on spots using a 1-micron beam, unless the sample location was homogeneous and a larger scan area was used. This technique was helpful when a sample was not stable under the electron beam and would dissolve before a full scan could be completed. Each scan ran for 1500 seconds. Results from each diffracting crystal in the microprobe (TAP, PET, LLIF) produced a graph with relative element peak

heights in counts per second. All SEM images and qualitative scan spectra are given in Appendix D, available on DVD-ROM.

3.2.2 X-Ray Diffraction (XRD)

Salts were identified by X-ray Diffraction (XRD) on a PANalytical x'Pert PRO XRD in the New Mexico Bureau of Geology XRD lab. Salt samples that did not rehydrate were ground prior to selection to avoid any preferred orientations; unstable salt deposits were not ground in order to avoid accelerating rehydration. Samples were selected under a microscope and were generally 50 μ m in size to limit the potential number of salt phases present. Each sample was placed in the center of a depressed zero background stage, which spun during analysis. Samples were run for 60 minutes with a 0.0170 $^{\circ}$ 2 theta (θ) step between each 2 θ position, ranging from 6.00 to 70.0 $^{\circ}$ 2 θ under Cu K α radiation run at 45kV and a current of 40mA in order to obtain peaks large enough to resolve. Mineral identifications were complicated due to the presence of multiple phases, so several identification techniques were used. Measured XRD patterns were compared to patterns of previously identified salt phases on Erebus, patterns of tentatively identified salt phases on Erebus, and patterns of unidentified chemical compounds on Erebus. Potential XRD patterns were also retrieved based on the elemental components determined in the EMP work and the batch mineral identification software was also used to determine the computers best XRD pattern fit. In order for an XRD pattern to be accepted the three largest peaks had to be present and match the measured pattern.

3.3 Snow Analysis

General water chemistry was determined on snow samples at the New Mexico Bureau of Geology Water Chemistry Lab. Analyses were made by Ion Chromatography (IC) and Inductively Coupled Plasma-Optical Emission Spectroscopy (ICP-OES). Conductivity and pH measurements were determined by standard methods. Samples were filtered prior to ICP-OES analysis, but all other analysis used unfiltered samples. The following species were determined:

ICP-OES: Ca, Fe, K, Na, Si, Mn, Al, Ba, Li, S, Sr

IC: Cl, F, NO₃, PO₄, SO₄

Measured: pH, Conductivity

4. RESULTS

4.1 Salt Samples

4.1.1 Field Characteristics

Salt samples from the summit region were located at or above 3000 meters elevation, flank samples between 2000-1000 meters elevation, and coastal samples were collected below 1000 meters elevation. Salt deposits are commonly found under rocks as massive deposits, as well as in vertical cracks and as needles in the snow and efflorescences on rock surfaces. Most exposed rock surfaces in the summit region of Erebus are covered in a white to tan coating, presumably due to reaction and alteration from the volcanic gas acidic plume. Figure 4 shows typical salt deposits located within the summit caldera. Salt accumulation rates are highest on the summit crater, especially in the dominant wind direction, and decrease down the slopes of the crater. Table 4 shows field estimated accumulation with field location, morphology, color, and contamination noted. Salt deposit size ranges from greater than 20cm³ to less than 1cm³. Overall, salt deposits range from pure white powder, usually void of any rock contamination, to waxy bright yellow often intermixed with rock

fragments. Pele's hairs of phonolite glass are also common in salt deposits in the summit region and absent from flank and coastal samples. Bright yellow deposits are common on the Main Crater rim and transition to pale yellow, and eventually pure white at the coast; pure white deposits are not constrained strictly to the coast, but are also found in the summit region. Transitions from yellow to white can be seen in vertical cracks on a cm scale as seen in Figure 4B. Salt deposits accumulated under rocks were most commonly sampled only because surface encrustation deposits were too thin to obtain a reasonable sample.

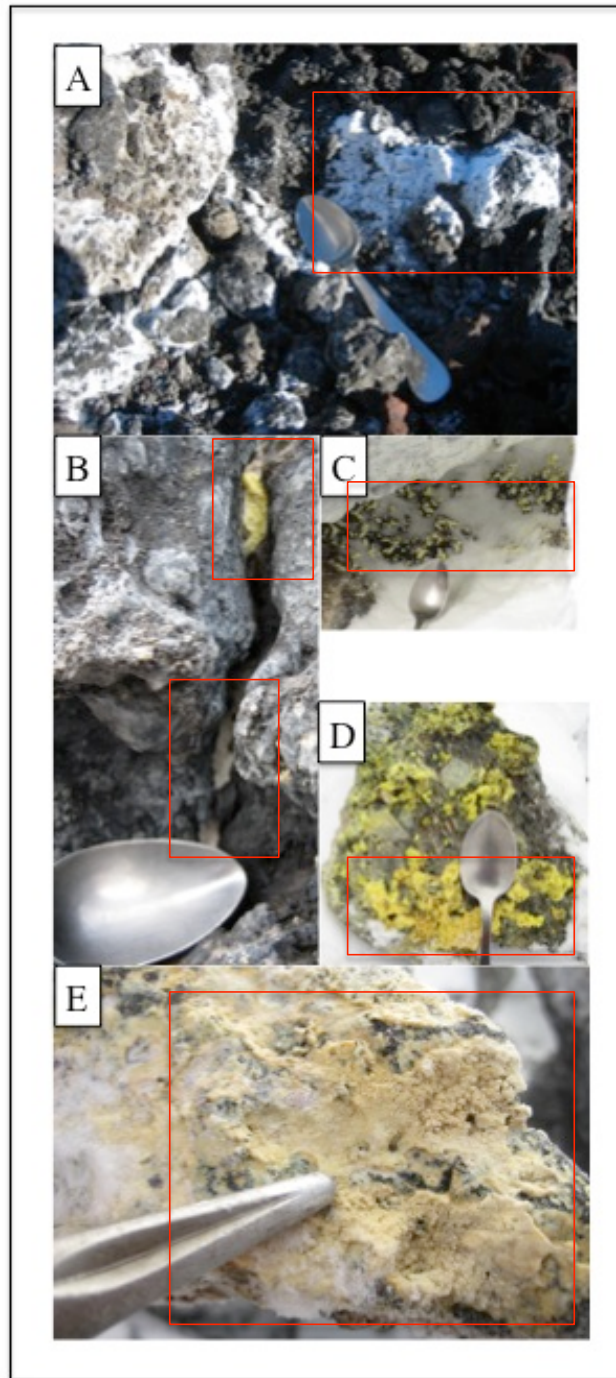


Figure 4. Field characteristics of salt deposits (teaspoon head (5.5cm long) and ice axe spike (10cm) for scale) with salt accumulations indicated by the boxes: A-White surface deposit, B-Vertical crack deposit, note transition from pale yellow to white, C-Pale yellow surface deposit on rock surface, surrounded by snow, D-Bright yellow under rock deposit, attached to rock bottom, E-Tan under rock deposit, attached to rock bottom.

Table 4. Field characteristics of salt deposits with a visual estimate of deposit size, salt color, and location from which salt was sampled. The samples with an asterisk are salts that dehydrated when brought to room temperature.

Sample	Deposit Size (cm ³)	Color	Field Location
Summit Samples			
ERE-09-001	<2	py, w, b	under rock
ERE-09-002	2 to 3	br	under rock
ERE-09-003		y	encrustation
ERE-09-004		by, b	under rock
ERE-09-005	2 to 3	w, b	under rock
ERE-09-006			rock sample
ERE-09-007*	10 to 20	dw, y, b	under rock
ERE-09-008*		g, br, y, w	under loose rock and in crack
ERE-09-009		py, dw, b	vertical crack
ERE-09-010	2 to 3	by, b	under rock
ERE-09-011*	<1	o, t, b	under rock
ERE-09-012	5 to 10	by, b	under rock
ERE-09-013	10+	by, b	vertical crack
ERE-09-014	2	w, py, b	under rock
ERE-09-015	1	w, t, br, b	under rock
ERE-09-016	4 to 5	py, w, b	under rock
ERE-09-017		br	rock surface
ERE-09-018	<1	w, py, b	under rock
ERE-09-019	2 to 3	vw, b	under rock
ERE-09-020	1	w, g	surface deposit
ERE-09-021*	5 to 10	w, g, br	under rock
ERE-09-022*	2	vw, py, b	under rock
ERE-09-023*	1 to 2	vw, g, py, b	under rock
ERE-09-024	2	vw, dw, t, b	under rock
ERE-09-025*	1 to 2	w, t, g, b	surface deposit
ERE-09-026*	1	w, t, g, b	surface deposit
ERE-09-034	20+	br, w, o, t, b	under rock
ERE-09-035	20+	w, t, br, b	surface deposit
ERE-09-036	1 to 2	br, b	under rock
ERE-09-037	<1	w, py, b, g	under rock
ERE-09-038	2	cw, py, o, br, b	under rock
ERE-09-039		y	encrustation
ERE-09-040*	1	cw, py, br, b	under rock
ERE-09-041*	5 to 10	vw, cw, t, b	under rock
ERE-09-042	5 to 10	br, t, vw	under rock
ERE-09-043	3	py, w, b	surface deposit
ERE-09-CR		by, b	under rock deposit
ERE-09-MC-1		br, w, g, b	low temp. gas vent deposit
ERE-09-MC-2		py, cw, br, b	low temp. gas vent deposit
Flank Samples			
ERE-09-027	2 to 3	vw, b	under rock
ERE-09-028	5	vw, b	under rock, on ground surface
ERE-09-029	10+	vw, b	under rock
ERE-09-031	2 to 3	vw, g, t, b	surface deposit
ERE-09-032	1	vw, t, b	surface deposit
ERE-09-033	1	vw, cw, b	surface deposit
Coastal Samples			
ERE-09-030	<1	g, w, py	surface efflorescence

b-black, br-brown, by-bright yellow, cw-cream white, dw-dirty white, g-grey, o-orange, py-pale yellow, t-tan, vw-very white, w-white, y-yellow

4.1.2 Electron Microprobe (EMP) Results

Twenty-seven samples were examined by EMP, with SEM images and qualitative element scans collected (Table 5). SEM images are in Appendix B.1 and qualitative scans are in Appendix B.3 (both on DVD-ROM). SEM imaging of salt deposits show distinct crystalline habits present in all samples examined. Images (Figure 5) show the range of morphologies present, ranging from stacked plates, needles, cubes, fibrous, hexagonal, sub-angular, and sub-rounded habits, and shark-tooth and cauliflower texture. Multiple morphologies and textures are present on a micron scale, with very few samples having only one morphology present. Despite effort to minimize contamination by rock samples on EMP slides, some volcanic glass shards and anorthoclase feldspar crystals fragments were observed in SEM images. Salts from the summit typically have a fibrous, sub-angular, or stacked plate texture. Hexagonal crystals, needles and cubes are also present with a few occurrences of rounded crystals and spindles. Shark-tooth texture is found in a few samples and cauliflower texture is only found in the summit samples. Flank samples primarily have sub-angular crystals, with stacked plates, spindles, needles, angular and hexagonal crystals and shark-tooth texture also present. The coastal sample only had stacked plates, cubic, and sub-angular crystals present.

Table 5. Basic elemental composition of salt samples measured via qualitative scans on an electron microprobe with the salt habits present as determined by SEM imaging.

Sample	Morphologies Present	Microprobe Qualitative Scan Composition														
		Al	Ca	Cl	Cu	F	Fe	K	Mg	Mn	Na	Ni	P	S	Si	Ti
Summit Samples																
ERE-09-001	sa, f, sp	A		A		A	A	A	P	P	A			A	M	
ERE-09-002	f, sp	A	M	P		M	P	P	P	P			M	A	P	M
ERE-09-004	f, h	A	M	A		A	P	P		M	A				M	
ERE-09-005	sp, h, n	A	M	M		M	P	P	M	M	A			A	P	M
ERE-09-009	f, sp, h	A		A		A	A	P	P	P	A			A		M
ERE-09-012	f, sp, h, n	A	M	A		A	A	A	A	M	A		M	P	M	P
ERE-09-014	f, h	A	P	A		A	A	A	P	P	A		M	M	M	M
ERE-09-015	sp, c, r	A	A	M		P	A	P	P	M	A			A	P	M
ERE-09-016	f, sp, ca, sa	A	P	A		A	P	P	A	P	A		M	A	P	M
ERE-09-018	f, s, c, sp, sa	A	M	A		A	A	A	A	A	A			A	P	
ERE-09-019	sp, s, c	P	M	A		M	M	P	M	M	A			M		
ERE-09-020	sp, sa	A	P	P		M	P	A	P	M	A			A	P	M
ERE-09-034	f, c, sp, sa	A		A		P		M			A			A		
ERE-09-036	sp, sa	A	P			P	A	A	M	M	M			P	A	P
ERE-09-037	n, st, f, sa	A	P	P		P	P	P	M	P	P			A	A	
ERE-09-038	f, sp, s, sa	A	M	A		A	M	A	A	M	A			A	M	M
ERE-09-043	f, sa	A	M	A		A	M	M	P	M	A			M	M	
ERE-09-CR	sp	P	P	P	P		P	P	M			P	M		A	
ERE-09-MC-1	sp, sa	A	P			A		P	P			P		A	A	
ERE-09-MC-2	f, c, sa	A		P		P		M			M			A		
Flank Samples																
ERE-09-027	sa								M			A		A		
ERE-09-028	sa	P	M						M			A		A	P	
ERE-09-029	sp, st, sa	M	M				M	M	M			A		A	M	M
ERE-09-031	s, h, st, sa		P									A		A		
ERE-09-032	s, n, sp, a	M	A				M	M				A		A	M	
ERE-09-033	n, st, sa	P	M					M	M			A		A	M	
Coastal Samples																
ERE-09-030	sp, c, sa	A	P	A			A	A	A			A		M	A	P

A: Abundant, P: Present, M: Minor

a-angular, c-cubic, ca-cauliflower texture, f-fibrous, h-hexagonal, n-needles, r-rectangular, s-spindles, sa-sub-angular, sp- stacked plates, st-shark tooth texture

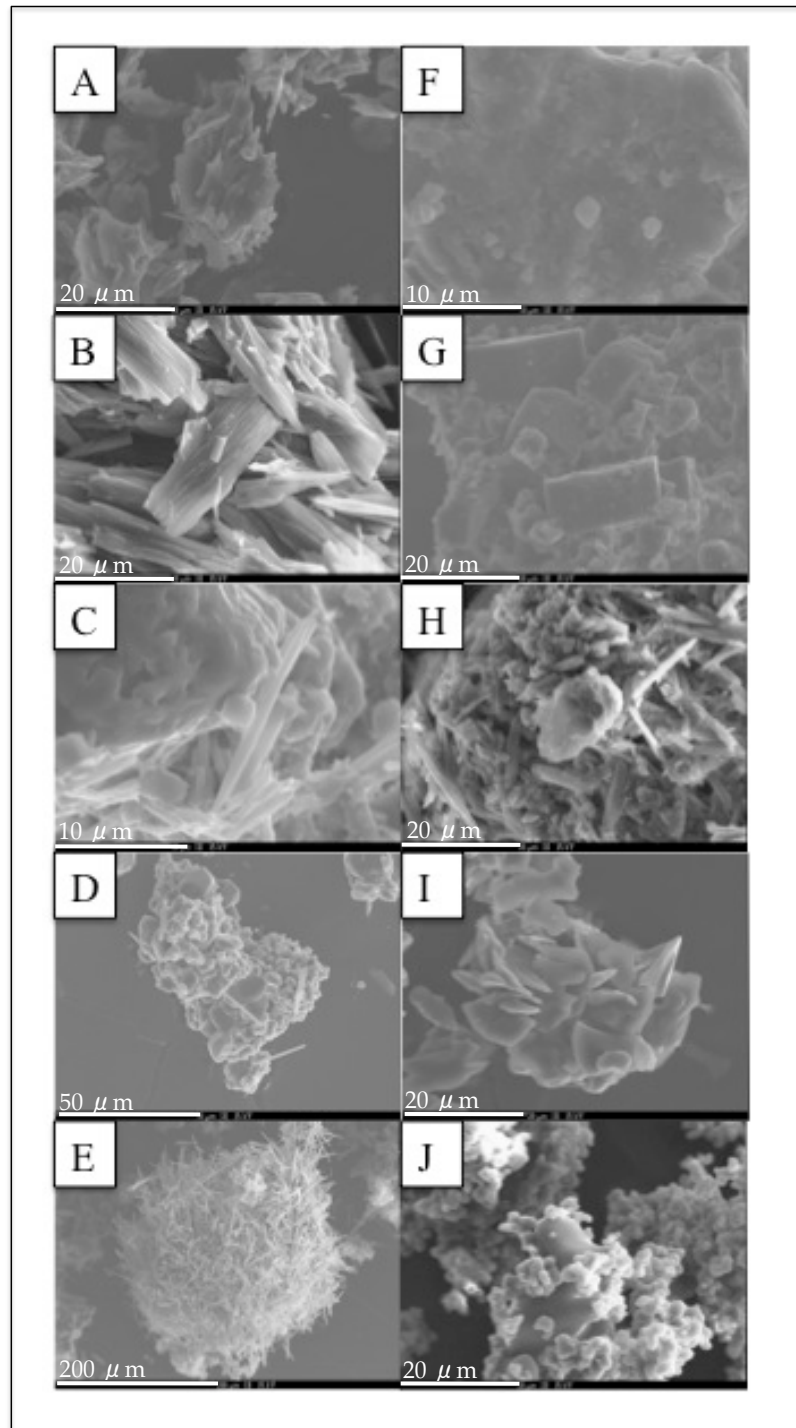


Figure 5. SEM images of habits present in salt samples showing distinct habits on a micron scale, with multiple habits present in samples on a micron scale. Dominant structures present include: A-Sub-angular, B-Fibrous, C-Stacked plates, D-Hexagonal, E-Needles, F-Cubes, G-Rectangular, H-Cauliflower texture, I-Shark-tooth texture, J-Sub-rounded salt crystals surrounding a volcanic glass shard.

Individual crystals were generally scanned on a 1 micron scale at a fixed position, however, due to the relative instability of salt phases under the beam charging and dissolution of material did occur. At the conclusion of some scans a hole would be present where the scan was conducted. In this case, the chemical composition of an underlying crystal may have influenced the results of the qualitative scan.

Qualitative element scans show a basic elemental composition of mixed Al, Ca, Cl, Cu, F, Fe, K, Mg, Mn, Na, Ni, P, S, Si, and Ti. On average at least ten scans were performed per sample. Table 5 lists all samples examined with relative abundances of each element present. For an element to be considered abundant it must be measured in 66% of the qualitative scans completed on each sample. For an element to be considered present it must be measured in 33-66% of the qualitative scans completed on each sample. For an element to be considered minor it must be present in at least one scan, but does not occur in more than 33% of the qualitative scans performed on one sample.

Individual salt samples contained multiple phases so determining a basic chemical composition of each grain was not possible. There were no consistencies between scans of similar habits. Based on the basic elemental makeup of the summit, flank, and coastal samples a basic chemical composition can be inferred for the three sub-groups. Summit samples primarily contain Al, Cl, F, Fe, Na, S with lesser amounts of K, Mg, Mn, Si, and traces of Ca, P, and Ti. Both Cu and Ni were detected in only one sample, and may reflect contamination from nearby scientific equipment such as metal tripods. Flank samples are dominantly composed of Na and S with lesser amounts of Si and Al,

trace amounts of Ca and K, with Fe, Mg, and Ti detected in a few samples. There was only one coastal sample analyzed and therefore the measured elemental composition cannot be concretely linked to the flank and summit samples. The coastal sample contained significant amounts of Al, Cl, Fe, K, Mg, Na, and Si, with lesser amounts of Ca and Ti, and minor amounts of S.

4.1.3 XRD Results

Thirty-seven salt samples were examined by XRD to determine mineral phases present. This data is given in Appendix C.1 (DVD-ROM). On average, each XRD scan had 21 distinct peaks, with a high of 58 peaks in one sample, and a low of 2 peaks in two of the samples. An example XRD scan is given in Figure 6. Overall, mineral identifications were easier on samples that had more distinct peaks to resolve. In order for a mineral identification to be considered positive the main three peaks for a mineral species had to be present in the measured sample spectra. The basic chemical composition and salt morphology observed on the electron microprobe was used to help determine best mineral fits. Observations from SEM images showed multiple morphologies present at a micron scale. For this reason it was impossible to isolate a single morphology for XRD analysis. Also, despite the zero background sample stage used, a sample measuring at least 50 μm had to be used in order to generate higher counts and peak resolution. Identifications were also complicated by the fact that a single peak could be assigned to multiple potential mineral phases. The use of a single peak for multiple mineral identifications is only possible if the peak is broad and

therefore encompasses several peaks into one. In the case of multiple minerals fitting one peak, the exact peak position and intensity of the measured peak and potential mineral species was used to make identifications. Identifications were tricky, and in some cases no identifications (positive or tentative) could be made. Table 6 lists the minerals identified in each XRD scan, with multiple minerals identified some scans. It is important to note that not all peaks were resolved.

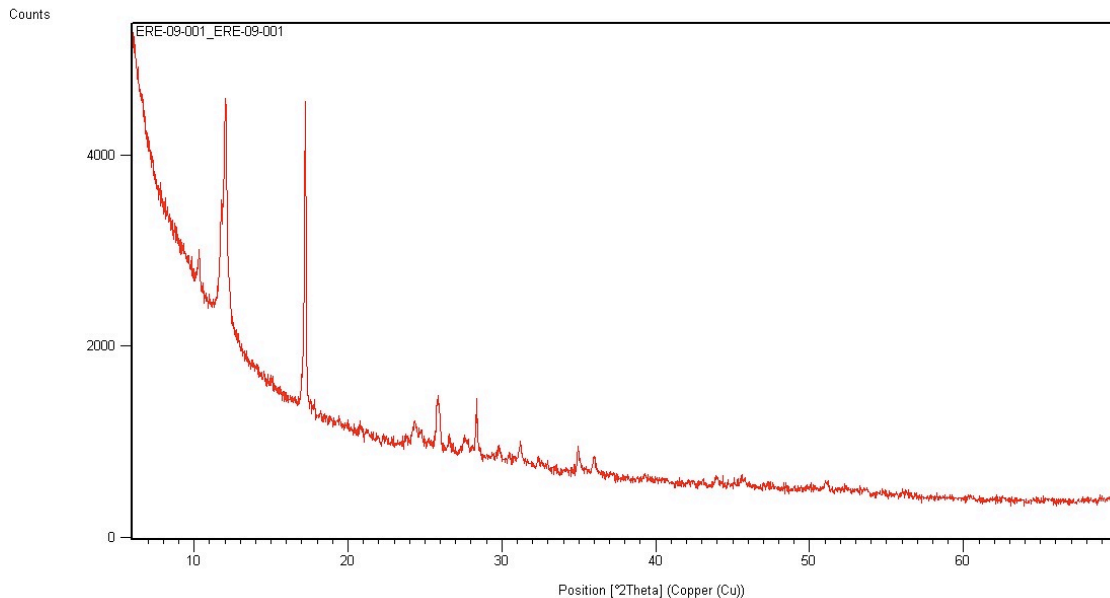


Figure 6. Example XRD pattern for Erebus salt sample ERE-09-001. Note distinct peaks at approximate $^{\circ}2\theta$ positions 10, 12, 17, 24, 26, 28, 30, 31, 35, 36 $^{\circ}$. Exact peak locations were determined by X'pert PRO software. Identified peaks were matched to known peaks of database minerals to make salt mineral identifications. In some case not all peaks could be resolved by known mineral species.

Table 6. XRD mineral identifications for all thirty-seven salt samples analyzed.

Sample	Alumite $KAl_3(SO_4)_2(OH)_6$	Calcite $Ca(CO_3)$	Cristobalite $Ca_{0.05}(Al_{1.0}Si_{1.0}O_4)$	Gypsum $Ca(SO_4)(H_2O)_2$	Halite NaCl	Halite, potassian Na_2K_2Cl	Illite $(K,H_2O)Al_2(Si_3Al)O_{10}(OH)_2 \cdot xH_2O$	Kaolinite $Al_2Si_2O_5(OH)_4$
Summit Samples								
ERE-09-001								
ERE-09-002								
ERE-09-004	x					x		x
ERE-09-005	x							
ERE-09-007								
ERE-09-008				x	x			
ERE-09-009								x
ERE-09-010								x
ERE-09-011					x			
ERE-09-012	x			x	x			x
ERE-09-013	x							x
ERE-09-014						x		x
ERE-09-015	x				x			
ERE-09-016								
ERE-09-018								
ERE-09-019	x				x			
ERE-09-020								
ERE-09-021					x			
ERE-09-022								
ERE-09-023							x	
ERE-09-024	x							
ERE-09-025								
ERE-09-026					x			
ERE-09-034					x			
ERE-09-036							x	
ERE-09-038	x							
ERE-09-040					x			
ERE-09-043	x							x
ERE-09-CR			x					
ERE-09-MC-1								
ERE-09-MC-2				x				
Flank Samples								
ERE-09-027								
ERE-09-028		x			x			
ERE-09-031								
ERE-09-032	x							
ERE-09-033				x				
Coastal Samples								
ERE-09-030								x

Table 6 Cont.

Sample	Katoite $\text{Ca}_3\text{Al}_2(\text{H}_2\text{O})_6$	Khademite $\text{Al}(\text{SO}_4)_2 \cdot 5\text{H}_2\text{O}$	Millosevichite $\text{Al}_2(\text{SO}_4)_3$	Ralstonite $\text{NaMgAl}(\text{F},\text{OH})_2 \cdot \text{H}_2\text{O}$	Rancieite $(\text{Ca},\text{Mn})\text{Mn}_2\text{O}_7 \cdot 3\text{H}_2\text{O}$	Sodiumalum $\text{NaAl}(\text{SO}_4)_2 \cdot (\text{H}_2\text{O})_{12}$	Sulfur S	Sylvite KCl	Thenardite Na_2SO_4
Summit Samples									
ERE-09-001	x				x			x	
ERE-09-002	x								
ERE-09-004	x								
ERE-09-005	x								
ERE-09-007	x	x					x		
ERE-09-008				x					x
ERE-09-009					x				
ERE-09-010	x								
ERE-09-011									
ERE-09-012									
ERE-09-013			x		x				
ERE-09-014									
ERE-09-015									
ERE-09-016								x	
ERE-09-018								x	
ERE-09-019					x				
ERE-09-020									x
ERE-09-021		x							
ERE-09-022		x		x					
ERE-09-023				x		x			x
ERE-09-024					x			x	
ERE-09-025									
ERE-09-026					x				x
ERE-09-034									
ERE-09-036									
ERE-09-038									
ERE-09-040									
ERE-09-043	x								
ERE-09-MC-1									
ERE-09-MC-2									
Flank Samples									
ERE-09-027	x								
ERE-09-028									x
ERE-09-031	x								
ERE-09-032	x								
ERE-09-033							x		
Coastal Samples									
ERE-09-030	x							x	

This study does reaffirm some mineral identifications made in previous studies (Keys, 1980; Keys and Williams, 1981; Zreda-Gostynska, 1995). Table 7 lists the positive, tentative, and new identifications made in this study. Salt identifications that agree with previous studies of Erebus salts include sylvite, alunite, khademite, halite, ralstonite, gypsum, mirabilite (thenardite), and calcite. Illite is the only mineral that was previously tentatively identified on Erebus and tentatively identified again in this study. Several minerals never before identified on Erebus are positively and tentatively identified in this study. Commonly occurring new identifications include rancieite, katoite, potassian-halite, and sodiumalum. Identified species that are not common and represent very tentative identifications include kaolinite, native sulfur, millosevichite, and cristobalite. Their chemistry and morphology fit with EMP observations, however due to their low abundance these minerals cannot be positively identified.

Table 7. Mineral identifications of Erebus salt samples.

Mineral	Chemical Formula
Mineral phases positively identified on Erebus	
Alunite	$K(Al_3(SO_4)_2(OH)_6)$
Calcite	$Ca(CO_3)$
Gypsum	$CaSO_4 \cdot 2H_2O$
Halite	$NaCl$
Khademite	$Al(SO_4)F \cdot 5H_2O$
Mirabilite	$Na_2SO_4 \cdot 10H_2O$
Ralstonite	$NaMgAl(F,OH)_6 \cdot H_2O$
Sylvite	KCl
Thenardite	Na_2SO_4
Mineral phases tentatively identified on Erebus	
Illite	$(K,H_3O)Al_2(Si_3Al)O_{10}(OH)_2 \cdot xH_2O$
Mineral phases previously not identified on Erebus	
Cristobalite	$Ca_{0.05}((Al_{0.1}Si_{1.9})O_4)$
Potassian-Halite	$NaKCl$
Kaolinite	$Al_2Si_2O_5(OH)_4$
Katoite	$Ca_3Al_2O_6(H_2O)_6$
Millosevichite	$Al_2(SO_4)_3$
Rancieite	$(Ca,Mn)Mn_4O_9 \cdot 3H_2O$
Sodiumalum	$NaAl(SO_4)_2(H_2O)_{12}$
Sulfur	S

There are a few unidentified peaks that are common throughout Erebus salt samples. The 2θ ranges that have several unidentified peaks are shown in Figure 7. Most peaks past $29.9^\circ 2\theta$ are not significant peaks and therefore are not included in Figure 7. These common grouping of peaks may represent a family of minerals that were not identified in this study. Due to issues with sample height or preferred orientations during sample analysis, an incomplete spectra or shifted peaks could also be responsible for these unidentified peak groupings. It

is possible that there could be many more minerals that were not identified in this study. Also, consistent unidentified peaks that occur in the same scan could be used to create a new spectrum to identify potentially new salt mineral phases. This process would be complicated due to the small sample size and other mineral phases present in the sample.

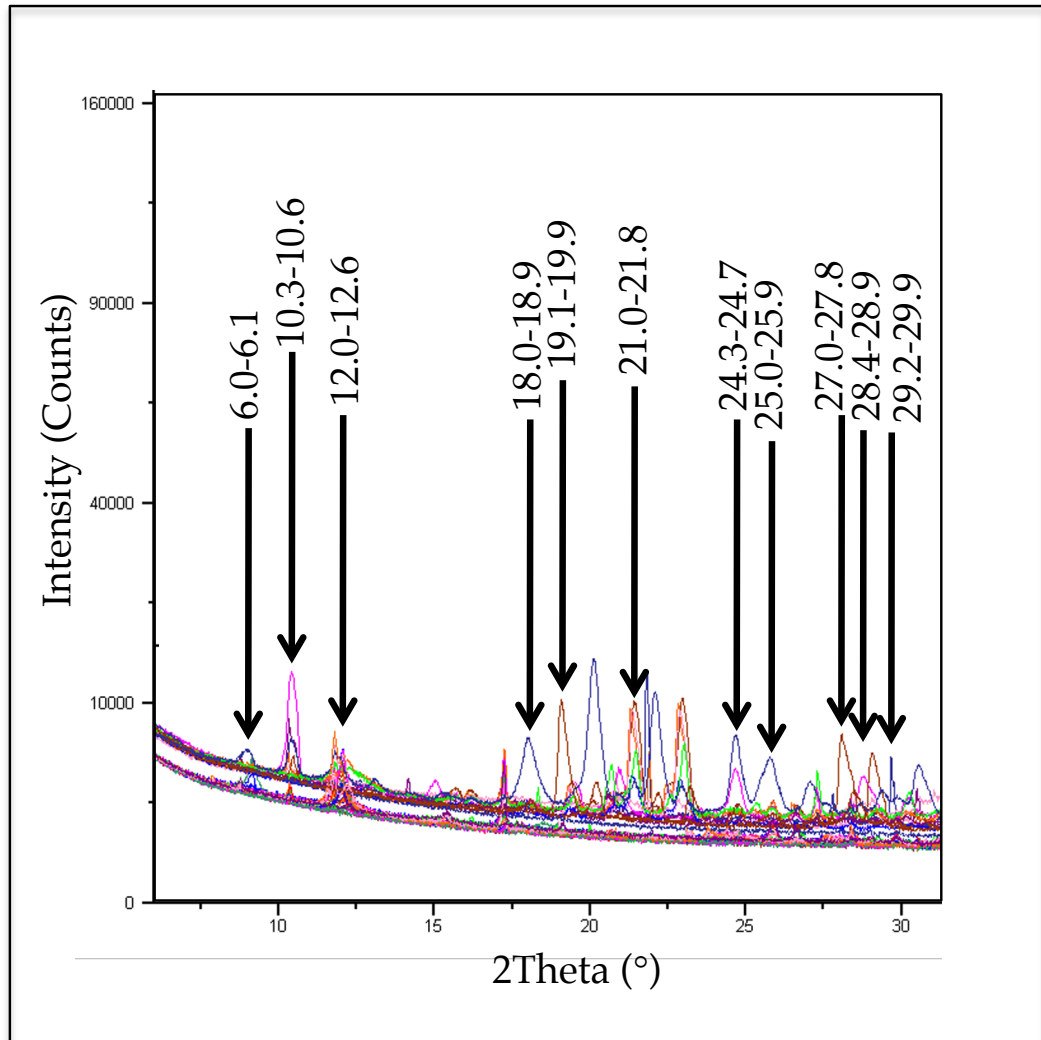


Figure 7. XRD Spectra for all 37 samples analyzed with major unidentified peak groupings indicated by the arrows. Peaks past 30°2θ are not shown since they do not represent any major peaks.

4.2 Snow Chemistry

Thirty-five snow samples were collected at the nearest snow patch adjacent to where the salt samples were collected. The snow was analyzed to determine major cations and anions present. From the reported results an ionic balance was calculated from the measured cations and anions in order to determine if all cations and anions were measured, or if some were not represented in the analysis. Table 8 lists the major cations and anions present in Erebus snow, along with the calculated ionic balance. Measured cations used in the ionic balance calculation include: Na^+ , K^+ , Mg^{2+} , Ca^{2+} . Measured anions used in the ionic balance calculation include: HCO_3^- , F^- , Cl^- , NO_2^- , NO_3^- , Br^- , CO_3^{2-} , SO_4^{2-} , PO_4^{3-} . If an ionic balance does not equal zero, then either a cation or anion was not included in the analysis. The recalculation of ionic balances to account for missing components will be addressed in the discussion. Ionic balances were calculated using the following formula:

$$\left[\frac{\text{Sum Total Cations (meq/L)} - \text{Sum Total Anions (meq/L)}}{\text{Sum Total Cations (meq/L)} + \text{Sum Total Anions (meq/L)}} \right] \times 100$$

The snow predominately contains Al, Cl, F, Na, SO_4 , and S. Also present is Fe, Ca, and K with traces of Ba, Br, Li, Mn, NO_3 , PO_4 , and Sr. The ionic balance ranges from -93.1 to -9.6 percent difference. In Figure 8 the major cations and anions present in the snow were plotted against elevation in order to determine the variability of these elements with relation to the main crater. The highest concentrations of all major cations and anions is at the main crater (3600m), with

the lowest concentrations in the coastal or lower flank regions. It is important to note that there is not a linear trend linking the change in concentration to elevation. However, the highest concentrations of all snow components are in the summit region. This implies that you need to be at high elevation for the concentration to increase. Each cation and anion represented in Figure 8 is individually plotted in Figures 9a, 9b, and 9c in order to illustrate the scattering in concentrations for these elements with relation to elevation. The clustering of points in the summit region for each snow chemistry component indicates that you need to be at higher elevations to get an increase in concentration, but not all snow samples show the same increase in concentration in the summit region.

Table 8. Raw snow chemistry data with measured cations and anions, pH, and conductivity along with the calculated ionic balance. A report of *na* is for measurements below detection limits and a report of *na* is for measurements that were not conducted.

Sample (all units in mg/L)	Al ³⁺	Ba ²⁺	Ca ²⁺	Fe ³⁺	K ⁺	Li ⁺	Min ²⁺	Na ⁺	Total Cations (meq/L)	Br	Cl	F	NO ₃ ⁻	PO ₄ ³⁻	SO ₄ ²⁻	Total Anions (meq/L)	pH	Conductivity (uS/cm)	Ionic Balance	
Summit Samples																				
001--compacted surface snow	2.86	0.016	1	1.19	1.00	0.001	0.069	2.00	0.18	<i>na</i>	28	8.2	<i>na</i>	0.20	2	1.28	3.2	275	-75.8	
001--ice	14.3	0.037	3	1.45	6.00	0.005	0.394	10.0	0.89	<i>na</i>	20	16.4	<i>na</i>	<i>na</i>	92	3.33	3.1	485	-57.9	
002--compacted surface snow	3.68	0.024	1	1.40	2.00	0.002	0.084	3.00	0.26	<i>na</i>	15	13.5	<i>na</i>	0.30	4	1.24	3.4	220	-65.4	
003--ice	185	0.151	40	69.3	229	0.059	3.597	197	17.35	<i>na</i>	439	889	1.00	7.40	192	63.46	2.5	3510	-57.1	
009--compacted snow	1.55	0.009	<i>na</i>	0.602	1.00	<i>na</i>	0.035	2.00	0.13	<i>na</i>	14	7.0	<i>na</i>	0.10	2	0.81	3.5	205	-73.0	
009--surface powder snow	0.439	0.003	<i>na</i>	0.153	<i>na</i>	<i>na</i>	0.009	<i>na</i>	0.03	<i>na</i>	9	1.2	<i>na</i>	0.20	1	0.33	3.7	105	-81.5	
010--compacted surface snow	4.52	0.024	1	1.84	4.00	0.002	0.098	4.00	0.35	<i>na</i>	22	22.1	<i>na</i>	0.20	3	1.85	3.3	300	-68.5	
011--compacted surface snow	0.967	0.006	<i>na</i>	0.422	1.00	<i>na</i>	0.028	1.00	0.07	<i>na</i>	13	4.2	<i>na</i>	<i>na</i>	1	0.62	3.5	170	-79.7	
012--compacted snow	17.6	0.085	3	5.55	9.02	0.004	0.435	12.3	0.99	<i>na</i>	46	51.2	0.073	0.36	10	4.21	3.3	390	-62.1	
012--surface powder snow	7.82	0.045	1	3.11	3.98	0.002	0.160	5.48	0.43	<i>na</i>	17	20.9	0.055	<i>na</i>	2	1.62	3.9	130	-58.0	
018--compacted snow	10.6	0.062	2	3.68	6.10	0.004	0.258	11.4	0.83	<i>na</i>	43	31.1	0.055	0.25	21	3.31	3.1	440	-59.9	
018--surface powder snow	3.11	0.017	1	1.20	1.70	0.001	0.068	2.37	0.19	<i>na</i>	15	7.3	0.044	<i>na</i>	1	0.84	3.7	115	-63.7	
020--compacted snow	4.81	0.027	1	1.98	3.22	0.002	0.108	4.15	0.33	<i>na</i>	21	15.3	0.051	0.22	4	1.51	3.4	225	-64.4	
020--surface powder snow	1.30	0.009	<i>na</i>	0.511	0.93	<i>na</i>	0.034	1.26	0.10	<i>na</i>	24	6.3	0.064	0.18	1	1.03	3.2	275	-82.5	
021--compacted surface snow	0.807	0.005	<i>na</i>	0.288	0.53	<i>na</i>	0.017	0.769	0.06	0.021	11	2.8	0.083	0.16	1	0.48	3.5	140	-78.2	
021--ice	1.75	0.010	<i>na</i>	0.702	1.24	0.001	0.035	1.64	0.12	0.021	9	4.7	0.049	<i>na</i>	6	0.63	3.5	130	-67.3	
022--compacted snow	0.441	0.003	<i>na</i>	0.132	0.21	<i>na</i>	0.009	0.313	0.03	<i>na</i>	5	1.5	<i>na</i>	0.16	1	0.24	3.8	74	-80.7	
022--surface powder snow	0.039	0.001	<i>na</i>	0.013	0.03	<i>na</i>	0.001	0.049	0.01	<i>na</i>	4	0.2	0.069	<i>na</i>	1	0.13	3.9	45	-93.1	
023--compacted snow	<i>na</i>	<i>na</i>	<i>na</i>	<i>na</i>	<i>na</i>	<i>na</i>	<i>na</i>	<i>na</i>	<i>na</i>	<i>na</i>	6	2.9	0.052	0.21	2	0.36	3.9	70	<i>na</i>	
023--surface powder snow	<i>na</i>	<i>na</i>	<i>na</i>	<i>na</i>	<i>na</i>	<i>na</i>	<i>na</i>	<i>na</i>	<i>na</i>	<i>na</i>	4	0.2	0.057	<i>na</i>	1	0.14	<i>na</i>	<i>na</i>	<i>na</i>	
025--compacted surface snow	0.439	0.004	<i>na</i>	0.092	0.45	<i>na</i>	0.010	0.632	0.05	<i>na</i>	3	1.4	<i>na</i>	<i>na</i>	1	0.19	3.9	44	-57.9	
026--compacted snow	0.726	0.003	<i>na</i>	0.101	0.23	<i>na</i>	0.015	0.765	0.05	<i>na</i>	3	2.2	0.051	0.20	1	0.23	4.0	49	-64.7	
026--surface powder snow	0.113	0.001	<i>na</i>	0.035	0.06	<i>na</i>	0.002	0.158	0.02	0.030	3	0.2	0.052	<i>na</i>	<i>na</i>	0.11	4.0	36	-76.5	
040--compacted snow	5.58	0.047	1	1.91	4.80	0.003	0.098	6.91	0.53	<i>na</i>	13	26.8	0.041	<i>na</i>	9	1.97	3.4	225	-57.8	
040--surface powder snow	0.308	0.124	<i>na</i>	0.025	0.14	<i>na</i>	0.005	0.251	0.02	<i>na</i>	4	1.2	0.055	0.32	1	0.22	3.8	61	-81.7	
043--compacted surface snow	5.29	0.105	1	1.85	2.74	0.002	0.113	3.90	0.31	<i>na</i>	20	13.6	0.072	<i>na</i>	6	1.41	3.4	195	-64.5	
CR--surface snow	871	0.313	131	416	415	0.301	18.855	886	60.10	6.58	3320	3558	10.7	<i>na</i>	403	289.60	1.6	18890	-65.6	
Flank Samples																				
027--compacted snow	0.075	0.117	<i>na</i>	0.001	0.14	<i>na</i>	0.002	1.74	0.10	<i>na</i>	3	0.4	0.016	0.10	1	0.17	5.4	26	-25.0	
027--surface powder snow	0.084	0.091	<i>na</i>	0.002	0.09	<i>na</i>	0.001	1.06	0.06	0.035	2	0.3	0.106	0.17	1	0.12	5.6	18	-30.6	
031--compacted surface snow	0.003	0.070	<i>na</i>	0.001	0.06	<i>na</i>	0.001	0.459	0.03	<i>na</i>	1	0.1	0.045	0.07	1	0.08	5.6	9.2	-47.6	
032--compacted surface snow	0.098	0.061	<i>na</i>	0.003	0.23	<i>na</i>	0.003	0.703	0.05	<i>na</i>	2	0.2	0.046	<i>na</i>	1	0.10	5.2	13	-38.8	
033--compacted snow	0.505	0.045	<i>na</i>	0.048	0.35	<i>na</i>	0.009	0.750	0.05	<i>na</i>	3	1.2	0.029	0.11	2	0.18	4.2	33	-55.2	
033--surface powder snow	1.00	0.026	<i>na</i>	0.056	0.92	<i>na</i>	0.014	2.29	0.15	0.038	5	2.6	0.020	0.09	4	0.36	4.0	54	-41.9	
Coastal Samples																				
030--compacted surface snow	0.025	0.077	<i>na</i>	0.002	0.36	<i>na</i>	0.002	3.178	0.18	0.042	6	0.1	0.133	0.07	1	0.22	5.5	30	-9.90	
030--ice	0.035	0.068	<i>na</i>	0.002	0.17	<i>na</i>	0.004	4.259	0.22	0.063	7	0.2	0.078	0.09	1	0.27	5.7	34	-9.60	

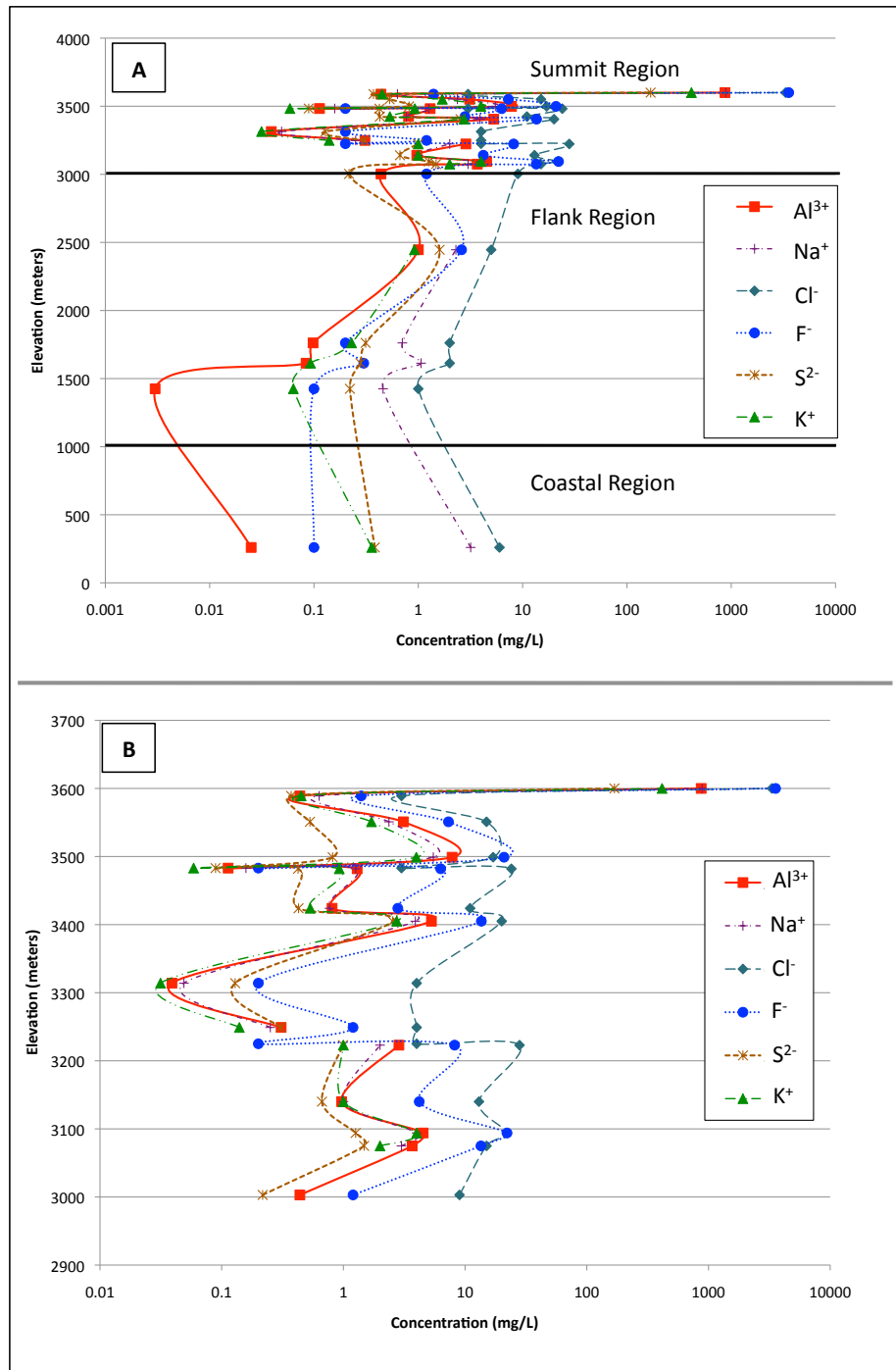


Figure 8. Fluctuations in the concentration of major elements found in Erebus snow samples. A. Coast to summit: Concentrations increase from coast to summit, with high variability in samples from the summit region. B. Summit region: There is high variability in snow chemistry within the summit region, with no clear trend linked to changes in elevation, with the exception of a steep increase in concentration at the summit (3600m).

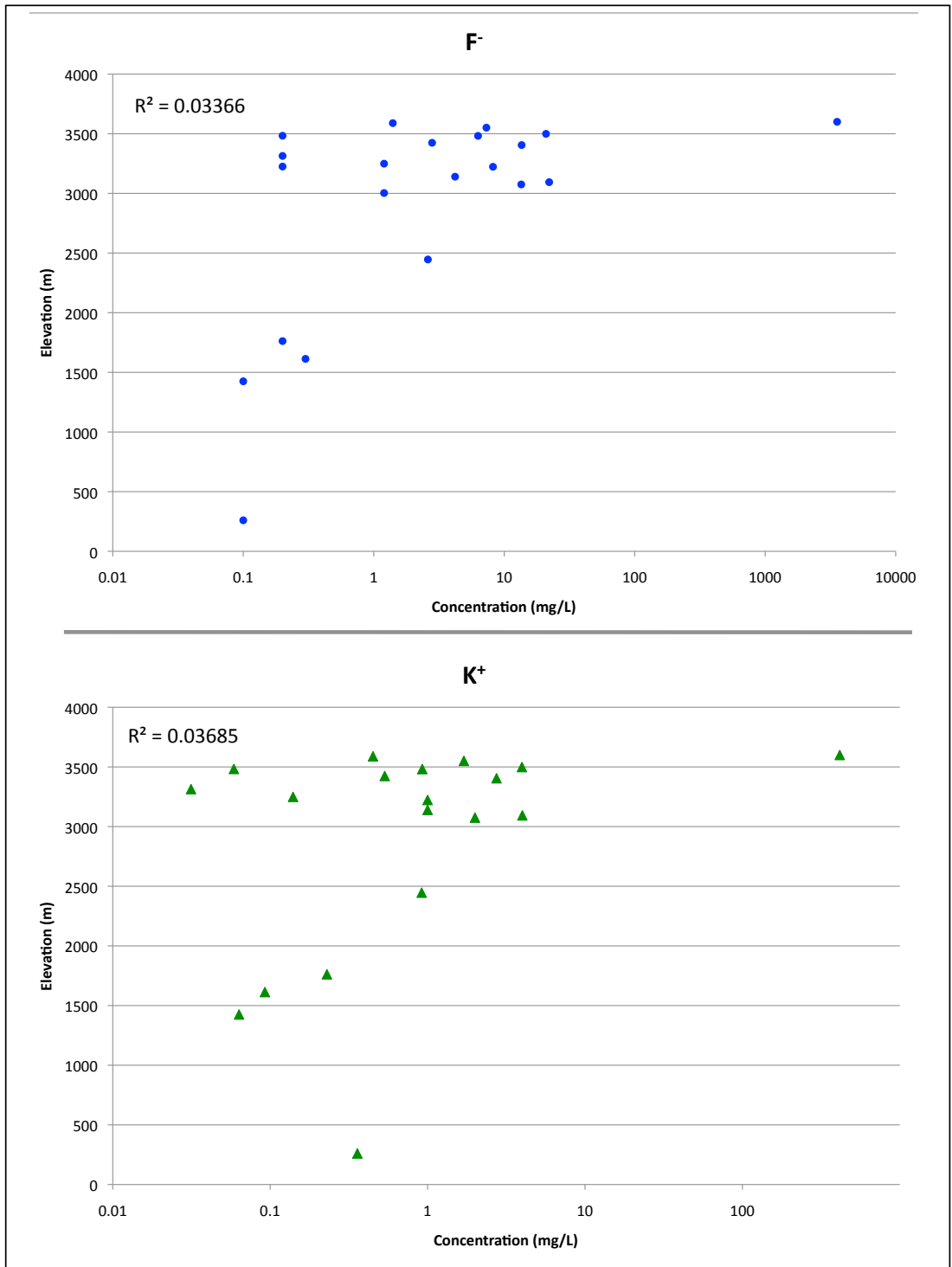


Figure 9b. Concentrations of major cation K⁺ and anion F⁻ in Erebus snow plotted individually against elevation. An R² value was calculated to determine the correlation between elevation and concentration for each cation and anion.

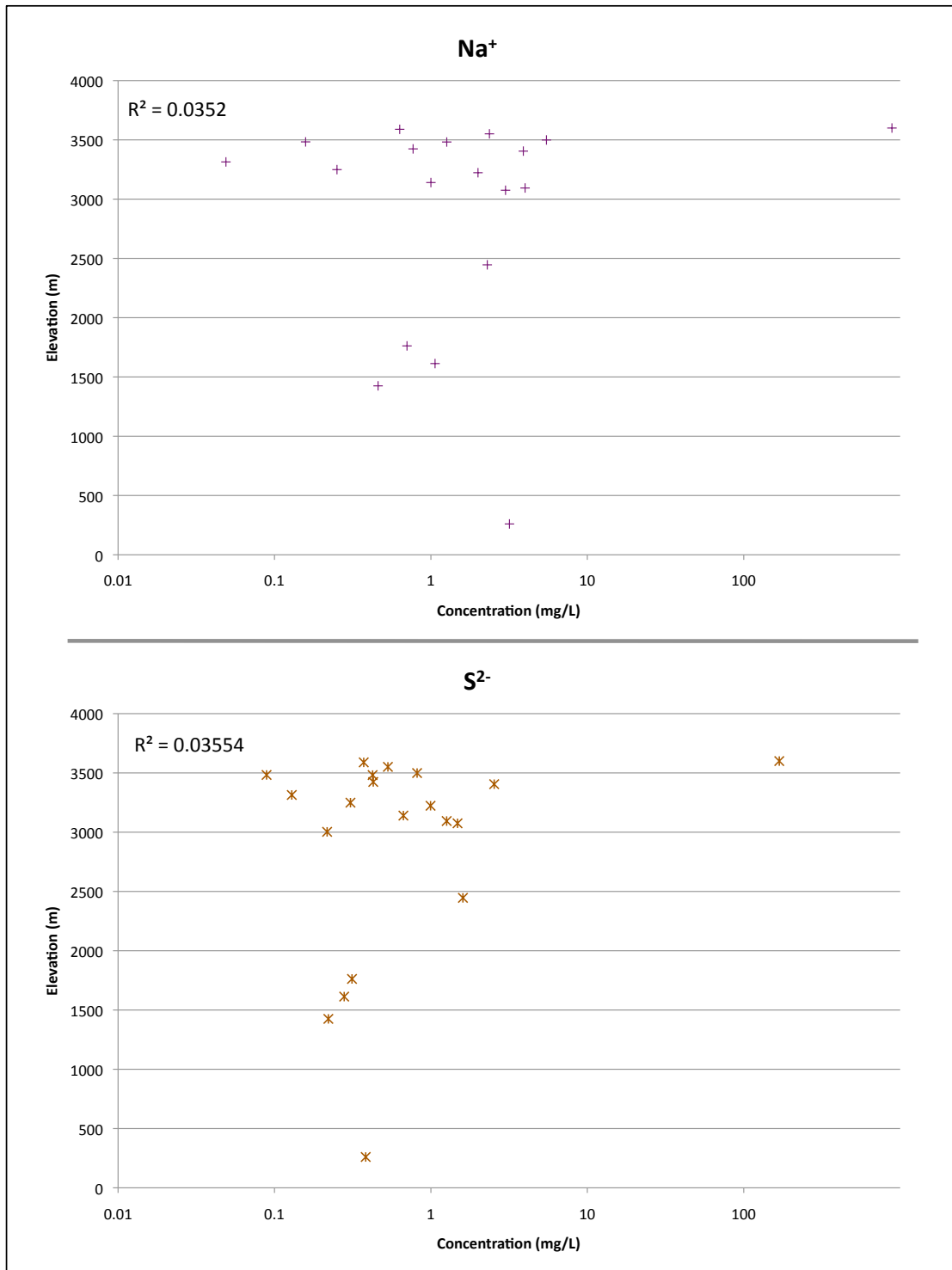


Figure 9c. Concentrations of major cation Na⁺ and anion S²⁻ in Erebus snow plotted individually against elevation. An R² value was calculated to determine the correlation between elevation and concentration for each cation and anion.

5. DISCUSSION

5.1 Plume Influence On Snow Chemistry

Snow chemistry on Erebus appears to be linked to the plume chemistry, and the snow may serve as a record of plume distribution in the summit region of Erebus. The initial indicator of the influence of the plume on snow chemistry can be seen in Figure 8A. The highest elemental concentrations in the snow are found at the summit of Erebus, with varying concentrations along the flanks of the volcano. There is high variability in the concentration of Al, F, Cl, Na, K, and SO_2^{2-} in the summit region. The main source for these major snow chemistry components in the summit region is the plume. As mentioned earlier, the minor gas species measured in the plume include HF, HCl, and SO_2 (Oppenheimer and Kyle, 2008; Oppenheimer et al., 2010; Zreda-Gostynska, 1995; Zreda-Gostynska et al., 1997). These acidic volcanic gases in combination with aerosol particles, which are rich in Cl, S, F, Na, K, and Al, are distributed in the summit region of the volcano (Chuan, 1994; Chuan et al., 1986; Ilyinskaya et al., 2010; Zreda-Gostynska, 1995). The occurrence of Al, F, Cl, Na, K, and S as major components in both the snow and plume is another indicator that the plume is the source for the elements in the snow.

It is important to note that pure snow has a baseline of 0 concentration for all snow chemistry components listed above. Therefore, the presence of these elements in snow samples from Erebus volcano indicates that something is contributing these elements to the snow chemistry. Antarctic snow from the McMurdo region was used as a baseline for comparison between Erebus snow samples and pure Antarctic snow. Snow from the McMurdo Sound region is heavily influenced by a marine effect (Margolin, 2006). High concentrations of Na, Cl, and S are expected in these samples, with concentrations at or near zero for all other components. Aside from Na, Cl, and S, any increase in concentration for Erebus snow samples over the baseline McMurdo Sound region snow samples would reflect an accumulation factor. Since the change in elevation alone was determined not to be the reason for an increase in concentration near the summit, and there is not a significant change in the rock chemistry between the summit and coast, the only remaining source for the increase in concentration is the Erebus plume. The presence of F in Erebus snow samples serves as the main evidence of plume chemistry reflected in Erebus snow chemistry. Fluorine is not present in any concentration in the McMurdo Sound region, but has high concentrations in the summit region. The only source of F in the summit region is the plume.

Despite the apparent lack in correlation between elevation and snow chemistry, a correlation coefficient was calculated between the snow chemistry components Al, Cl, F, K, Na, and S (Table 9). Correlation coefficients illustrate whether the fluctuations in concentration for each snow component follow the same trend. A strong correlation between snow chemistry components may indicate a similar source for these elements. Overall, correlations exist between

these six elements, with two distinct populations present. A strong correlation exists between elements F, Al, K, and Na, with correlation coefficients above 0.9. The second population is only weakly correlated in the 0.6 range and includes Cl and S interacting with the other four elements. It appears that F is the link between the strong correlations and it is possible that F, Al, K, and Na are depositing out together from the plume. The F is most likely complexing with the Al, K, and Na and these heavy particles are falling out together. The weak correlations between Cl and S with F, Al, K, and Na indicate that Cl and S are not deposited from the plume with the other components in the summit region. The correlation coefficients are an initial indicator of the reflection on the plume chemistry on the snow chemistry, but further evidence of this is necessary.

Table 9. Correlation coefficients for six prominent elements in Erebus summit snow chemistry. A correlation coefficient [R²] close to 1 indicates a strong correlation and no correlation is present at 0 (n=16).

Element	Al	Cl	F	K	Na	S
Al	1					
Cl	0.6084	1				
F	0.9301	0.6863	1			
K	0.9348	0.5803	0.9817	1		
Na	0.9911	0.6182	0.9623	0.9689	1	
S	0.6895	0.5807	0.6783	0.6478	0.6958	1

Enrichment factors for snow components were calculated in order to establish a link between the plume and snow compositions. They were calculated relative to the chemical composition of coastal Antarctic snow from the McMurdo Sound area determined by Margolin (2006) and to the Erebus plume composition determined by Zreda-Gostynska (1995). It is important to note that the plume does not influence snow from the McMurdo Sound area, and its

chemistry has been established as being near zero for all components reported. Antarctic snow from the McMurdo Sound area and the Erebus plume were selected as the source for each calculation because they represent two potential sources for influencing snow chemistry on Erebus. The plume is a constant factor in the summit region and its components may be reflected in the summit region snow chemistry, and snow in the summit region typically isn't fresh snowfall, but is blown in, possibly from the McMurdo Sound area. These two potential influences on snow chemistry in the summit region represent two end-members and the largest factors of change.

Enrichment factors (EF) are calculated using:

$$EF_{\text{Sample}} = \frac{(X/R)_{\text{Snow}}}{(X/R)_{\text{Antarctic snow, Erebus plume}}}$$

where EF_{Snow} is the enrichment factor of element X in the sample, $(X/R)_{\text{sample}}$ is the ratio of element X to the reference element R in the sample, and $(X/R)_{\text{Antarctic snow, Erebus plume}}$ is the ratio of element X to the reference element in the Antarctic snow or the Erebus plume. Iron was selected as the reference element in this study since it has a well-established concentration in the two sources used (Antarctic snow, and the Erebus plume) and low reactivity of its compounds in the atmosphere (Zreda-Gostynska, 2005). Other common reference elements used in enrichment factor calculations include Al and Sc. Only common elements measured in the plume and snow chemistry could be used in EF calculations. Aluminum was not selected as a reference element since it is a major component in the salts, snow, plume, and rock, and Sc was not measured in the snow chemistry.

Figures 10a and 10b illustrate the trends in calculated EF for snow samples in the summit region (above 3000 m) and ranging from the coastal region of Erebus up to the summit relative to potential sources: McMurdo Sound region snow and the Erebus plume. Erebus snow samples were averaged in 100-meter elevation intervals for the summit region, and 500-meter elevation intervals for the coast to summit regions. A dark black line plotted horizontally at 0 for each EF plot indicates the source. The ratio of X/Fe is enriched relative to the source if it is above 0, and depleted relative to the source if it is below 0. It is important to note that the enrichment or depletion of X/Fe relative to the source is only a relative indicator for potential sources for snow chemistry components. This calculation is only a ratio and can also be affected by changes in the concentrations of the reference element Fe. In general, if the ratio of X/Fe is enriched relative to the source then it is interpreted that the element X is most likely not from the source being examined. However, it is also possible that an element is deposited in excess from the source and has accumulated to a higher concentration than the source. For example, if Al/Fe is enriched relative to the plume source, then the Al present in Erebus snow is either not deposited from the plume, or the Al from the plume is depositing out into the snow in excess; the first case is more likely over the latter. EF calculations are typically used to determine the volatility of melt components into the gas phase, but their use here presents a new application for determining sources for snow chemistry components.

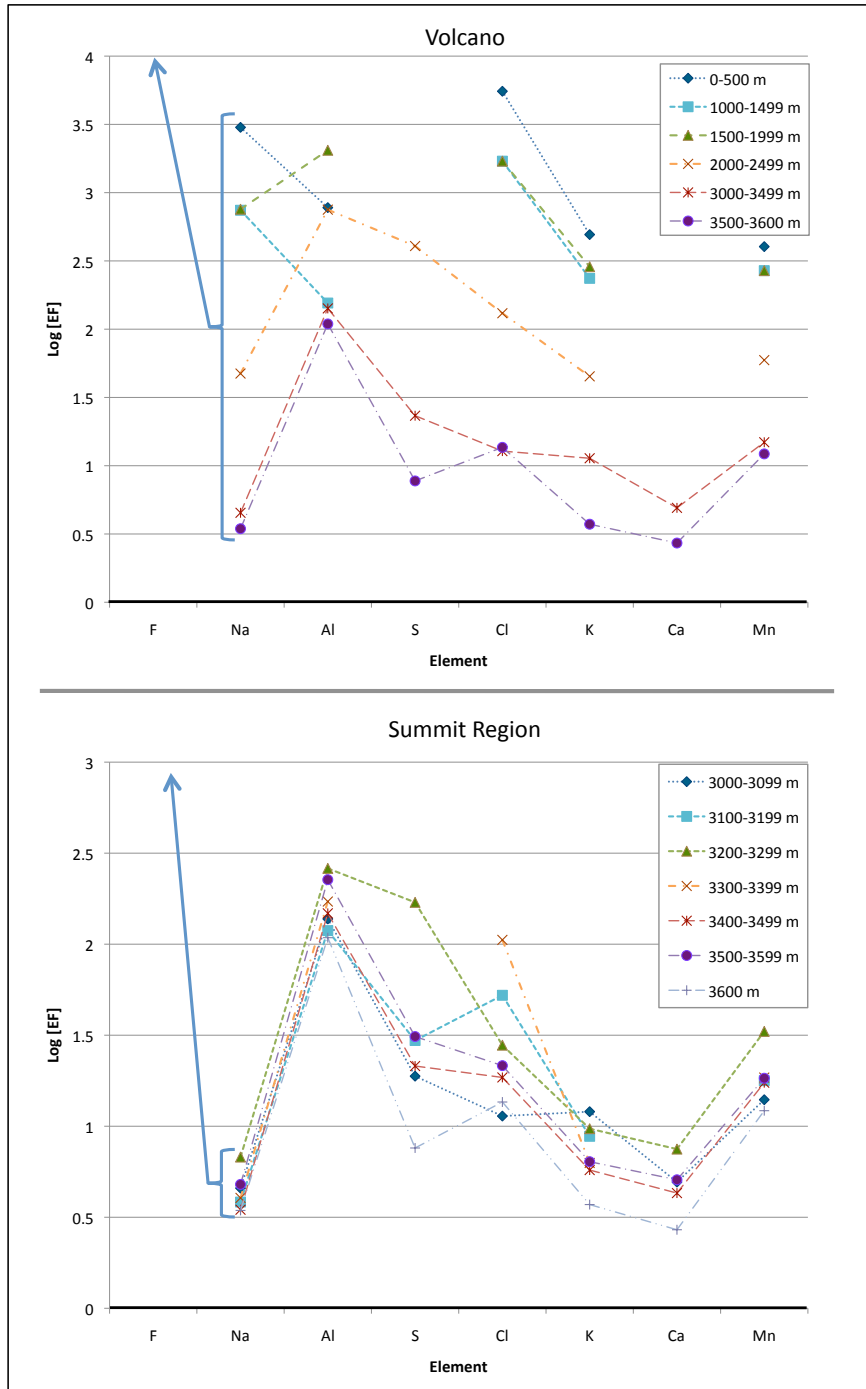


Figure 10a. Enrichment factors (EF) for Erebus snow samples Fe normalized relative to McMurdo Sound region snow. Erebus snow samples were averaged within 500-meter elevation intervals for the volcano, ranging from the coast to the summit and into 100-meter elevation intervals for the summit region. Omitted elevation ranges did not contain any snow samples. The arrow indicated the inferred F enrichment. McMurdo Sound region snow is not influenced by the Erebus plume and values are from Margolin (2006).

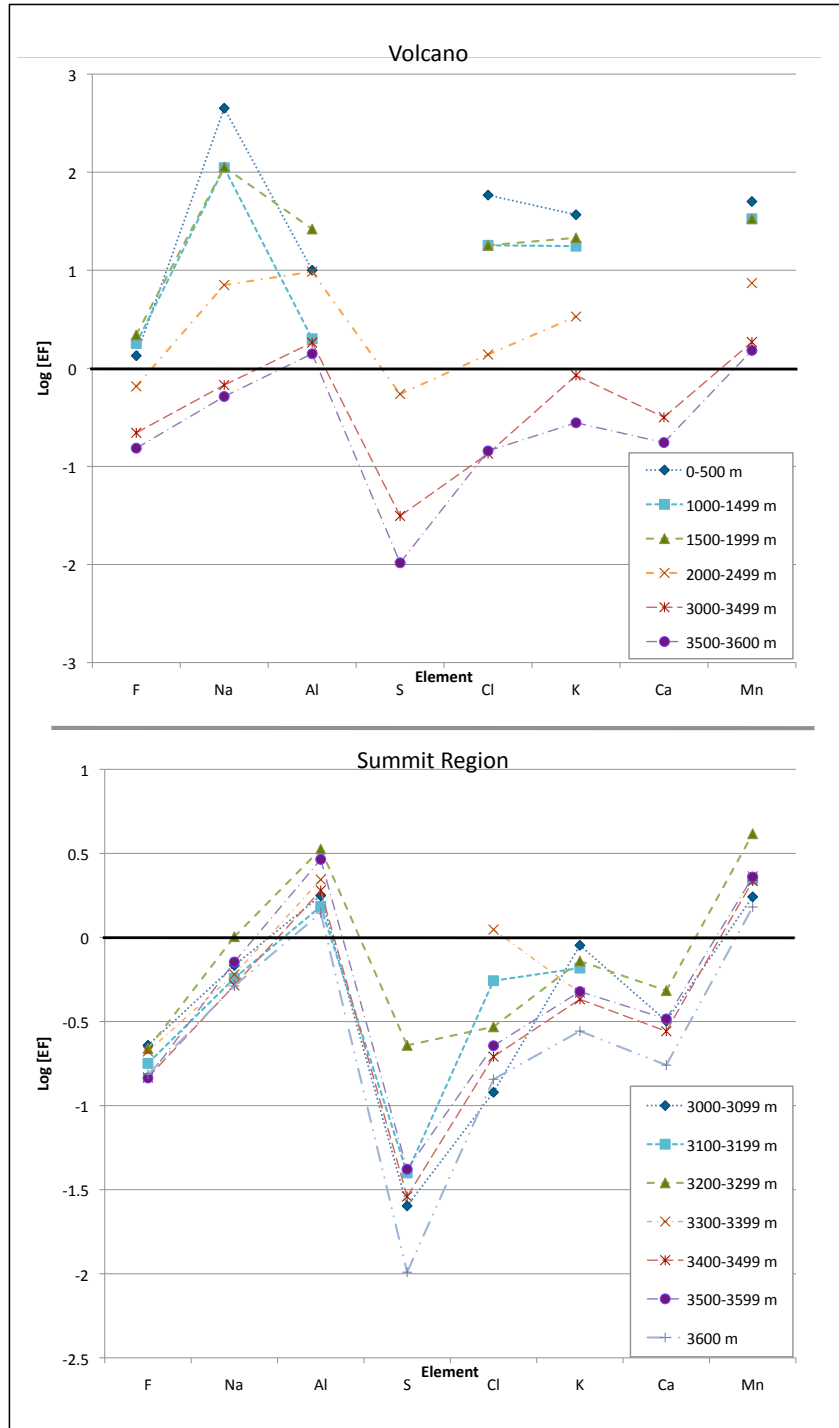


Figure 10b. Enrichment factors (EF) for Erebus snow samples Fe normalized relative to the Erebus plume. Erebus snow samples were averaged within 500-meter elevation intervals for the volcano, ranging from the coast to the summit and into 100-meter elevation intervals for the summit region. Omitted elevation ranges did not contain any snow samples. Erebus plume values are from Zreda-Gostynska (1995).

Erebus summit snow samples are all enriched relative to McMurdo Sound region snow (Figure 10a). Enrichment factors for F could not be calculated since the McMurdo Sound region snow does not contain any F, but it is assumed that their EF would be highly enriched relative to McMurdo snow and the arrow in Figure 10a reflects this assumption. The lack of plume influence on McMurdo Sound region snow is evident by the absence of F in snow samples from this region. The enrichment of Erebus snow components over McMurdo snow components represents an accumulation factor for elements not present in McMurdo Sound region snow. This holds true for all elements, with the exception of Na, Cl, and S. These three components are all reported in McMurdo Sound region snow and are from a marine source. Therefore, the presence of these components in Erebus summit snow cannot be linked strictly to the plume, but instead may also reflect a marine component present in the summit region. The near zero concentration for all McMurdo Sound region snow components indicates that it would be unlikely that concentrations in Erebus snow components are a reflection of the accumulation of McMurdo Sound snow at the summit of Erebus. This observation illustrates that the chemistry of the Erebus summit region snow is not a reflection of McMurdo Sound region snow.

The Erebus plume EF plot is the best representation of the plume component reflected in the summit snow (Figure 10b). Erebus summit snow is depleted in F, Na, S, Cl, K, and Ca relative to the Erebus plume. This depletion relative to the plume illustrates the effectiveness of the plume components depositing in the snow in the summit region. As stated earlier F, Na, S, Cl, and K are all major components in the plume. The Log[EF] of F, Na, Cl, and K are all similar to the plume and may represent direct transfer from the plume to the

snow in the summit region. The enrichment of Al and Mn relative to the plume indicates that they are likely from a source other than the plume. The source of the Al and Mn is most likely from the weathering of exposed rock surfaces by acidic plume gases in the summit region. Overall, Figures 10a and 10b illustrate the link between the plume chemistry and snow chemistry, indicating the influence of the plume on the snow chemistry and sources of elements available for salt formation on Erebus.

The chemistry of the Erebus plume is not reflected in the snow along the coast and flanks of the volcano. Both Na and Cl are major components of seawater, so their extreme enrichment in coastal and flank samples relative to both McMurdo Sound region snow and the Erebus plume is seawater influenced and not plume influenced. Snow samples from the Erebus summit region are depleted in all components relative the Erebus plume, whereas flank and coastal samples are all enriched compared to the Erebus plume. This indicates that the chemistry of the two end members (summit snow and coastal snow) have different sources, or the measurable influence of the plume is constrained to the summit region. The flank samples trend as an intermediate between the summit and coastal samples, indicating a transition between plume influenced snow chemistry and marine influenced snow chemistry. Snow chemistry components Cl, Na, and S are all found in seawater chemistry. It is safe to assume that the source for the Cl, Na, and S in the coastal region is of marine origin and the source in the summit region is of plume origin, with the possibility of a small marine influence in the summit region.

5.2 Snow Chemistry Ionic Balance

The negative ionic balances calculated for the snow chemistry indicate that a major cation was not represented in snow chemistry analyses. Hydrogen is the logical missing cation since it is present in most of the salt species identified, and is present in Erebus plume gas species. Hydrogen is represented in the plume as HCl, HF, H₂O, HNO₃, and HO₂NO₂ (Oppenheimer et al., 2010; Zreda-Gostynska et al., 1997). The missing hydrogen can be calculated by difference to achieve an ionic balance of zero (Table 10). Hydrogen is also the element responsible for the pH values measured. It is expected that the calculated hydrogen concentration in Erebus snow should be linked to the measured pH of Erebus snow and this trend is illustrated in Figure 11. Snow samples with a high concentration of H⁺ have the lowest pH values, while samples with low H⁺ concentrations have the highest pH values. It is also important to note that, in general, pH increases from the summit of Erebus down to the coast. This trend indicates that the hydrogen content in the acidic plume gases near the summit influences the pH of the snow.

Table 10. Calculated hydrogen component of snow chemistry with measured pH.

Summit Samples	H (mg/L)	pH
001--compacted surface snow	1.10	3.2
001--ice	2.44	3.1
002--compacted surface snow	0.98	3.4
003--ice	46.1	2.5
009--compacted snow	0.68	3.5
009--surface power snow	0.30	3.7
010--compacted surface snow	1.50	3.3
011--compacted surface snow	0.55	3.5
012--compacted snow	3.22	3.3
012--surface powder snow	1.19	3.9
018--compacted snow	2.48	3.1
018--surface powder snow	0.65	3.7
020--compacted snow	1.18	3.4
020--surface powder snow	0.93	3.2
021--compacted surface snow	0.42	3.5
021--ice	0.51	3.5
022--compacted snow	0.21	3.8
022--surface powder snow	0.12	3.9
025--compacted surface snow	0.14	3.9
026--compacted snow	0.18	4.0
026--surface powder snow	0.09	4.0
040--compacted snow	1.44	3.4
040--surface powder snow	0.20	3.8
043--compacted surface snow	1.11	3.4
CR--surface snow	230	1.6
Flank Samples		
027--compacted snow	0.07	5.4
027--surface powder snow	0.06	5.6
031--compacted surface snow	0.05	5.6
032--compacted surface snow	0.06	5.2
033--compacted snow	0.13	4.2
033--surface powder snow	0.21	4.0
Coastal Samples		
030--compacted surface snow	0.04	5.5
030--ice	0.05	5.7

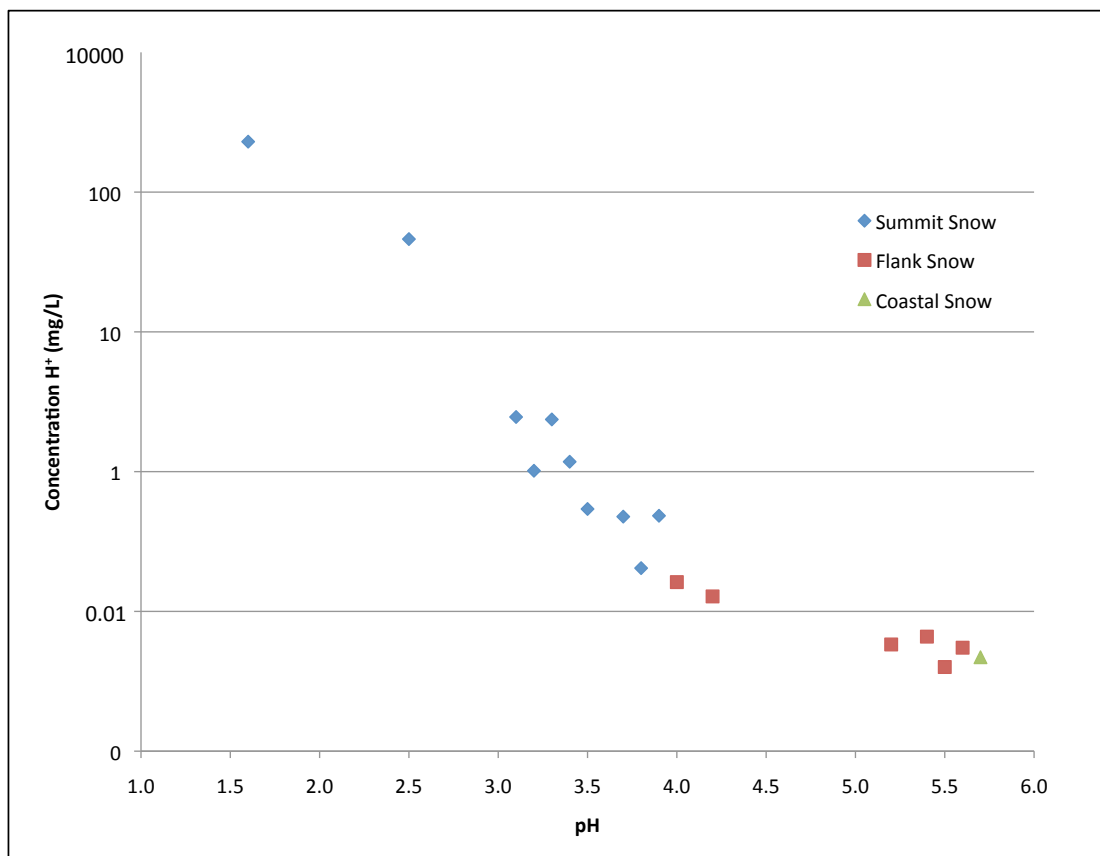


Figure 11. Measured pH for Erebus snow samples relative to the calculated concentration of H⁺.

5.3 Summit Region Mineral Identifications

Identifications of the salt compositions were complicated due to multiple phases present in each sample examined. Identifications presented are subdivided into positive, tentative, and phases never before identified on Erebus. The addition of the EMP data assisted in identifications by taking elemental compositions determined by qualitative scans, and habits observed in SEM images into account. The identifications of salts formed on Erebus give an

indication of formation processes and environmental influences. Salts on Erebus are grouped into three main categories: those formed by dry deposition of solid aerosols, evaporative salt deposits, and salts formed by weathering processes. Minerals formed by alteration processes are a fourth group of minerals associated with salt deposits on Erebus. Salts were grouped into these categories by using information on established formation conditions for the minerals identified. The combination of salt identifications, plume chemistry, rock chemistry, and snow chemistry were also used to determine salt formation process. The most commonly identified salt deposits in the summit region include halite, sylvite, alunite, mirabilite, and gypsum.

Salts formed by the dry deposition of solid aerosols include halite and potassian-halite. The formation of these minerals from aerosol particles is possible since Cl (39 wt%), Na (3 wt%), and K (3 wt%) are the dominant aerosols (Zreda-Gostynska, 1995). These particles, seen by Chuan (1983) and implied by Zreda-Gostynska's (1995) plume chemistry, can combine to form NaCl and NaKCl and are then deposited as a salt within the summit region. Overall, sulfate and halide salts (NaCl, NaF, KCl, and KF) compose 90% of measured aerosol species and are available for dry deposition within the summit region (Ilyinskaya et al., 2010). Potassian-halite formation is also possible through solid solution of halite and sylvite also in solid solution. Since these salt identifications are linked to volcanic aerosol particles, salts formed by these processes are considered to be VSDs. It is important to note that the presence of marine halite in the summit region cannot be ruled out.

Although not a salt by definition, native sulfur is also deposited as an aerosol particle within the summit region of Erebus. Chuan (1994) had reported

the identification of native sulfur in Erebus aerosol samples in addition to the presence of H₂SO₄. Sulfur is a major component on Erebus filter packs (30 wt. %) and is readily available for the formation of sulfur deposits in the summit region (Zreda-Gostynska, 1995). Oppenheimer and Kyle (2008) recorded SO₂ as the fourth most dominant gas in the Erebus plume at 1.40 mol percent.

Measurements of SO₂ emission rates indicate that rates are normally distributed with a mean of 61 ± 27 Mg d⁻¹ (Sweeney et al., 2008). Heavy sulfur particles fallout of the plume and are deposited within the summit region of Erebus.

Evaporative salt deposits found in the summit region include gypsum, sylvite, halite, and, mirabilite; all of which have been previously positively identified on Erebus. Since mirabilite is so unstable it quickly dehydrates in air and turns into thenardite. For this reason mirabilite was not actually identified, but samples identified as thenardite from the summit region would have been mirabilite under Antarctic environmental conditions. Evaporate salt deposits are common in desert settings, and Antarctica, specifically the McMurdo Sound region, has been classified as a cold desert (Keys and Williams, 1981). With the exception of sylvite, all of these salt minerals fall within the ten most abundant minerals in the McMurdo Sound Region and would most likely be present with or without the influence of the volcano. Although not a major salt deposit in the McMurdo Sound Region, sylvite is present in the summit region and can be considered a volcano influenced deposit in the summit region.

The identification of alunite (KAl₃(SO₄)₂(OH)₆) is an indication of weathering on Erebus since it typically forms as an alteration product. Alunite forms as a chemical reaction product between sulfuric acid in the plume and potassium rich feldspars through the process of alunitization. Alunite has been

positively identified in the summit region of Erebus in this study and previous studies of Erebus salt deposits. Since alunite forms from weathering processes aided by acidic plume gases, it is also considered a volcano influenced salt deposit.

Formation of clay as an alteration product on Erebus was first proposed by Zreda-Gostynska (1995) as a weathering product from the interaction of rock, mobile ions, acidic plume gases and solid aerosols. Clay minerals identified in this study include illite and kaolinite, which may both form as a result of chemical weathering of feldspars and glass. Anorthoclase feldspar crystals and volcanic glass are the main minerals subjected to chemical weathering by acidic plume gases, especially HF. Exposed rock surfaces in the summit region of Erebus contain approximately 70% glass, and are likely the primary source available for the formation of clays in the summit region. Also, bombs erupted from Erebus contain approximately 30% anorthoclase feldspar crystals and 70% glass, indicating that exposed rock surfaces are subjected to weathering by acidic plume gases (Kelly et al., 2008). Kaolinite formation on Erebus is possible by the following reaction:



Turner and Fishman (1991) noted that clay formation is possible by the initial reaction between glass and pore water. Through this reaction H^+ ions from the water are exchanged for K^+ , Na^+ , Ca^{2+} , and Mg^{2+} ions from the glass surface. All

of these are components in Erebus volcanic glass. This exchange results in an increase in pH, which is necessary for clay formation. Overall, the alteration of glass to clay occurs in conditions of low pH, and the snow in the Erebus summit region indicates the presence of the necessary low pH values below 4.0 (Leggo et al., 2001).

Kaolinite can also form directly when Al is present in solution (Krauskopf and Bird, 1995). Kaolinite typically won't form at low pH values, however if the pH is neutralized to a value above 6, kaolinite becomes more likely to precipitate out of the Al solution. The phase diagram illustrating the solubility of kaolinite under these conditions is presented in Figure 12. At low pH values kaolinite will form in solution, and as this reaction takes place, the pH of the solution will increase. Kaolinite will then precipitate out of solution when the pH reaches a high enough value, resulting in a kaolinite deposit.

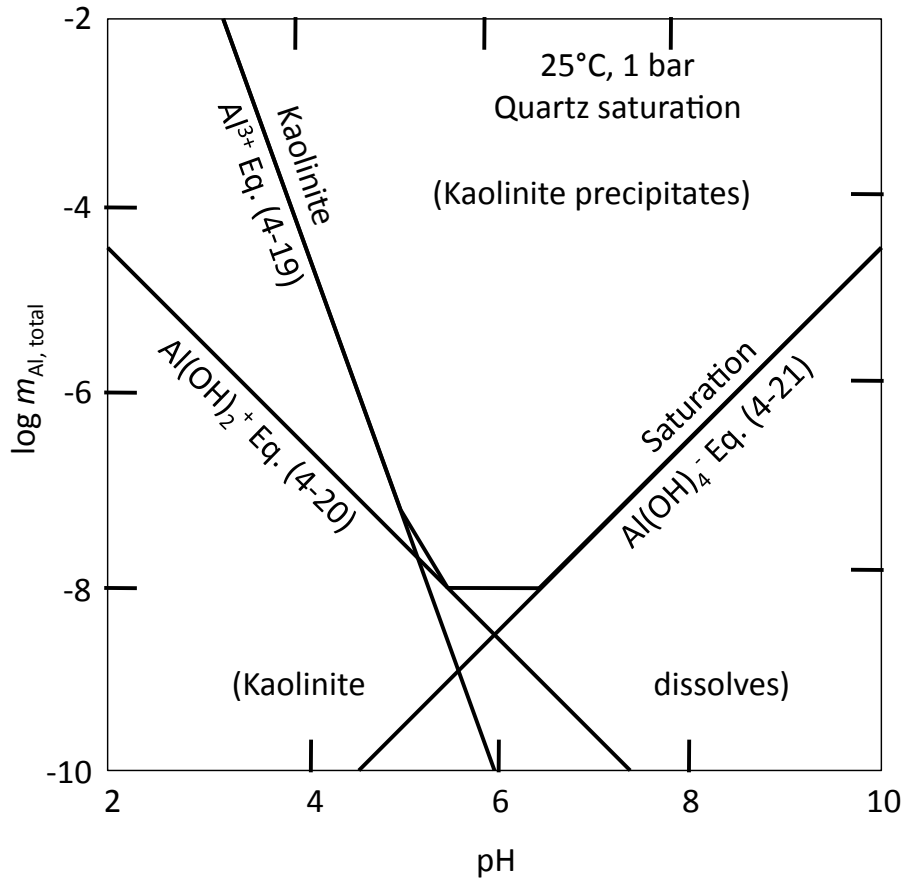


Figure 12. Phase diagram for the solubility of kaolinite (from Krauskopf and Bird, 1995).

Illite was tentatively identified by Zreda-Gostynska (1995) and is again tentatively identified in this study. The identifications of illite and kaolinite in this study can only be considered tentative due to their sporadic occurrence in salt samples. However, their presence in the summit region of Erebus must be considered due to the presence of formation conditions for both of these clay minerals. SEM image observations did show some stacked plate habits, which could be interpreted as a clay like habit. Unfortunately, it is impossible to isolate a single grain for XRD identification. Since clays form as a simple weathering

product, their presence in the summit region of Erebus is considered to be volcano influenced because the acidic plume gases aid in the weathering process.

The identification of Al-bearing minerals on Erebus is very common, but is limited to tentative identifications. Several Al-bearing minerals tentatively identified in this study have not previously been identified as a secondary mineral in the summit region of Erebus. These include katoite ($\text{Ca}_3\text{Al}_2\text{O}_6(\text{H}_2\text{O})_6$), millosevichite ($\text{Al}_2(\text{SO}_4)_3$), and sodialum ($\text{NaAl}(\text{SO}_4)_2(\text{H}_2\text{O})_{12}$). Katoite is a mineral commonly found as a chemical weathering product in the cavities of phonolitic lavas, which are present in the summit region of Erebus. The formation of Al-bearing minerals on Erebus warrants discussion of the source of Al in the summit region for salt formation. Filter pack samples measuring the aerosol composition of the Erebus plume show Al as a very minor component (1%) (Zreda-Gostynska, 1995). However, (Rosenberg, 1988) identified several aluminum-fluoride hydrates in salts he considered to be VSDs from Erebus, including aluminum trifluoride (AlF_3). Despite the previous identification of AlF_3 , no identifications of AlF_3 were made in this study. Every salt sample in this study was examined for the presence of AlF_3 , with no major peaks being present in any of the XRD spectra. Rosenberg postulated that aluminum fluoride hydrates, such as $\text{AlF}_3 \cdot 3\text{H}_2\text{O}$, are formed as incrustations in the summit region as assemblages of crystals that sublime directly from the plume. It is important to note that these identifications are tentative and AlF_3 has not been identified as a mineral. With the low concentration of Al in the Erebus plume the occurrence of AlF_3 would not be common. Instead, the main source of Al in the summit region is from Al liberated from the break-up of phonolite lavas. The average Al content of whole-rock phonolite lavas erupted over the past 17 ka on Erebus is

19.80 wt. %, matrix glass separated from tephra erupted from Erebus contain 19.74 wt. % Al_2O_3 and anorthoclase feldspar crystals in recently erupted lava bombs contain 22.81 wt. % Al_2O_3 (Kelly et al., 2008). This is a significantly higher percentage compared to the plume aerosol contribution. Therefore, most, if not all, of the Al found in Erebus salt deposits would have originated from Erebus glass or feldspars, and not the plume aerosol.

The tentative identification in previous studies of the proposed VSD mineral “Erebusite” ($\text{NaAl}_4\text{O}_4\text{Cl}_5$) is also noteworthy. This substance is only known as a man made substance and has never been observed in nature. Rose (1987), Zreda-Gostynska (1995), and Rosenberg (1988) all made tentative identifications of the new VSD “Erebusite”. In all three studies the identifications were extremely tentative and relied on the substitution of F and Fe to explain the change in sample color from white in the man made substance, to the observed bright yellow. Again, all XRD spectra were examined for the presence of “Erebusite” and no identifications were made in this study. In light of the research presented in this study the thought is that “Erebusite” is not present on Erebus, but instead is the combination of several salt mineral phases. The combination of SEM images and XRD spectra indicate that it is impossible to isolate a single salt phase for identification. Therefore, all samples analyzed represent multiple salt phases. However, the lack of any major “Erebusite” peaks in all samples examined indicates that either “Erebusite” was not sampled or it does not exist.

5.4 Salt Formation On Erebus

It has been postulated that salts found in the summit region of Erebus may form by acid-rock interactions or by direct deposition from the plume (Jones et al., 1983). Overall, Erebus salts seem to form through a complex interaction between the plume, exposed rocks, and the snow (Zreda-Gostynska, 1995). Zreda-Gostynska (1995) proposed potential pathways for salt formation on Erebus, including interactions between acidic gases, exposed rock surfaces, elements liberated from the acidic gases and rock, and clay minerals formed in the process (Figure 13). The major plume components include H₂O, CO₂, and SO₂; the major aerosol components include Cl, F, and S; and the major rock components include SiO₂, Al₂O₃, and Na₂O. These major components, and minor components listed earlier, are the available materials for salt formation on Erebus. Table 11 indicates potential sources for elements found in Erebus salts. Many of these elements are present in the snow, indicating that the snow is the major reservoir for elements found in the plume and liberated from rock fragments. In addition to the snow, wind also plays a role in plume and snow distribution in the summit region of Erebus. Since snow is the major transport mechanism for salt forming elements, the presence of certain elements in the snow indicates which salt minerals may form. More Al, F, Fe, and Mn rich salts will form in the summit region, while coastal salts will predominately be Cl, Na, and S rich. Coastal salts identified include halite, sylvite, and mirabilite; and flank salts identified include halite, mirabilite, gypsum, calcite, ralstonite, and gypsum. A much larger variety of salts are formed in the summit region due to the presence of more salt forming species.

Table 11. Possible element sources for Erebus salts. Elements with an * were also detected in snow measurements.

Salt Component	Source
Al*	Aerosol, Rock
Ca*	Rock
Cl*	Plume, Aerosol
F*	Plume, Aerosol
Fe*	Rock
K*	Aerosol, Rock
Mg	Rock
Mn*	Rock
Na*	Aerosol, Rock
P	Rock
S*	Plume, Aerosol
Si	Rock
Ti	Rock

Weathering processes also play a major role in salt formation on Erebus. Weathering on Erebus can occur as wind scour, chemical weathering, or freeze-thaw break-up of volcanic rock. Frost cracks are present in the summit region, along with small pooling of water under some rocks. In the latter case, snow on a rock surface melts as the sun heats up the rock; the melted snow then flows under the rock, where it can refreeze in a crack. An example of melting, and re-freezing snow flow can be seen in Figure 14. The expansion of the water as it freezes can expand the crack, breaking up the rock, and liberating small rock fragments for alteration into salts and clays. As mentioned earlier, the largest salt accumulations are on the underside of rocks. The low average snow pH of 3.4 in the summit region aids in the chemical weathering of rocks in the area. Chemical weathering results in the alteration of rock surfaces and the formation

of thin encrustations on all exposed rock surfaces. It has been observed that newly erupted bombs quickly alter in a period of months from a dark glassy surface to a grey to tan covered surface from the interaction with acidic gases in the plume. It was proven earlier that the plume distribution is represented in the snow chemistry. This point is reiterated by the increase in pH moving from summit to coast, with an average flank snow pH of 5.0 and an average coastal snow pH of 5.6.

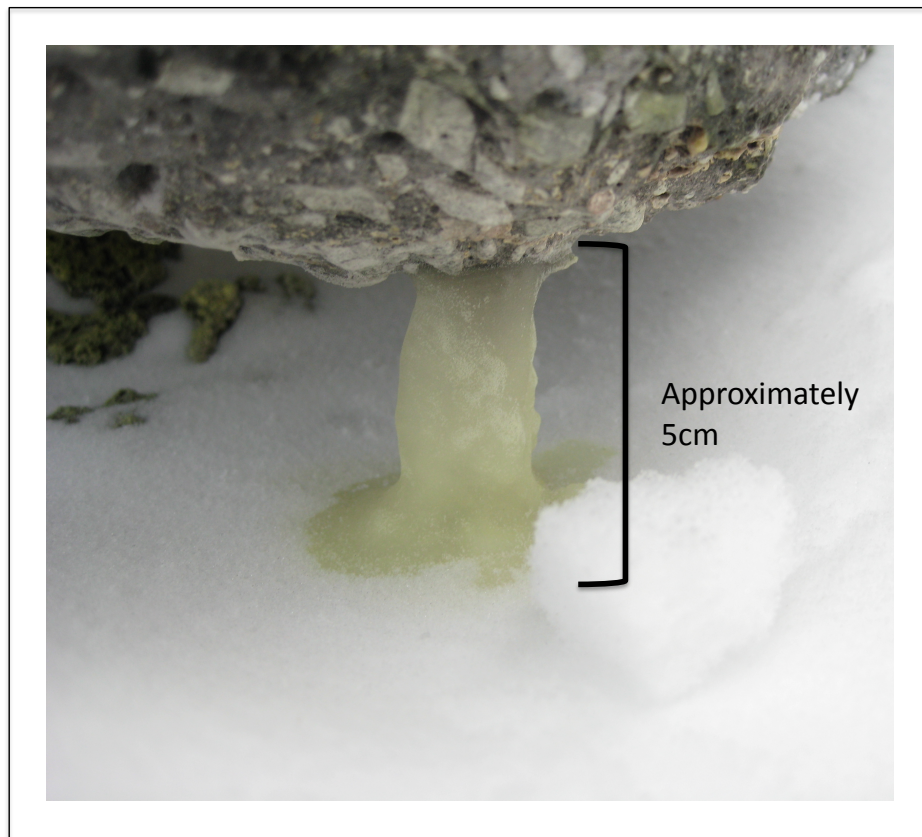


Figure 14. Flow feature found in the summit region of Erebus. Note the contrast in color from the pure white snow to the yellowed flow feature extending from the rock bottom to the snow surface. This example serves as evidence of snow melt and flow within the summit region, and the use of snow as a transport mechanism for acidic gases in the plume, aerosol particles, and elements liberated from rock fragments.

6. CONCLUSIONS

Salt deposits on Erebus are formed through the complex interaction between dry deposition of aerosols from the plume, exposed rock surfaces, acidic volcanic gases, and snow. The influence of the plume decreases outside the summit region, resulting in a decrease in variety of salt minerals identified. Salt deposits at the coast have a marine source and the plume heavily influences deposits in the summit region. Salts on the flank of Erebus have some traces of a plume influence and represent a transition between plume influenced and marine salts.

This study reaffirms the previous positive identification of several salt minerals on Erebus, and also identifies salt minerals previously never identified on Erebus. These new tentative identifications share a common chemical make-up and crystal habit as previously identified salts, but need further study to confirm their identification. Due to the complicated nature of salts on Erebus, it is impossible to isolate a single salt crystal and produce an XRD spectra with high enough counts to produce an identification. As it stands, there are several commonly occurring unidentified XRD peaks. These peaks may reflect the influence of unidentified phases. The two main previously tentatively identified mineral species (Erebusite and AlF_3) were not identified in this study. These

species may simply represent multiple phases present in one sample and does not exist as a new mineral phase.

Most salts on Erebus are not true VSDs, but instead are volcanic influenced salts. Only salt deposits formed by dry deposition of aerosols from the plume are true VSDs. Due to the climate conditions operating in Antarctica, salt deposits would form with or without the presence of an actively degassing volcano. The plume provides a wider range of elements available for salt formation in the summit region, evident by the plume enrichment factor in the snow chemistry.

Future work on Erebus salts could include more detailed chemical analysis of samples under $10\mu\text{m}$, as well as trying to quantify the rate of salt formation on Erebus. Also, the marine or volcanic salt source could be quantified by analyzing the salt samples for $\delta^{34}\text{S}$ and $^{87}\text{Sr}/^{86}\text{Sr}$ values.

APPENDIX A: DETAILED MATERIALS AND METHODS

A.1 Sample Locations

Table A-1. Salt sample locations (sample locations with an asterisk indicate a corresponding snow sample taken at the same location)

Sample Number	Latitude	Longitude	Elevation (m)	Sample Number	Latitude	Longitude	Elevation (m)
Summit Samples							
ERE-09-001*	S 77°30.577'	E 167°08.897'	3223	ERE-09-025*	S 77°32.097'	E 167°06.818'	3589
ERE-09-002*	S 77°30.434'	E 167°09.578'	3075	ERE-09-026*	S 77°32.283'	E 167°06.168'	3483
ERE-09-003*	S 77°30.434'	E 167°09.558'	3075	ERE-09-034	S 77°30.813'	E 167°13.163'	3168
ERE-09-004	S 77°30.434'	E 167°09.558'	3104	ERE-09-035	S 77°30.813'	E 167°13.163'	3168
ERE-09-005	S 77°30.434'	E 167°09.558'	3105	ERE-09-036	S 77°30.794'	E 167°13.217'	3154
ERE-09-006	S 77°30.432'	E 167°09.587'	3103	ERE-09-037	S 77°30.754'	E 167°13.382'	3123
ERE-09-007	S 77°30.425'	E 167°09.631'	3095	ERE-09-038	S 77°30.754'	E 167°13.382'	3123
ERE-09-008	S 77°30.315'	E 167°09.700'	3003	ERE-09-039	S 77°31.279'	E 167°13.609'	3304
ERE-09-009*	S 77°30.315'	E 167°09.700'	3003	ERE-09-040*	S 77°31.478'	E 167°14.241'	3249
ERE-09-010*	S 77°30.396'	E 167°09.101'	3094	ERE-09-041	S 77°31.478'	E 167°14.241'	3192
ERE-09-011*	S 77°30.421'	E 167°08.172'	3140	ERE-09-042	S 77°31.478'	E 167°14.241'	3405
ERE-09-012*	S 77°31.315'	E 167°08.910'	3499	ERE-09-043*	S 77°31.587'	E 167°12.265'	3405
ERE-09-013	S 77°31.315'	E 167°08.910'	3499	ERE-09-CR*	S 77°31.538'	E 167°09.476'	3600
ERE-09-014	S 77°31.311'	E 167°08.924'	3497	ERE-09-MC-1	S 77°31.363'	E 167°09.205'	3632
ERE-09-015	S 77°31.536'	E 167°08.925'	3606	ERE-09-MC-2	S 77°31.404'	E 167°09.094'	3662
ERE-09-016	S 77°31.307'	E 167°08.920'	3495	Flank Samples			
ERE-09-017	S 77°31.307'	E 167°08.920'	3495	ERE-09-027*	S 77°25.750'	E 167°01.487'	1613
ERE-09-018*	S 77°31.446'	E 167°08.347'	3551	ERE-09-028	S 77°25.730'	E 167°01.353'	1613
ERE-09-019	S 77°31.395'	E 167°07.121'	3482	ERE-09-029	S 77°25.731'	E 167°01.354'	1613
ERE-09-020*	S 77°31.395'	E 167°07.121'	3482	ERE-09-031*	S 77°27.179'	E 166°48.874'	1425
ERE-09-021*	S 77°31.413'	E 167°05.561'	3424	ERE-09-032*	S 77°28.609'	E 166°53.411'	1762
ERE-09-022*	S 77°31.346'	E 167°03.709'	3314	ERE-09-033*	S 77°29.879'	E 167°01.321'	2446
ERE-09-023*	S 77°31.461'	E 167°02.899'	3225	Coastal Samples			
ERE-09-024	S 77°32.070'	E 167°05.175'	3477	ERE-09-030*	S 77°27.358'	E 166°29.868'	260

A.2 Salt Sample Analysis

A.2.1 Electron Microprobe Methods

The Cameca SX-100 has three crystals that are able to analyze for the following relevant elements:

TAP (SP2): F, Na, Mg, Al, Si, P

PET (SP1): Si, P, S, Cl, K, Ca, Ti, Mn, Fe

LLIF (SP3): Ca, Ti, Mn, Fe, Ni, Cu, Zn

All qualitative scan spectra are given in Appendix B, available on DVD-ROM.

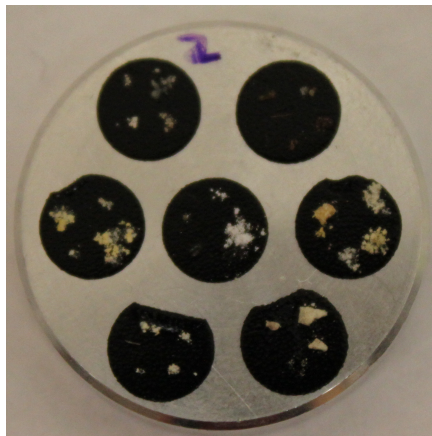


Figure A-1. Electron microprobe sample plug. Each round black carbon tape represents one bulk salt sample that has been sub-sampled. The entire sample plug measures 2.54cm in diameter.

APPENDIX B: ELECTRON MICROPROBE DATA

B.1 SEM Images (DVD-ROM)

B.2 BSE Images (DVD-ROM)

B.3 Qualitative Scans (DVD-ROM)

B.4 Normalized Qualitative Scan Data

Peak intensity (in counts) was visually estimated from the qualitative scan spectra produced for each measured sample. Intensity was recorded for every element measured per sample. Only Ka lines were estimated. Si is measured on both the PET and TAP crystal, but only estimates from the PET crystal were used. Also, both Fe and Mn are measured on both the PET and LLIF crystals, but only estimates from the LLIF crystal was used. Peak intensity was then normalized to 100 counts per sample for each sample analyzed. The results of this normalization are given in Table B-1.

Table B-1. Normalized Probe Data

Sample	Habit Scanned	Counts per Second Normalized to 100														
		Al	Ca	Cl	Cu	F	Fe	K	Mg	Mn	Na	Ni	P	S	Si	Ti
Summit Samples																
ERE-09-001																
583		7.2	0.0	5.8	0.0	0.0	66.2	12.2	0.0	0.0	0.0	0.0	0.0	8.6	0.0	0.0
585		6.9	0.0	5.8	0.0	0.0	53.2	11.6	1.7	0.0	2.9	0.0	0.0	11.6	6.4	0.0
586	fibrous	58.2	0.0	0.0	0.0	3.6	10.5	13.8	0.0	1.5	7.3	0.0	0.0	5.1	0.0	0.0
587	fibrous	73.7	0.0	4.1	0.0	4.6	0.0	0.0	0.0	16.6	0.0	0.0	0.0	0.9	0.0	0.0
588	stacked plate	69.9	0.0	0.0	0.0	2.3	1.0	0.9	18.6	0.0	2.8	0.0	0.0	4.4	0.0	0.0
589	fibrous	0.0	0.0	34.2	0.0	0.0	11.2	23.6	0.0	0.0	0.0	0.0	0.0	31.1	0.0	0.0
590	sub-angular	42.7	0.0	8.7	0.0	0.0	13.9	16.1	6.2	3.7	0.0	0.0	0.0	8.7	0.0	0.0
591	stacked plate	57.0	0.0	3.8	0.0	0.0	0.0	15.8	6.3	0.0	3.2	0.0	0.0	13.9	0.0	0.0
592		82.3	0.0	1.6	0.0	2.3	1.4	2.9	4.5	0.5	2.3	0.0	0.0	2.3	0.0	0.0
597		53.4	0.0	7.3	0.0	1.5	0.0	0.0	15.6	0.0	1.5	0.0	0.0	20.6	0.0	0.0
599		81.0	0.0	3.1	0.0	4.5	3.4	1.3	0.0	0.7	4.5	0.0	0.0	1.6	0.0	0.0
600	fibrous	83.2	0.0	1.5	0.0	2.1	4.0	1.0	4.2	1.0	2.1	0.0	0.0	1.0	0.0	0.0
601	sub-angular	79.3	0.0	2.9	0.0	3.4	1.1	1.2	2.1	0.9	6.9	0.0	0.0	2.2	0.0	0.0
602	stacked plate	78.6	0.0	2.1	0.0	1.9	7.3	0.6	0.0	1.2	7.7	0.0	0.0	0.5	0.0	0.0
603	stacked plate	69.7	0.0	2.1	0.0	3.5	9.1	3.0	2.6	1.5	4.4	0.0	0.0	3.5	0.6	0.0
604	sub-angular	67.6	0.0	11.1	0.0	2.7	3.4	0.0	6.8	1.7	6.8	0.0	0.0	0.0	0.0	0.0
605	fibrous	69.6	0.0	0.7	0.0	3.6	2.2	0.0	7.9	1.6	11.9	0.0	0.0	1.2	1.4	0.0
ERE-09-002																
606	stacked plate	77.0	0.0	2.0	0.0	4.1	3.6	1.4	4.1	1.4	4.1	0.0	0.0	2.4	0.0	0.0
607	stacked plate	45.1	3.2	4.3	0.0	0.0	6.1	5.8	3.2	0.0	0.0	0.0	0.0	0.0	32.2	0.0
608	fibrous	86.4	0.0	0.0	0.0	3.9	0.0	0.8	0.0	0.0	5.9	0.0	0.0	0.6	2.4	0.0
610	fibrous	22.9	0.0	0.0	0.0	0.0	9.2	0.0	0.0	3.8	0.0	0.0	0.0	0.0	64.1	0.0
611	sub-angular	54.1	0.0	0.0	0.0	2.4	0.0	0.0	24.2	0.0	14.5	0.0	0.0	4.8	0.0	0.0
614	stacked plate	4.1	74.4	0.0	0.0	0.0	0.0	0.0	0.0	1.2	0.0	0.0	0.0	20.3	0.0	0.0
615	stacked plate	68.1	0.0	1.5	0.0	2.1	4.1	1.1	16.4	0.8	2.5	0.0	0.0	3.5	0.0	0.0
616	fibrous	48.1	3.0	1.0	0.0	0.0	7.8	6.0	3.0	1.2	3.0	0.0	6.0	1.0	18.7	1.2
617	sub-angular	76.2	0.0	0.9	0.0	3.1	1.3	0.5	4.6	0.7	10.8	0.0	0.0	1.9	0.0	0.0
620	stacked plate	18.3	0.0	9.2	0.0	0.0	0.0	0.0	4.6	0.0	0.0	0.0	0.0	9.2	58.7	0.0
621	stacked plate	11.6	0.0	5.8	0.0	0.0	3.5	0.0	0.0	0.0	0.0	0.0	0.0	4.7	69.8	4.7
622	stacked plate	11.1	5.9	0.0	0.0	0.0	11.9	14.8	0.0	0.0	5.9	0.0	0.0	0.0	44.4	5.9
623	stacked plate	38.8	7.1	0.0	0.0	0.0	0.0	7.1	11.8	1.2	0.0	0.0	0.0	2.8	28.2	3.1
624	stacked plate	10.0	0.0	5.0	0.0	0.0	0.0	0.0	0.0	0.0	0.0	0.0	0.0	5.0	70.0	10.0
625	fibrous	75.0	0.0	10.4	0.0	0.0	0.0	0.0	0.0	0.0	7.1	0.0	0.0	7.5	0.0	0.0
ERE-09-004																
627	fibrous	81.1	0.0	0.4	0.0	2.2	1.0	0.6	0.0	0.0	14.7	0.0	0.0	0.0	0.0	0.0
628	fibrous	60.9	3.1	2.1	0.0	8.7	4.9	5.2	0.0	0.0	13.9	0.0	0.0	0.0	1.2	0.0
629	fibrous	83.0	0.0	1.9	0.0	13.8	1.2	0.0	0.0	0.0	0.0	0.0	0.0	0.0	0.0	0.0
630	fibrous	78.9	0.0	1.4	0.0	3.2	0.7	0.0	0.0	0.0	15.8	0.0	0.0	0.0	0.0	0.0
631	fibrous	49.3	0.0	10.1	0.0	0.0	0.0	40.6	0.0	0.0	0.0	0.0	0.0	0.0	0.0	0.0
632	fibrous	83.7	0.0	2.7	0.0	6.1	0.0	0.0	0.0	0.0	7.6	0.0	0.0	0.0	0.0	0.0
633	fibrous	84.5	0.0	1.4	0.0	4.7	0.0	0.0	0.0	0.0	9.4	0.0	0.0	0.0	0.0	0.0
634	fibrous	87.9	0.0	2.0	0.0	3.8	0.0	0.0	0.0	0.0	6.3	0.0	0.0	0.0	0.0	0.0
635	fibrous	64.1	0.0	5.7	0.0	6.7	4.7	3.3	0.0	1.1	13.4	0.0	0.0	0.0	1.1	0.0
636	fibrous	75.9	0.0	5.4	0.0	2.7	0.0	7.1	0.0	0.0	8.9	0.0	0.0	0.0	0.0	0.0
ERE-09-005																
637	stacked plate	55.7	2.7	0.0	0.0	2.7	2.2	23.0	2.7	0.0	0.0	0.0	0.0	2.2	8.7	0.0
639	stacked plate	42.1	3.0	0.0	0.0	2.4	1.6	27.7	3.0	0.0	9.0	0.0	0.0	3.0	8.1	0.0
640		36.6	4.9	0.0	0.0	7.3	8.5	17.1	6.1	0.0	9.8	0.0	0.0	3.7	6.1	0.0
641	stacked plate	18.0	0.0	0.0	0.0	0.0	0.0	1.4	0.0	0.0	72.0	0.0	0.0	8.6	0.0	0.0
642	stacked plate	22.2	0.0	0.0	0.0	0.0	0.0	4.4	0.0	0.0	55.6	0.0	0.0	15.6	2.2	0.0
643	stacked plate	8.1	0.0	0.0	0.0	0.0	0.0	0.0	0.0	0.0	72.6	0.0	0.0	19.4	0.0	0.0
644	stacked plate	24.4	0.0	0.0	0.0	0.0	0.0	0.0	0.0	0.0	18.7	0.0	0.0	56.9	0.0	0.0
645		0.0	0.0	11.8	0.0	0.0	0.0	0.0	0.0	0.0	0.0	0.0	0.0	0.0	88.2	0.0
646	needles	13.8	0.0	0.0	0.0	0.0	0.0	0.0	0.0	0.0	60.6	0.0	0.0	25.7	0.0	0.0
647	sub-angular	15.4	0.0	0.0	0.0	0.0	0.0	0.0	0.0	0.0	53.8	0.0	0.0	30.8	0.0	0.0
648	sub-angular	32.5	0.0	0.0	0.0	0.0	20.3	16.3	0.0	0.0	8.1	0.0	0.0	8.1	11.4	3.3
649	sub-angular	34.1	0.0	0.0	0.0	2.7	17.1	6.8	3.4	1.4	20.5	0.0	0.0	7.8	3.4	2.7
650		7.7	0.0	0.0	0.0	0.0	0.0	0.0	0.0	0.0	67.3	0.0	0.0	25.0	0.0	0.0

Table B-1. Continued

Sample	Habit Scanned	Counts per Second Normalized to 100														
		Al	Ca	Cl	Cu	F	Fe	K	Mg	Mn	Na	Ni	P	S	Si	Ti
ERE-09-009																
651	stacked plate	41.2	0.0	2.1	0.0	2.6	1.4	2.6	30.9	0.8	5.1	0.0	0.0	13.4	0.0	0.0
652	fibrous	84.9	0.0	2.0	0.0	0.0	5.7	3.6	0.0	0.0	0.0	0.0	0.0	3.7	0.0	0.0
653	fibrous	79.0	0.0	1.3	0.0	5.1	1.6	0.5	6.1	0.0	5.1	0.0	0.0	1.5	0.0	0.0
654	stacked plate	76.8	0.0	3.5	0.0	8.8	0.0	0.0	0.0	0.0	11.0	0.0	0.0	0.0	0.0	0.0
655	sub-angular	45.6	0.0	0.8	0.0	3.0	0.8	1.9	34.2	0.8	3.0	0.0	0.0	9.9	0.0	0.0
656	sub-angular	43.5	0.0	0.0	0.0	2.2	0.0	2.2	30.4	0.0	4.3	0.0	0.0	17.4	0.0	0.0
657	fibrous	65.6	0.0	1.6	0.0	4.1	9.8	0.0	8.2	1.6	7.4	0.0	0.0	1.6	0.0	0.0
658	fibrous	81.6	0.0	2.4	0.0	2.0	5.3	0.0	0.0	0.8	4.1	0.0	0.0	2.0	0.0	1.6
659	fibrous	45.3	0.0	1.8	0.0	2.0	1.5	2.0	30.2	0.5	2.5	0.0	0.0	14.1	0.0	0.0
660	fibrous	71.4	0.0	1.4	0.0	2.4	2.4	1.2	13.9	0.8	4.0	0.0	0.0	2.6	0.0	0.0
ERE-09-012																
525		17.9	0.0	25.1	0.0	0.0	3.2	0.0	0.0	0.0	53.8	0.0	0.0	0.0	0.0	0.0
526	fibrous	59.4	0.0	2.7	0.0	3.7	7.8	1.4	9.1	0.9	13.7	0.0	0.0	1.4	0.0	0.0
527		46.8	0.0	5.0	0.0	3.6	17.3	6.5	3.6	0.0	11.5	0.0	1.1	2.2	0.0	2.4
528	sub-rounded	22.6	0.0	3.2	0.0	1.6	40.4	11.3	5.2	0.0	7.3	0.0	1.2	5.6	0.0	1.6
529	fibrous	71.6	0.0	3.3	0.0	3.1	4.6	1.4	5.1	0.9	9.2	0.0	0.0	0.8	0.0	0.0
530	fibrous	76.5	0.0	1.6	0.0	3.3	9.3	0.0	5.5	1.1	2.7	0.0	0.0	0.0	0.0	0.0
533	fibrous	63.4	0.0	1.5	0.0	3.9	8.8	1.0	9.8	1.0	9.8	0.0	0.0	1.0	0.0	0.0
534	stacked plate	25.2	0.0	5.0	0.0	2.9	38.7	11.8	3.4	0.0	5.0	0.0	1.3	5.0	0.0	1.7
535	sub-rounded	40.7	0.0	3.7	0.0	3.1	24.7	6.2	6.2	0.0	9.9	0.0	1.2	3.1	0.0	1.2
536	needles	27.9	0.0	12.7	0.0	4.0	5.3	3.2	0.0	0.8	44.6	0.0	0.0	1.6	0.0	0.0
537	needles	30.4	0.0	20.3	0.0	2.0	1.2	0.0	3.5	0.0	42.6	0.0	0.0	0.0	0.0	0.0
538	stacked plate	75.8	0.0	5.5	0.0	1.9	0.7	0.0	4.7	0.0	11.4	0.0	0.0	0.0	0.0	0.0
539	fibrous	64.5	0.0	2.5	0.0	3.6	1.9	0.0	7.2	0.0	20.1	0.0	0.0	0.4	0.0	0.0
540	fibrous	77.3	0.0	9.9	0.0	0.0	3.0	0.0	0.0	1.3	8.6	0.0	0.0	0.0	0.0	0.0
541	sub-rounded	5.4	0.0	4.0	0.0	0.0	51.5	15.8	0.0	0.0	1.0	0.0	1.0	11.9	5.9	3.5
542	fibrous	16.8	0.0	54.6	0.0	0.0	21.8	0.0	0.0	0.0	6.7	0.0	0.0	0.0	0.0	0.0
543	stacked plate	26.3	0.0	6.6	0.0	0.0	4.7	0.0	0.0	0.0	0.0	0.0	0.0	0.0	59.1	3.3
544	stacked plate	24.0	0.0	3.4	0.0	3.0	35.9	10.3	3.4	0.0	3.8	0.0	0.9	9.4	3.4	2.6
545	stacked plate	26.7	0.0	3.0	0.0	3.0	44.8	7.3	3.0	0.0	7.3	0.0	0.9	0.7	0.9	2.3
546	fibrous	71.2	0.0	2.0	0.0	3.6	0.7	0.6	7.1	0.6	14.2	0.0	0.0	0.0	0.0	0.0
547	sub-rounded	63.5	0.0	4.5	0.0	3.1	8.7	1.9	6.8	0.9	9.3	0.0	0.0	1.1	0.0	0.0
550	fibrous	45.5	0.0	6.1	0.0	0.0	23.3	6.1	5.1	0.0	5.9	0.0	0.0	5.1	1.0	2.0
551	fibrous	59.7	0.0	2.0	0.0	3.3	13.9	2.8	6.6	1.3	6.6	0.0	0.3	1.7	0.3	1.3
552	stacked plate	41.8	3.5	2.4	0.0	0.0	3.5	5.6	4.2	0.0	11.1	0.0	0.0	0.0	27.9	0.0
553	stacked plate	19.0	0.0	5.4	0.0	0.0	49.0	6.8	0.0	0.0	0.0	0.0	0.7	4.1	9.5	5.4
554	stacked plate	45.4	3.6	2.4	0.0	0.0	7.3	7.3	5.4	0.0	8.2	0.0	0.0	0.0	18.2	2.3
555	fibrous	65.4	0.0	5.9	0.0	3.9	3.9	1.0	6.5	0.0	9.2	0.0	0.0	0.9	2.0	1.2
556	stacked plate	73.0	0.0	3.8	0.0	5.8	3.8	0.0	4.9	0.5	8.3	0.0	0.0	0.0	0.0	0.0
557	stacked plate	70.0	0.0	3.5	0.0	4.4	2.0	0.9	6.1	0.0	13.1	0.0	0.0	0.0	0.0	0.0
558	stacked plate	75.2	0.0	1.0	0.0	3.4	5.1	0.7	6.8	0.7	6.8	0.0	0.0	0.2	0.0	0.0
ERE-09-014																
661	fibrous	83.2	0.0	1.7	0.0	3.8	1.1	0.4	1.9	0.4	7.6	0.0	0.0	0.0	0.0	0.0
662	fibrous	84.7	0.0	0.6	0.0	4.8	1.2	1.0	3.0	0.0	4.8	0.0	0.0	0.0	0.0	0.0
663	fibrous	86.3	0.0	3.5	0.0	2.9	1.4	0.0	0.0	0.2	5.8	0.0	0.0	0.0	0.0	0.0
665	fibrous	86.8	0.3	1.6	0.0	3.9	1.2	0.4	2.0	0.2	3.6	0.0	0.0	0.0	0.0	0.0
666	sub-rounded	64.7	1.7	1.4	0.0	4.6	1.5	2.8	10.2	0.0	8.3	0.0	0.7	0.7	0.5	3.0
667	fibrous	78.2	0.0	1.0	0.0	7.4	2.2	0.0	3.0	0.7	7.4	0.0	0.0	0.0	0.0	0.0
668	sub-angular	6.7	0.0	6.7	0.0	0.0	8.7	8.1	0.0	0.0	0.0	0.0	0.0	0.0	67.1	2.7
669	stacked plate	44.1	2.2	2.2	0.0	3.5	5.3	5.3	0.0	1.2	5.3	0.0	0.0	0.0	30.9	0.0
670	fibrous	73.9	0.0	5.1	0.0	8.5	1.1	0.0	0.0	0.0	11.4	0.0	0.0	0.0	0.0	0.0
671	fibrous	90.2	0.0	1.4	0.0	2.3	1.0	0.7	0.0	0.0	4.5	0.0	0.0	0.0	0.0	0.0
672	fibrous	71.7	0.5	0.7	0.0	4.5	2.7	0.5	9.0	0.7	9.0	0.0	0.0	0.7	0.0	0.0
ERE-09-015																
673	stacked plate	27.6	13.2	0.0	0.0	6.0	3.5	15.0	6.0	0.0	16.8	0.0	0.0	1.8	10.2	0.0
674	stacked plate	51.9	2.6	0.6	0.0	5.2	9.2	0.9	5.8	1.2	13.8	0.0	0.0	1.3	4.6	2.9

Table B-1. Continued

Sample	Habit Scanned	Counts per Second Normalized to 100														
		Al	Ca	Cl	Cu	F	Fe	K	Mg	Mn	Na	Ni	P	S	Si	Ti
ERE-09-016																
559	stacked plate	42.3	0.0	7.5	0.0	8.1	9.2	3.7	5.0	2.0	18.7	0.0	0.0	2.5	1.0	0.0
560	fibrous	77.6	0.0	1.3	0.0	2.8	4.3	1.0	5.5	0.8	5.5	0.0	0.2	0.7	0.1	0.0
562	fibrous	13.6	63.3	0.0	0.0	1.8	0.0	0.0	0.0	0.0	3.2	0.0	0.0	18.1	0.0	0.0
563	stacked plate	5.3	73.7	0.0	0.0	0.0	0.0	0.0	0.0	0.0	0.0	0.0	0.0	21.1	0.0	0.0
564	fibrous	46.9	0.0	9.1	0.0	7.8	4.4	4.2	5.2	4.7	15.6	0.0	0.0	1.3	0.8	0.0
565	sub-angular	51.7	0.0	1.6	0.0	3.7	7.2	1.5	4.4	1.8	8.9	0.0	0.0	1.3	17.7	0.0
566	fibrous	26.4	1.1	2.2	0.0	20.8	3.2	0.8	13.9	2.4	27.8	0.0	0.0	0.8	0.6	0.0
567	stacked plate	12.5	0.0	8.3	0.0	0.0	4.2	4.2	4.2	2.1	8.3	0.0	0.0	0.0	52.1	4.2
568	cauliflower	53.8	0.0	1.5	0.0	3.9	7.3	1.0	5.9	1.5	5.9	0.0	0.0	0.8	16.6	2.0
569	fibrous	54.2	0.0	3.3	0.0	8.1	6.0	2.8	8.1	1.5	10.8	0.0	0.0	2.7	0.7	1.7
570	flat hexagonal	1.9	72.8	0.0	0.0	1.0	0.0	0.0	0.0	0.0	0.0	0.0	0.0	24.3	0.0	0.0
571	flat hexagonal	3.1	72.7	0.0	0.0	1.9	0.9	0.0	0.0	0.0	2.3	0.0	0.0	19.1	0.0	0.0
572	fibrous	61.1	22.2	1.1	0.0	2.8	0.0	0.0	3.3	0.0	5.6	0.0	0.0	2.8	0.0	1.1
573	fibrous	43.5	0.0	9.6	0.0	8.7	0.0	0.0	6.5	3.3	23.9	0.0	0.0	1.1	3.5	0.0
574	fibrous	65.9	0.0	3.9	0.0	3.9	0.0	0.0	3.9	2.3	19.4	0.0	0.0	0.0	0.8	0.0
ERE-09-018																
675	stacked plate	53.9	0.0	7.8	0.0	0.0	15.7	4.9	0.0	4.9	9.8	0.0	0.0	2.9	0.0	0.0
676	sub-angular	76.4	0.0	3.2	0.0	3.2	3.2	1.3	2.5	0.7	7.0	0.0	0.0	2.5	0.0	0.0
677		69.6	0.0	0.8	0.0	8.0	4.4	0.0	7.0	0.4	9.9	0.0	0.0	0.0	0.0	0.0
678	stacked plate	61.3	0.0	3.3	0.0	4.7	0.0	0.0	0.0	0.0	7.1	0.0	0.0	4.7	18.9	0.0
679	fibrous	81.6	0.0	1.2	0.0	3.3	3.8	0.8	2.7	0.3	5.4	0.0	0.0	0.9	0.0	0.0
680	stacked plate	78.7	0.0	1.7	0.0	3.4	3.9	1.4	3.4	0.0	6.7	0.0	0.0	0.8	0.0	0.0
681	stacked plate	86.6	0.7	0.0	0.0	0.0	1.2	0.0	3.7	0.5	6.2	0.0	0.0	0.7	0.3	0.0
682	fibrous	57.5	0.0	3.7	0.0	2.6	3.1	2.6	5.2	0.5	20.9	0.0	0.0	3.4	0.4	0.0
683	cubic	74.4	0.0	1.8	0.0	3.1	2.8	1.4	3.1	0.3	10.5	0.0	0.0	2.1	0.4	0.0
684	cubic	73.2	0.0	2.1	0.0	4.6	2.7	1.7	4.6	0.0	9.1	0.0	0.0	1.6	0.4	0.0
685	stacked plate	74.5	1.0	1.0	0.0	2.6	3.9	2.2	6.5	1.9	2.6	0.0	0.0	3.9	0.0	0.0
686	fibrous	79.8	0.0	0.9	0.0	3.8	2.1	1.1	3.0	0.6	7.6	0.0	0.0	1.0	0.0	0.0
687	fibrous	75.0	0.0	1.7	0.0	2.9	2.6	1.4	4.6	0.5	10.4	0.0	0.0	0.9	0.0	0.0
688	fibrous	80.8	0.0	1.3	0.0	2.0	1.5	1.0	3.2	0.3	8.9	0.0	0.0	0.7	0.2	0.0
689	sub-angular	77.1	0.0	1.3	0.0	4.6	2.0	0.7	4.1	0.4	9.1	0.0	0.0	0.8	0.0	0.0
690	stacked plate	61.0	0.0	1.9	0.0	4.1	15.3	3.6	5.1	1.0	6.1	0.0	0.0	1.9	0.0	0.0
691	stacked plate	51.5	1.5	1.4	0.0	5.1	6.0	1.7	5.1	0.0	13.7	0.0	0.0	1.9	12.0	0.0
ERE-09-019																
692	stacked plate	12.3	0.0	14.8	0.0	0.0	39.4	14.8	0.0	4.9	3.9	0.0	0.0	9.9	0.0	0.0
693	fibrous	75.9	0.0	3.2	0.0	3.8	3.5	2.5	2.5	0.0	6.3	0.0	0.0	2.2	0.0	0.0
694	stacked plate	0.0	0.0	44.9	0.0	0.0	0.0	0.0	0.0	0.0	55.1	0.0	0.0	0.0	0.0	0.0
695	flat hexagonal	0.0	0.0	34.3	0.0	0.0	0.0	0.0	0.0	0.0	65.7	0.0	0.0	0.0	0.0	0.0
696	fibrous	71.9	1.4	3.7	0.0	3.6	1.4	2.5	5.8	2.9	3.6	0.0	0.0	3.2	0.0	0.0
697	stacked plate	0.0	0.0	9.7	0.0	0.0	0.0	0.0	0.0	0.0	90.3	0.0	0.0	0.0	0.0	0.0
698	fibrous	76.9	0.0	7.7	0.0	0.0	0.0	0.0	0.0	0.0	15.4	0.0	0.0	0.0	0.0	0.0
699	sub-rounded	13.6	0.0	8.5	0.0	0.0	0.0	1.5	0.0	0.0	76.4	0.0	0.0	0.0	0.0	0.0
700	cubic	0.0	0.0	18.5	0.0	0.0	0.0	0.0	0.0	0.0	81.5	0.0	0.0	0.0	0.0	0.0
701	sub-rounded	0.0	0.0	29.6	0.0	0.0	0.0	0.0	0.0	0.0	70.4	0.0	0.0	0.0	0.0	0.0
702	stacked plate	2.5	0.0	32.5	0.0	0.0	0.0	0.0	0.0	0.0	65.0	0.0	0.0	0.0	0.0	0.0
ERE-09-020																
703	sub-rounded	34.2	0.0	0.0	0.0	2.6	0.0	1.7	1.7	0.0	34.2	0.0	0.0	25.6	0.0	0.0
704	sub-rounded	35.9	0.0	0.0	0.0	0.0	0.0	3.8	0.0	0.0	44.9	0.0	0.0	15.4	0.0	0.0
705	sub-rounded	32.2	0.0	2.7	0.0	2.7	0.0	2.0	0.0	0.0	41.6	0.0	0.0	18.8	0.0	0.0
706	sub-rounded	34.1	0.0	3.6	0.0	0.0	0.0	5.4	0.0	0.0	33.7	0.0	0.0	21.7	1.4	0.0
707	sub-angular	45.1	1.0	0.0	0.0	0.0	1.8	0.0	5.0	2.2	34.1	0.0	0.0	10.0	0.8	0.0
708	sub-angular	23.4	0.0	0.0	0.0	0.0	0.0	6.4	0.0	0.0	35.1	0.0	0.0	35.1	0.0	0.0
709	sub-rounded	47.2	1.4	1.5	0.0	0.0	2.6	1.4	3.8	1.5	28.3	0.0	0.0	10.8	1.4	0.0
710	sub-rounded	23.9	0.0	19.3	0.0	0.0	5.1	0.0	0.0	3.6	17.8	0.0	0.0	30.5	0.0	0.0
711	stacked plate	52.6	1.9	0.0	0.0	0.0	3.4	3.8	3.0	0.0	7.5	0.0	0.0	0.0	26.3	1.5
712	sub-angular	54.5	2.7	0.0	0.0	0.0	3.8	6.8	2.7	0.0	14.4	0.0	0.0	15.0	0.0	0.0

Table B-1. Continued

Sample	Habit Scanned	Counts per Second Normalized to 100														
		Al	Ca	Cl	Cu	F	Fe	K	Mg	Mn	Na	Ni	P	S	Si	Ti
ERE-09-034																
800	fibrous	54.9	0.0	13.7	0.0	7.8	0.0	0.0	0.0	0.0	23.5	0.0	0.0	0.0	0.0	0.0
801	stacked plate	55.4	0.0	0.0	0.0	0.0	0.0	0.0	0.0	0.0	30.8	0.0	0.0	13.8	0.0	0.0
803	stacked plate	44.0	0.0	19.0	0.0	0.0	0.0	0.0	0.0	0.0	17.9	0.0	0.0	19.0	0.0	0.0
804	fibrous	50.9	0.0	12.7	0.0	12.7	0.0	0.0	0.0	0.0	20.0	0.0	0.0	3.6	0.0	0.0
885	fibrous	60.8	0.0	3.5	0.0	8.7	0.0	0.0	0.0	0.0	26.1	0.0	0.0	1.0	0.0	0.0
805	fibrous	56.3	0.0	6.3	0.0	12.7	0.0	0.0	0.0	0.0	24.6	0.0	0.0	0.0	0.0	0.0
806	stacked plate	66.7	0.0	0.0	0.0	0.0	0.0	15.6	0.0	0.0	0.0	0.0	0.0	17.8	0.0	0.0
886	stacked plate	61.4	0.0	0.0	0.0	0.0	0.0	19.3	0.0	0.0	0.0	0.0	0.0	19.3	0.0	0.0
807	fibrous	52.4	0.0	10.1	0.0	11.5	0.0	0.0	0.0	0.0	25.9	0.0	0.0	0.0	0.0	0.0
887	fibrous	71.7	0.0	1.1	0.0	7.6	0.0	0.0	0.0	0.0	19.1	0.0	0.0	0.5	0.0	0.0
ERE-09-036																
810	stacked plate	25.3	0.0	0.0	0.0	6.3	13.9	10.1	0.0	0.0	0.0	0.0	0.0	6.3	38.0	0.0
811	sub-angular	21.3	0.0	0.0	0.0	0.0	25.5	7.1	0.0	2.8	0.0	0.0	0.0	2.1	35.5	5.7
812	stacked plate	37.5	5.0	0.0	0.0	0.0	10.0	12.5	0.0	0.0	0.0	0.0	0.0	0.0	31.3	3.8
813	sub-rounded	40.0	0.0	0.0	0.0	0.0	18.0	8.0	0.0	0.0	0.0	0.0	0.0	0.0	30.0	4.0
814	sub-angular	38.3	2.9	0.0	0.0	4.8	13.4	9.6	0.0	0.0	0.0	0.0	0.0	0.0	28.7	2.4
815	sub-angular	63.1	3.8	0.0	0.0	4.0	4.6	3.2	8.6	0.0	10.3	0.0	0.0	1.1	1.3	0.0
816	stacked plate	22.2	3.7	0.0	0.0	0.0	22.7	7.4	0.0	0.0	0.0	0.0	0.0	2.7	38.4	3.0
817	sub-angular	5.9	0.0	0.0	0.0	0.0	0.0	0.0	0.0	0.0	72.9	0.0	0.0	21.2	0.0	0.0
ERE-09-037																
819	stacked plate	78.3	1.5	0.0	0.0	2.6	2.4	1.2	2.6	0.4	9.6	0.0	0.0	0.8	0.6	0.0
820	sub-angular	47.9	15.5	1.3	0.0	2.6	0.0	2.8	10.3	2.1	2.6	0.0	0.0	12.9	1.9	0.0
821	sub-angular	76.6	0.0	1.3	0.0	4.3	0.0	0.4	0.0	0.0	17.0	0.0	0.0	0.0	0.4	0.0
822	sub-angular	14.3	30.6	0.0	0.0	0.0	8.2	0.0	0.0	32.7	0.0	0.0	0.0	10.2	4.1	0.0
823	cauliflower	61.8	0.0	7.2	0.0	9.7	0.0	1.0	0.0	0.0	19.3	0.0	0.0	0.5	0.5	0.0
824	sub-angular	14.3	21.4	7.1	0.0	0.0	21.4	0.0	0.0	26.2	0.0	0.0	0.0	4.8	4.8	0.0
ERE-09-038																
825	fibrous	71.5	0.0	2.2	0.0	3.2	0.0	2.3	6.5	0.0	13.0	0.0	0.0	1.3	0.0	0.0
826	stacked plate	46.3	0.0	4.0	0.0	0.0	0.0	10.8	30.4	1.9	6.6	0.0	0.0	0.0	0.0	0.0
827	sub-rounded	60.7	0.0	0.9	0.0	3.0	0.0	2.0	7.6	1.5	16.7	0.0	0.0	7.6	0.0	0.0
828	fibrous	74.9	0.0	2.4	0.0	4.4	0.0	0.4	4.4	0.0	13.2	0.0	0.0	0.0	0.2	0.0
829	stacked plate	49.5	0.0	0.0	0.0	0.0	5.9	5.0	2.0	0.0	0.0	0.0	0.0	0.0	35.6	2.0
830	fibrous	69.2	0.0	2.9	0.0	5.3	0.0	1.9	10.6	0.0	8.0	0.0	0.0	1.6	0.4	0.0
831	sub-angular	89.6	0.0	0.0	0.0	1.8	0.0	0.0	0.0	0.0	4.5	0.0	0.0	4.1	0.0	0.0
832	stacked plate	0.0	0.0	24.4	0.0	0.0	0.0	0.0	0.0	0.0	75.6	0.0	0.0	0.0	0.0	0.0
833	sub-angular	64.6	8.2	3.1	0.0	5.9	0.0	4.7	11.8	0.0	0.0	0.0	0.0	1.8	0.0	0.0
834	fibrous	70.5	0.0	0.6	0.0	5.9	0.0	0.9	4.7	0.0	16.5	0.0	0.0	0.8	0.0	0.0
ERE-09-043																
835	sub-angular	75.0	0.8	0.9	0.0	5.0	0.0	0.8	10.0	0.0	5.0	0.0	0.0	0.8	1.8	0.0
836	fibrous	70.2	0.0	0.0	0.0	8.8	0.0	0.0	4.7	0.0	16.4	0.0	0.0	0.0	0.0	0.0
837	fibrous	75.5	0.0	2.7	0.0	4.4	0.0	1.0	0.0	0.0	16.4	0.0	0.0	0.0	0.0	0.0
838	fibrous	85.0	0.0	2.8	0.0	3.1	0.0	0.0	3.9	1.3	3.9	0.0	0.0	0.0	0.0	0.0
840	fibrous	78.6	0.0	5.0	0.0	3.3	0.0	0.0	0.0	0.0	13.1	0.0	0.0	0.0	0.0	0.0
841	sub-angular	80.6	0.0	0.7	0.0	3.5	0.5	0.0	4.4	1.0	8.9	0.0	0.0	0.4	0.0	0.0
842	fibrous	61.3	0.0	5.1	0.0	12.3	0.0	1.1	0.0	0.0	20.2	0.0	0.0	0.0	0.0	0.0
843	fibrous	74.0	0.0	0.3	0.0	6.3	0.7	0.0	0.0	1.1	17.6	0.0	0.0	0.0	0.0	0.0
844	fibrous	59.4	0.0	5.1	0.0	10.1	0.0	0.0	0.0	0.0	25.4	0.0	0.0	0.0	0.0	0.0
ERE-09-CR																
846	sub-rounded	90.7	6.8	0.0	0.0	0.0	0.0	0.0	0.0	0.0	0.0	0.0	0.0	0.0	2.4	0.0
847	stacked plate	1.6	12.6	6.3	40.0	0.0	7.5	1.9	2.5	0.0	0.0	23.9	1.9	0.0	1.8	0.0
849	stacked plate	0.0	0.0	1.2	11.4	0.0	1.9	1.0	0.0	0.0	0.0	83.8	0.0	0.0	0.6	0.0
ERE-09-MC-1																
851	stacked plate	68.7	1.4	0.0	0.0	4.1	0.0	3.4	8.2	0.0	2.7	0.0	0.0	1.8	9.6	0.0
852	sub-angular	54.1	33.8	0.0	0.0	1.4	0.0	0.0	2.7	0.0	0.0	0.0	0.0	6.8	1.4	0.0
853	sub-angular	71.4	0.0	0.0	0.0	2.4	0.0	2.4	0.0	0.0	0.0	0.0	0.0	23.8	0.0	0.0
854	sub-angular	60.9	9.9	0.0	0.0	2.8	0.0	0.0	0.0	0.0	0.0	0.0	0.0	25.5	0.8	0.0
855	sub-angular	66.7	0.0	0.0	0.0	0.0	0.0	0.0	0.0	0.0	0.0	0.0	0.0	33.3	0.0	0.0
856	stacked plate	90.8	1.0	0.0	0.0	0.6	0.0	0.0	5.1	0.0	0.6	0.0	0.0	0.0	2.0	0.0
857	sub-rounded	52.9	3.9	0.0	0.0	2.0	0.0	29.4	2.9	0.0	2.9	0.0	0.0	3.9	2.0	0.0
858	flat hexagonal	0.0	0.0	0.0	0.0	0.0	0.0	100.0	0.0	0.0	0.0	0.0	0.0	0.0	0.0	0.0
859	sub-rounded	74.1	4.6	0.0	0.0	5.6	0.0	1.9	4.2	0.0	0.0	0.0	0.0	9.3	0.5	0.0
860	sub-angular	52.1	18.3	0.0	0.0	3.0	0.0	2.4	3.0	0.0	0.0	0.0	0.0	11.8	9.5	0.0
861	sub-angular	58.5	0.0	0.0	0.0	4.7	0.0	4.7	5.8	0.0	4.7	0.0	0.0	2.9	18.7	0.0

Table B-1. Continued

Sample	Habit Scanned	Counts per Second Normalized to 100														
		Al	Ca	Cl	Cu	F	Fe	K	Mg	Mn	Na	Ni	P	S	Si	Ti
ERE-09-MC-2																
862	spindle	80.7	0.0	0.0	0.0	0.0	0.0	0.0	0.0	0.0	0.0	0.0	0.0	19.3	0.0	0.0
863	spindle	86.4	0.0	0.0	0.0	3.1	0.0	0.0	0.0	0.0	0.0	0.0	0.0	9.6	1.0	0.0
864	spindle	83.5	0.0	0.0	0.0	5.1	0.0	0.0	0.0	0.0	0.0	0.0	0.0	11.3	0.0	0.0
865	spindle	77.2	0.0	1.5	0.0	3.9	0.0	2.7	0.0	0.0	3.9	0.0	0.0	10.8	0.0	0.0
866	stacked plate	89.4	1.1	1.1	0.0	0.0	0.0	0.0	0.0	0.0	0.0	0.0	0.0	8.4	0.0	0.0
Flank Samples																
ERE-09-027																
713	sub-rounded	0.0	0.0	0.0	0.0	0.0	0.0	0.0	0.0	0.0	22.5	0.0	0.0	77.5	0.0	0.0
714	sub-rounded	0.0	0.0	0.0	0.0	0.0	0.0	22.1	0.0	0.0	39.7	0.0	0.0	38.2	0.0	0.0
715	sub-rounded	0.0	0.0	0.0	0.0	0.0	0.0	0.0	0.0	0.0	64.3	0.0	0.0	35.7	0.0	0.0
716	sub-rounded	0.0	0.0	0.0	0.0	0.0	0.0	0.0	0.0	0.0	50.0	0.0	0.0	50.0	0.0	0.0
ERE-09-028																
575	sub-rounded	0.0	0.0	0.0	0.0	0.0	0.0	0.0	0.0	0.0	77.9	0.0	0.0	22.1	0.0	0.0
576	sub-rounded	0.0	0.0	0.0	0.0	0.0	0.0	0.0	0.0	0.0	80.0	0.0	0.0	20.0	0.0	0.0
577	sub-angular	74.3	0.0	0.0	0.0	0.0	0.0	0.0	0.0	0.0	14.3	0.0	0.0	0.0	11.4	0.0
579	sub-angular	68.0	7.9	0.0	0.0	0.0	0.0	0.9	0.0	0.0	18.1	0.0	0.0	1.1	3.9	0.0
581	sub-rounded	0.0	0.0	0.0	0.0	0.0	0.0	0.0	0.0	0.0	44.4	0.0	0.0	55.6	0.0	0.0
582	sub-angular	55.4	12.1	0.0	0.0	0.0	0.0	0.0	0.0	0.0	12.1	0.0	0.0	2.0	18.3	0.0
ERE-09-029																
717	sub-angular	5.9	0.0	0.0	0.0	0.0	0.0	0.0	0.0	0.0	54.9	0.0	0.0	35.3	3.9	0.0
718	sub-angular	16.5	0.0	0.0	0.0	0.0	0.0	0.0	6.0	0.0	57.7	0.0	0.0	19.8	0.0	0.0
719	sub-angular	0.0	0.0	0.0	0.0	0.0	0.0	0.0	0.0	0.0	75.8	0.0	0.0	24.2	0.0	0.0
720	sub-angular	0.0	0.0	0.0	0.0	0.0	0.0	0.0	0.0	0.0	72.7	0.0	0.0	27.3	0.0	0.0
721	sub-rounded	0.0	0.0	0.0	0.0	0.0	0.0	0.0	0.0	0.0	50.0	0.0	0.0	50.0	0.0	0.0
722	sub-angular	0.0	0.0	0.0	0.0	0.0	0.0	0.0	0.0	0.0	75.0	0.0	0.0	25.0	0.0	0.0
723	sub-angular	0.0	0.0	0.0	0.0	0.0	0.0	0.0	0.0	0.0	65.2	0.0	0.0	34.8	0.0	0.0
724	sub-rounded	0.0	0.0	0.0	0.0	0.0	0.0	0.0	0.0	0.0	65.8	0.0	0.0	34.2	0.0	0.0
725	sub-angular	0.0	0.0	0.0	0.0	0.0	0.0	0.0	0.0	0.0	69.6	0.0	0.0	30.4	0.0	0.0
726	sub-angular	0.0	0.0	0.0	0.0	0.0	0.0	0.0	0.0	0.0	78.0	0.0	0.0	22.0	0.0	0.0
727	stacked plate	0.0	70.2	0.0	0.0	0.0	0.0	0.0	0.0	0.0	1.0	0.0	0.0	28.8	0.0	0.0
728	sub-angular	0.0	0.0	0.0	0.0	0.0	0.0	0.0	0.0	0.0	34.6	0.0	0.0	65.4	0.0	0.0
729	cubic	40.4	4.0	0.0	0.0	0.0	4.5	10.1	0.0	0.0	3.5	0.0	0.0	0.0	35.4	2.0
730	sub-angular	0.0	0.0	0.0	0.0	0.0	0.0	0.0	0.0	0.0	0.0	0.0	0.0	100.0	0.0	0.0
ERE-09-031																
760	flat hexagonal	0.0	0.0	0.0	0.0	0.0	0.0	0.0	0.0	0.0	66.4	0.0	0.0	33.6	0.0	0.0
761	spindle	0.0	48.4	0.0	0.0	0.0	0.0	0.0	0.0	0.0	32.7	0.0	0.0	18.9	0.0	0.0
873	spindle	0.0	25.9	0.0	0.0	0.0	0.0	0.0	0.0	0.0	53.4	0.0	0.0	20.7	0.0	0.0
762	sub-rounded	0.0	0.0	0.0	0.0	0.0	0.0	0.0	0.0	0.0	55.6	0.0	0.0	44.4	0.0	0.0
763	sub-rounded	0.0	0.0	0.0	0.0	0.0	0.0	0.0	0.0	0.0	40.4	0.0	0.0	59.6	0.0	0.0
764	spindle	0.0	38.0	0.0	0.0	0.0	0.0	0.0	0.0	0.0	39.4	0.0	0.0	22.5	0.0	0.0
765	flat hexagonal	0.0	0.0	0.0	0.0	0.0	0.0	0.0	0.0	0.0	47.6	0.0	0.0	52.4	0.0	0.0
874	sub-rounded	0.0	0.0	0.0	0.0	0.0	0.0	0.0	0.0	0.0	66.9	0.0	0.0	33.1	0.0	0.0
766	sub-rounded	0.0	0.0	0.0	0.0	0.0	0.0	0.0	0.0	0.0	66.3	0.0	0.0	33.7	0.0	0.0
767	flat hexagonal	0.0	0.0	0.0	0.0	0.0	0.0	0.0	0.0	0.0	81.5	0.0	0.0	18.5	0.0	0.0
875	flat hexagonal	0.0	0.0	0.0	0.0	0.0	0.0	0.0	0.0	0.0	82.6	0.0	0.0	17.4	0.0	0.0
769	flat hexagonal	0.0	0.0	0.0	0.0	0.0	0.0	0.0	0.0	0.0	75.9	0.0	0.0	24.1	0.0	0.0
772	spindle	0.0	36.0	0.0	0.0	0.0	0.0	0.0	0.0	0.0	24.7	0.0	0.0	39.3	0.0	0.0
876	spindle	0.0	52.4	0.0	0.0	0.0	0.0	6.0	0.0	0.0	19.2	0.0	0.0	22.5	0.0	0.0
771		0.0	0.0	0.0	0.0	0.0	0.0	0.0	0.0	0.0	45.5	0.0	0.0	54.5	0.0	0.0
773	flat hexagonal	0.0	0.0	0.0	0.0	0.0	0.0	0.0	0.0	0.0	24.2	0.0	0.0	75.8	0.0	0.0
774	spindle	0.0	100.0	0.0	0.0	0.0	0.0	0.0	0.0	0.0	0.0	0.0	0.0	0.0	0.0	0.0
775	flat hexagonal	0.0	0.0	0.0	0.0	0.0	0.0	0.0	0.0	0.0	53.6	0.0	0.0	46.4	0.0	0.0
ERE-09-032																
776	needle	0.0	32.3	0.0	0.0	0.0	0.0	0.0	0.0	0.0	45.2	0.0	0.0	22.6	0.0	0.0
777	needle	0.0	39.2	0.0	0.0	0.0	0.0	0.0	0.0	0.0	21.6	0.0	0.0	39.2	0.0	0.0
877	needle	0.0	37.7	0.0	0.0	0.0	0.0	0.0	0.0	0.0	31.2	0.0	0.0	31.2	0.0	0.0
778	sub-angular	0.0	53.1	0.0	0.0	0.0	0.0	0.0	0.0	0.0	0.0	0.0	0.0	46.9	0.0	0.0
779	spindle	0.0	25.0	0.0	0.0	0.0	0.0	0.0	0.0	0.0	53.1	0.0	0.0	21.9	0.0	0.0
780	needle	0.0	37.8	0.0	0.0	0.0	0.0	0.0	0.0	0.0	43.2	0.0	0.0	18.9	0.0	0.0
878	needle	0.0	16.3	0.0	0.0	0.0	0.0	0.0	0.0	0.0	55.6	0.0	0.0	28.1	0.0	0.0
879	sub-angular	0.0	14.8	0.0	0.0	0.0	0.0	0.0	0.0	0.0	60.4	0.0	0.0	13.4	11.4	0.0
782	spindle	0.0	47.3	0.0	0.0	0.0	0.0	0.0	0.0	0.0	27.3	0.0	0.0	25.5	0.0	0.0
783	sub-angular	0.0	42.3	0.0	0.0	0.0	3.8	0.0	0.0	0.0	30.8	0.0	0.0	23.1	0.0	0.0
784	sub-angular	0.0	0.0	0.0	0.0	0.0	0.0	0.0	0.0	0.0	43.8	0.0	0.0	56.3	0.0	0.0
785	stacked plate	54.9	9.8	0.0	0.0	0.0	0.0	0.0	0.0	0.0	7.8	0.0	0.0	0.0	27.5	0.0
786	stacked plate	52.1	0.0	0.0	0.0	0.0	5.2	6.3	0.0	0.0	0.0	0.0	0.0	0.0	36.5	0.0
880	stacked plate	49.3	1.6	0.0	0.0	0.0	1.6	3.3	0.0	0.0	19.7	0.0	0.0	1.3	23.0	0.0
787	needle	0.0	83.9	0.0	0.0	0.0	0.0	0.0	0.0	0.0	0.0	0.0	0.0	16.1	0.0	0.0

Table B-1. Continued

Sample	Habit Scanned	Counts per Second Normalized to 100														
		Al	Ca	Cl	Cu	F	Fe	K	Mg	Mn	Na	Ni	P	S	Si	Ti
ERE-09-033																
788	sub-angular	0.0	0.0	0.0	0.0	0.0	0.0	0.0	0.0	0.0	34.9	0.0	0.0	65.1	0.0	0.0
789	sub-rounded	0.0	0.0	0.0	0.0	0.0	0.0	0.0	0.0	0.0	33.3	0.0	0.0	66.7	0.0	0.0
791	sub-angular	0.0	0.0	0.0	0.0	0.0	0.0	0.0	0.0	0.0	73.3	0.0	0.0	26.7	0.0	0.0
881	sub-angular	3.5	0.0	0.0	0.0	0.0	0.0	0.0	0.0	0.0	77.2	0.0	0.0	19.3	0.0	0.0
792	sub-angular	0.0	0.0	0.0	0.0	0.0	0.0	0.0	0.0	0.0	68.2	0.0	0.0	31.8	0.0	0.0
793	sub-angular	8.0	0.0	0.0	0.0	0.0	0.0	0.0	0.0	0.0	63.3	0.0	0.0	28.7	0.0	0.0
794	sub-angular	17.2	0.0	0.0	0.0	0.0	0.0	6.9	0.0	0.0	51.7	0.0	0.0	24.1	0.0	0.0
882	sub-angular	29.3	0.0	0.0	0.0	0.0	0.0	19.4	0.0	0.0	44.0	0.0	0.0	7.3	0.0	0.0
795	sub-angular	6.2	0.0	0.0	0.0	0.0	0.0	0.0	0.0	0.0	59.6	0.0	0.0	34.2	0.0	0.0
796	sub-angular	0.0	0.0	0.0	0.0	0.0	0.0	0.0	0.0	0.0	64.7	0.0	0.0	35.3	0.0	0.0
883	sub-angular	25.8	6.5	0.0	0.0	0.0	0.0	0.0	0.0	0.0	53.2	0.0	0.0	14.5	0.0	0.0
797	sub-rounded	5.0	0.0	0.0	0.0	0.0	0.0	0.0	0.0	0.0	65.0	0.0	0.0	30.0	0.0	0.0
884	sub-rounded	25.1	4.1	0.0	0.0	0.0	0.0	2.1	4.1	0.0	41.1	0.0	0.0	22.6	1.0	0.0
798	sub-angular	0.0	0.0	0.0	0.0	0.0	0.0	0.0	0.0	0.0	78.1	0.0	0.0	21.9	0.0	0.0
799	sub-rounded	0.0	0.0	0.0	0.0	0.0	0.0	0.0	0.0	0.0	65.7	0.0	0.0	34.3	0.0	0.0
Coastal Samples																
ERE-09-030																
731	stacked plate	35.0	4.2	0.0	0.0	0.0	7.5	4.2	16.7	0.0	8.3	0.0	0.0	0.0	22.5	1.7
732	stacked plate	34.3	1.7	2.6	0.0	0.0	8.2	6.0	12.9	0.0	3.4	0.0	0.0	0.0	29.2	1.7
734	cubic	30.8	4.6	7.7	0.0	0.0	0.0	3.1	0.0	0.0	30.8	0.0	0.0	0.0	23.1	0.0
735	stacked plate	50.0	8.3	0.0	0.0	0.0	0.0	4.2	0.0	0.0	8.3	0.0	0.0	0.0	29.2	0.0
736	stacked plate	38.9	3.5	3.5	0.0	0.0	9.7	7.1	7.1	0.0	4.4	0.0	0.0	0.0	23.9	1.8
747	sub-rounded	31.3	10.8	4.8	0.0	0.0	24.1	0.0	0.0	0.0	0.0	0.0	0.0	0.0	28.9	0.0
748	sub-rounded	0.0	0.0	13.4	0.0	0.0	0.0	0.0	0.0	0.0	85.4	0.0	0.0	0.0	1.2	0.0
749	sub-rounded	0.0	0.0	27.3	0.0	0.0	0.0	0.0	5.7	0.0	42.0	0.0	0.0	2.8	19.3	2.8
867	sub-rounded	4.9	0.0	16.7	0.0	0.0	0.0	0.0	0.0	0.0	66.7	0.0	0.0	9.8	2.0	0.0
750	sub-rounded	31.3	0.0	2.0	0.0	0.0	6.3	7.8	15.6	0.0	9.8	0.0	0.0	3.9	23.4	0.0
751	cubic	57.0	0.0	0.0	0.0	0.0	3.0	7.6	0.0	0.0	9.5	0.0	0.0	0.0	22.8	0.0
868	sub-angular	37.0	8.3	0.0	0.0	0.0	9.7	5.6	7.4	0.0	5.1	0.0	0.0	0.0	25.0	1.9
752	sub-rounded	0.0	14.3	33.3	0.0	0.0	15.5	0.0	0.0	0.0	25.0	0.0	0.0	7.1	4.8	0.0
869	sub-rounded	10.5	2.7	10.5	0.0	0.0	3.1	2.9	5.2	0.0	47.2	0.0	0.0	9.4	8.4	0.0
753	stacked plate	30.8	6.5	3.5	0.0	0.0	9.2	5.8	11.5	0.0	9.6	0.0	0.0	0.0	23.1	0.0
870	stacked plate	43.3	5.8	1.7	0.0	0.0	5.2	5.8	5.0	0.0	5.0	0.0	0.0	0.0	28.3	0.0
754	sub-rounded	46.5	3.9	0.0	0.0	0.0	18.6	8.5	11.6	0.0	0.0	0.0	0.0	0.0	10.9	0.0
871	sub-rounded	31.4	1.6	0.0	0.0	0.0	13.7	8.2	10.9	0.0	5.5	0.0	0.0	0.0	26.0	2.7
755	sub-angular	42.2	0.0	2.1	0.0	0.0	10.1	4.2	21.1	0.0	10.5	0.0	0.0	0.0	9.7	0.0
758	sub-angular	0.0	0.0	34.5	0.0	0.0	0.0	0.0	0.0	0.0	58.6	0.0	0.0	6.9	0.0	0.0
759	sub-angular	28.4	0.0	0.0	0.0	0.0	13.1	5.3	17.7	0.0	14.2	0.0	0.0	21.3	0.0	0.0
872	sub-angular	17.3	2.6	13.9	0.0	0.0	2.6	1.7	4.3	0.0	47.6	0.0	0.0	1.7	6.9	1.3

APPENDIX C: XRD PATTERNS

C.1 XRD Pattern Spectra Images with Pattern Tables (DVD-ROM)

C.2 XRD Reference Codes

Table C-1. XRD reference codes for all mineral phases identified.

Reference Code	Mineral Name	Compound Name	Chemical Formula	Crystal System	Quality
00-005-0628	Halite, syn	Sodium Chloride	NaCl	Cubic	S
00-005-0631	Thenardite, syn	Sodium Sulfate	Na ₂ SO ₄	Orthorhombic	I;ALT
00-021-0816	Gypsum	Calcium Sulfate Hydrate	CaSO ₄ ·2H ₂ O	Monoclinic	S
00-022-0718	Rancieite	Calcium Manganese Oxide Hydrate	(Ca,Mn)Mn ₂ O ₇ ·3H ₂ O	Hexagonal	B;D
00-024-0733	Sulfur, syn	Sulfur	S	Orthorhombic	C;D
00-026-1011	Khademite	Aluminum Sulfate Fluoride Hydrate	Al(SO ₄)F·5H ₂ O	Orthorhombic	S
00-041-1476	Sylvite, syn	Potassium Chloride	KCl	Cubic	S
00-042-1428	Millosevichite	Aluminum Sulfate	Al ₂ (SO ₄) ₃	Rhombohedral	I;ALT
00-045-1331	Ralstonite	Sodium Magnesium Aluminum Fluoride Hydroxide Hydrate	NaMgAl(F,OH) ₂ ·H ₂ O	Cubic	I
00-047-1884	Alunite, syn	Potassium Aluminum Sulfate Hydroxide	KAl ₃ (SO ₄) ₂ (OH) ₆	Rhombohedral	I
00-058-0466	Rancieite	Calcium Manganese Oxide Hydrate	CaMn ₂ O ₇ ·3H ₂ O	Hexagonal	S
00-058-2004	Kaolinite-1A	Aluminum Silicate Hydroxide	Al ₂ Si ₂ O ₅ (OH) ₄	Anorthic	I
00-058-2006	Kaolinite-1Ad	Aluminum Silicate Hydroxide	Al ₂ Si ₂ O ₅ (OH) ₄	Anorthic	B
00-058-2017	Illite-2M2, heated	Potassium Aluminum Silicate Hydroxide Hydrate	(K ₈ H ₃ O)Al ₂ (Si ₃ Al)O ₁₀ (OH) ₂ ·xH ₂ O	Monoclinic	B
00-058-2028	Kaolinite-1A	Aluminum Silicate Hydroxide	Al ₂ Si ₂ O ₅ (OH) ₄	Anorthic	I
01-070-1541	Thenardite, syn	Sodium Sulfate	Na ₂ SO ₄	Orthorhombic	S
01-070-2509	Halite, syn	Sodium Chloride	NaCl	Cubic	I
01-071-0735	Katoite	Calcium Aluminum Oxide Hydrate	Ca ₃ Al ₂ O ₇ (H ₂ O) ₆	Cubic	B;ALT
01-071-1776	Alunite	Potassium Aluminum Sulfate Hydroxide	K(Al ₃ (SO ₄) ₂ (OH) ₆)	Rhombohedral	B;ALT
01-071-3741	Halite	Sodium Chloride	NaCl	Cubic	I;ALT
01-072-1630	Alunite	Potassium Aluminum Sulfate Hydroxide	K(Al ₃ (SO ₄) ₂ (OH) ₆)	Rhombohedral	I
01-072-4582	Calcite	Calcium Carbonate	Ca(CO ₃)	Rhombohedral	B;ALT
01-073-9760	Cristobalite	Calcium Aluminum Silicate	Ca _{0.05} ((Al _{1.5} Si _{1.5})O ₄)	Tetragonal	B;NAT;NAP;ALT
01-074-1433	Gypsum	Calcium Sulfate Hydrate	Ca(SO ₄)(H ₂ O) ₂	Monoclinic	S;ALT
01-074-1904	Gypsum	Calcium Sulfate Hydrate	Ca(SO ₄)(H ₂ O) ₂	Monoclinic	B;ALT
01-074-5108	Sodiumalunite	Sodium Aluminum Sulfate Hydrate	NaAl(SO ₄) ₂ (H ₂ O) ₁₂	Cubic	B;ALT
01-074-6226	Katoite, syn	Calcium Aluminum Hydroxide	Ca ₃ (Al(OH) ₆) ₂	Cubic	S
01-074-9685	Sylvite, syn	Potassium Chloride	KCl	Cubic	S
01-075-0301	Halite, potassian, syn	Sodium Potassium Chloride	Na ₃₀₀₇ K ₄₉₆₃ Cl	Cubic	I
01-075-0303	Halite, potassian, syn	Sodium Potassium Chloride	Na ₆₉₉₀ K ₃₀₁₀ Cl	Cubic	I
01-075-1675	Ralstonite	Sodium Magnesium Aluminum Fluoride Hydroxide Hydrate	Na _{0.4} (Mg _{0.57} Al _{1.53} (F _{0.5} (OH) _{0.5}) ₆ (H ₂ O) _{0.8})	Cubic	B
01-075-1771	Ralstonite	Sodium Magnesium Aluminum Fluoride Hydroxide Hydrate	Na _{0.41} Mg _{0.492} Al _{1.548} F _{4.528} (OH) _{1.422} (H ₂ O) _{0.835}	Cubic	I
01-076-3453	Halite	Sodium Chloride	NaCl	Cubic	I;NAT;ALT
01-088-2380	Khademite	Aluminum Sulfate Fluoride Hydrate	Al(SO ₄)F(H ₂ O) ₅	Orthorhombic	S
01-089-3615	Halite, syn	Sodium Chloride	NaCl	Cubic	H;ALT

C.3 XRD Identifications

Table C-2. XRD identifications of Erebus salt deposits

Mineral Name	Chemical Formula	Compound Name	Crystal System	Score
ERE_001				
Rancieite	$\text{CaMn}_4\text{O}_9 \cdot 3\text{H}_2\text{O}$	Calcium Manganese Oxide Hydrate	Hexagonal	27
Sylvite, syn	KCl	Potassium Chloride	Cubic	23
Katoite	$\text{Ca}_3\text{Al}_2\text{O}_6(\text{H}_2\text{O})_6$	Calcium Aluminum Oxide Hydrate	Cubic	22
ERE_002				
Katoite	$\text{Ca}_3\text{Al}_2\text{O}_6(\text{H}_2\text{O})_6$	Calcium Aluminum Oxide Hydrate	Cubic	32
ERE_004				
Kaolinite-1A	$\text{Al}_2\text{Si}_2\text{O}_5(\text{OH})_4$	Aluminum Silicate Hydroxide	Anorthic	44
Katoite	$\text{Ca}_3\text{Al}_2\text{O}_6(\text{H}_2\text{O})_6$	Calcium Aluminum Oxide Hydrate	Cubic	29
Alunite	$\text{KAl}_3(\text{SO}_4)_2(\text{OH})_6$	Potassium Aluminum Sulfate Hydroxide	Rhombohedral	17
Halite, potassian, syn	$\text{Na}_{699}\text{K}_{301}\text{Cl}$	Sodium Potassium Chloride	Cubic	19
ERE_005				
Katoite	$\text{Ca}_3\text{Al}_2\text{O}_6(\text{H}_2\text{O})_6$	Calcium Aluminum Oxide Hydrate	Cubic	33
Alunite	$\text{KAl}_3(\text{SO}_4)_2(\text{OH})_6$	Potassium Aluminum Sulfate Hydroxide	Rhombohedral	23
ERE_007				
Katoite	$\text{Ca}_3\text{Al}_2\text{O}_6(\text{H}_2\text{O})_6$	Calcium Aluminum Oxide Hydrate	Cubic	38
Khademite	$\text{Al}(\text{SO}_4)\text{F} \cdot 5\text{H}_2\text{O}$	Aluminum Sulfate Fluoride Hydrate	Orthorhombic	27
Sulfur, syn	S	Sulfur	Orthorhombic	22
ERE_008				
Halite, syn	NaCl	Sodium Chloride	Cubic	37
Sylvite, syn	KCl	Potassium Chloride	Cubic	14
Ralstonite	$\text{NaMgAl}(\text{F},\text{OH})_6 \cdot \text{H}_2\text{O}$	Sodium Magnesium Aluminum Fluoride Hydroxide Hydrate	Cubic	9
Gypsum	$\text{CaSO}_4 \cdot 2\text{H}_2\text{O}$	Calcium Sulfate Hydrate	Monoclinic	4
ERE_009				
Kaolinite-1A	$\text{Al}_2\text{Si}_2\text{O}_5(\text{OH})_4$	Aluminum Silicate Hydroxide	Anorthic	25
ERE_010				
Rancieite	$\text{CaMn}_4\text{O}_9 \cdot 3\text{H}_2\text{O}$	Calcium Manganese Oxide Hydrate	Hexagonal	42
Kaolinite-1A	$\text{Al}_2\text{Si}_2\text{O}_5(\text{OH})_4$	Aluminum Silicate Hydroxide	Anorthic	25
Katoite	$\text{Ca}_3\text{Al}_2\text{O}_6(\text{H}_2\text{O})_6$	Calcium Aluminum Oxide Hydrate	Cubic	25
ERE_011				
Halite, syn	NaCl	Sodium Chloride	Cubic	25
ERE_012				
Halite, syn	NaCl	Sodium Chloride	Cubic	30
Gypsum	$\text{CaSO}_4 \cdot 2\text{H}_2\text{O}$	Calcium Sulfate Hydrate	Monoclinic	12
Alunite	$\text{KAl}_3(\text{SO}_4)_2(\text{OH})_6$	Potassium Aluminum Sulfate Hydroxide	Rhombohedral	9
ERE_013				
Rancieite	$\text{CaMn}_4\text{O}_9 \cdot 3\text{H}_2\text{O}$	Calcium Manganese Oxide Hydrate	Hexagonal	44
Alunite, syn	$\text{KAl}_3(\text{SO}_4)_2(\text{OH})_6$	Potassium Aluminum Sulfate Hydroxide	Rhombohedral	26
Kaolinite-1A	$\text{Al}_2\text{Si}_2\text{O}_5(\text{OH})_4$	Aluminum Silicate Hydroxide	Anorthic	16
Millosevichite	$\text{Al}_2(\text{SO}_4)_3$	Aluminum Sulfate	Rhombohedral	18
ERE_014				
Halite, potassian, syn	$\text{Na}_{699}\text{K}_{301}\text{Cl}$	Sodium Potassium Chloride	Cubic	22
Kaolinite-1Ad	$\text{Al}_2\text{Si}_2\text{O}_5(\text{OH})_4$	Aluminum Silicate Hydroxide	Anorthic	10
ERE_015				
Halite, syn	NaCl	Sodium Chloride	Cubic	38
Alunite	$\text{KAl}_3(\text{SO}_4)_2(\text{OH})_6$	Potassium Aluminum Sulfate Hydroxide	Rhombohedral	31
ERE_016				
Halite, syn	NaCl	Sodium Chloride	Cubic	32
Sylvite, syn	KCl	Potassium Chloride	Cubic	26
ERE_018				
Sylvite, syn	KCl	Potassium Chloride	Cubic	21
ERE_019				
Rancieite	$\text{CaMn}_4\text{O}_9 \cdot 3\text{H}_2\text{O}$	Calcium Manganese Oxide Hydrate	Hexagonal	45
Halite	NaCl	Sodium Chloride	Cubic	37
Alunite, syn	$\text{KAl}_3(\text{SO}_4)_2(\text{OH})_6$	Potassium Aluminum Sulfate Hydroxide	Rhombohedral	22
ERE_020				
Sylvite, syn	KCl	Potassium Chloride	Cubic	17
ERE_021				
Halite, syn	NaCl	Sodium Chloride	Cubic	29
Khademite	$\text{Al}(\text{SO}_4)\text{F} \cdot 5\text{H}_2\text{O}$	Aluminum Sulfate Fluoride Hydrate	Orthorhombic	24
Ralstonite	$\text{Na}_{0.4}(\text{Mg}_{0.5}\text{Al}_{1.5})(\text{F}_{0.5}(\text{OH})_{0.5})_6(\text{H}_2\text{O})_{0.8}$	Sodium Magnesium Aluminum Fluoride Hydroxide Hydrate	Cubic	19

Table C-2. Continued

Mineral Name	Chemical Formula	Compound Name	Crystal System	Score
ERE_022				
Ralstonite	$\text{Na}_{0.04}\text{Mg}_{0.5}\text{Al}_{1.5}(\text{F}_{0.5}\text{OH})_{0.5}(\text{H}_2\text{O})_{0.5}$	Sodium Magnesium Aluminum Fluoride Hydroxide Hydrate	Cubic	28
Khademite	$\text{Al}(\text{SO}_4)\text{F}\cdot 5\text{H}_2\text{O}$	Aluminum Sulfate Fluoride Hydrate	Orthorhombic	21
ERE_023				
Halite	NaCl	Sodium Chloride	Cubic	40
Illite-2M2, heated	$(\text{K},\text{H}_3\text{O})\text{Al}_2(\text{Si}_3\text{Al})\text{O}_{10}(\text{OH})_2\cdot x\text{H}_2\text{O}$	Potassium Aluminum Silicate Hydroxide Hydrate	Monoclinic	32
Sodiumalum	$\text{NaAl}(\text{SO}_4)_2(\text{H}_2\text{O})_{12}$	Sodium Aluminum Sulfate Hydrate	Cubic	32
Thenardite, syn	Na_2SO_4	Sodium Sulfate	Orthorhombic	12
Ralstonite	$\text{Na}_{0.041}\text{Mg}_{0.452}\text{Al}_{1.548}\text{F}_{4.578}(\text{OH})_{1.422}(\text{H}_2\text{O})_{0.835}$	Sodium Magnesium Aluminum Fluoride Hydroxide Hydrate	Cubic	20
ERE_024				
Rancieite	$(\text{Ca},\text{Mn})\text{Mn}_4\text{O}_7\cdot 3\text{H}_2\text{O}$	Calcium Manganese Oxide Hydrate	Hexagonal	43
Sylvite, syn	KCl	Potassium Chloride	Cubic	24
Alunite	$\text{KAl}_3(\text{SO}_4)_2(\text{OH})_6$	Potassium Aluminum Sulfate Hydroxide	Rhombohedral	20
ERE_025				
Halite	NaCl	Sodium Chloride	Cubic	37
Khademite	$\text{Al}(\text{SO}_4)\text{F}\cdot 5\text{H}_2\text{O}$	Aluminum Sulfate Fluoride Hydrate	Orthorhombic	16
ERE_026				
Halite, syn	NaCl	Sodium Chloride	Cubic	46
Rancieite	$\text{CaMn}_4\text{O}_7\cdot 3\text{H}_2\text{O}$	Calcium Manganese Oxide Hydrate	Hexagonal	24
Sodiumalum	$\text{NaAl}(\text{SO}_4)_2(\text{H}_2\text{O})_{12}$	Sodium Aluminum Sulfate Hydrate	Cubic	31
ERE_027				
Katoite	$\text{Ca}_3\text{Al}_2\text{O}_6(\text{H}_2\text{O})_6$	Calcium Aluminum Oxide Hydrate	Cubic	32
ERE_028				
Thenardite, syn	Na_2SO_4	Sodium Sulfate	Orthorhombic	76
Halite	NaCl	Sodium Chloride	Cubic	30
Calcite	$\text{Ca}(\text{CO}_3)$	Calcium Carbonate	Rhombohedral	19
ERE_030				
Rancieite	$(\text{Ca},\text{Mn})\text{Mn}_4\text{O}_7\cdot 3\text{H}_2\text{O}$	Calcium Manganese Oxide Hydrate	Hexagonal	46
Sylvite, syn	KCl	Potassium Chloride	Cubic	25
Halite, potassian, syn	$\text{Na}_{3037}\text{K}_{4963}\text{Cl}$	Sodium Potassium Chloride	Cubic	23
Katoite, syn	$\text{Ca}_3(\text{Al}(\text{OH})_6)_2$	Calcium Aluminum Hydroxide	Cubic	11
ERE_031				
Rancieite	$\text{CaMn}_4\text{O}_7\cdot 3\text{H}_2\text{O}$	Calcium Manganese Oxide Hydrate	Hexagonal	38
Katoite	$\text{Ca}_3\text{Al}_2\text{O}_6(\text{H}_2\text{O})_6$	Calcium Aluminum Oxide Hydrate	Cubic	26
ERE_032				
Katoite	$\text{Ca}_3\text{Al}_2\text{O}_6(\text{H}_2\text{O})_6$	Calcium Aluminum Oxide Hydrate	Cubic	35
Alunite	$\text{KAl}_3(\text{SO}_4)_2(\text{OH})_6$	Potassium Aluminum Sulfate Hydroxide	Rhombohedral	19
ERE_033				
Rancieite	$\text{CaMn}_4\text{O}_7\cdot 3\text{H}_2\text{O}$	Calcium Manganese Oxide Hydrate	Hexagonal	41
Ralstonite	$\text{NaMgAl}(\text{F},\text{OH})_6\cdot \text{H}_2\text{O}$	Sodium Magnesium Aluminum Fluoride Hydroxide Hydrate	Cubic	25
Gypsum	$\text{CaSO}_4\cdot 2\text{H}_2\text{O}$	Calcium Sulfate Hydrate	Monoclinic	11
ERE_034				
Sylvite, syn	KCl	Potassium Chloride	Cubic	27
Halite, potassian, syn	$\text{Na}_{3037}\text{K}_{4963}\text{Cl}$	Sodium Potassium Chloride	Cubic	15
ERE_036				
Illite-2M2, heated	$(\text{K},\text{H}_3\text{O})\text{Al}_2(\text{Si}_3\text{Al})\text{O}_{10}(\text{OH})_2\cdot x\text{H}_2\text{O}$	Potassium Aluminum Silicate Hydroxide Hydrate	Monoclinic	43
Ralstonite	$\text{Na}_{0.041}\text{Mg}_{0.452}\text{Al}_{1.548}\text{F}_{4.578}(\text{OH})_{1.422}(\text{H}_2\text{O})_{0.835}$	Sodium Magnesium Aluminum Fluoride Hydroxide Hydrate	Cubic	21
ERE_038				
Alunite	$\text{KAl}_3(\text{SO}_4)_2(\text{OH})_6$	Potassium Aluminum Sulfate Hydroxide	Rhombohedral	24
ERE_040				
Halite, syn	NaCl	Sodium Chloride	Cubic	39
ERE_043				
Kaolinite-1A	$\text{Al}_2\text{Si}_2\text{O}_5(\text{OH})_4$	Aluminum Silicate Hydroxide	Anorthic	46
Katoite	$\text{Ca}_3\text{Al}_2\text{O}_6(\text{H}_2\text{O})_6$	Calcium Aluminum Oxide Hydrate	Cubic	34
Alunite	$\text{KAl}_3(\text{SO}_4)_2(\text{OH})_6$	Potassium Aluminum Sulfate Hydroxide	Rhombohedral	20
ERE_MC1				
Rancieite	$\text{CaMn}_4\text{O}_7\cdot 3\text{H}_2\text{O}$	Calcium Manganese Oxide Hydrate	Hexagonal	40
ERE_MC2				
Rancieite	$\text{CaMn}_4\text{O}_7\cdot 3\text{H}_2\text{O}$	Calcium Manganese Oxide Hydrate	Hexagonal	46
Gypsum	$\text{CaSO}_4\cdot 2\text{H}_2\text{O}$	Calcium Sulfate Hydrate	Monoclinic	14
ERE_CR				
Illite-2M2, heated	$(\text{K},\text{H}_3\text{O})\text{Al}_2(\text{Si}_3\text{Al})\text{O}_{10}(\text{OH})_2\cdot x\text{H}_2\text{O}$	Potassium Aluminum Silicate Hydroxide Hydrate	Monoclinic	36
Ralstonite	$\text{Na}_{0.041}\text{Mg}_{0.452}\text{Al}_{1.548}\text{F}_{4.578}(\text{OH})_{1.422}(\text{H}_2\text{O})_{0.835}$	Sodium Magnesium Aluminum Fluoride Hydroxide Hydrate	Cubic	28
Cristobalite	$\text{Ca}_{0.05}(\text{Al}_{0.1}\text{Si}_{1.9})\text{O}_4$	Calcium Aluminum Silicate	Tetragonal	20

REFERENCES

- Bernard, A. and Le Guern, F., 1986. Condensations of volatile elements in high-temperature gases of Mount St. Helens. *Journal of Volcanology and Geothermal Research*, 28: 91-105.
- Bowser, C.J., Rafter, T.A. and Black, R.F., 1970. Geochemical evidence for the origin of the mirabilite deposits near Hobbs Glacier, Victoria Land, Antarctica. In: B. Morgan (Editor), *Fifttieth Anniversary Symposia: Mineralogy and Petrology of the Upper Mantle Sulfides Mineralogy and Geochemistry of Non-Marine Evaporites*. Mineralogical Society of America, New Jersey, pp. 261-272.
- Caldwell, D.A. and Kyle, P.R., 1994. Mineralogy and geochemistry of ejecta erupted from Mount Erebus, Antarctica between 1972 and 1986. *Volcanological and Environmental Studies of Mount Erebus, Antarctica; Antarctic Research Series*, 66: 147-162.
- Chuan, R.L., 1994. Dispersal of volcano-derived particles from Mount Erebus in the Antarctic atmosphere. *Volcanological and Environmental Studies of Mount Erebus, Antarctica; Antarctic Research Series* 66: 97-102.
- Chuan, R.L., Palais, J., Rose, W.I. and Kyle, P.R., 1986. Fluxes, sizes, morphology, and compositions of particles in the Mt. Erebus volcanic plume, December 1983. *Journal of Atmospheric Chemistry*, 4: 467-477.
- Claridge, G.G.C. and Campbell, I.B., 1977. The salts in Antarctic soils, their distribution and relationship to soil processes. *Soil Science*, 123: 377-384.
- Esser, R.P., Kyle, P. and McIntosh, W.C., 2004. $^{40}\text{Ar}/^{39}\text{Ar}$ dating of the eruptive history of Mount Erebus, Antarctica: volcano evolution. *Bulletin of Volcanology*, 66: 671-686.
- Faure, G., 1998. *Principles and applications of geochemistry*. Prentice Hall, Upper Saddle River, 600 pp.

- Faure, G. and Jones, L.M., 1989. Distribution of marine salts along the west coast of Ross Island, Antarctica, based on isotopic compositions of strontium and sulfur, *Weathering; its products and deposits. Volume I. Processes.* Theophrastus Publications, S.A., Athens, pp. 369-381.
- Ferreira, T. and Oskarsson, N., 1999. Chemistry and isotopic composition of fumarole discharge of Furnas Caldera. *Journal of Volcanology and Geothermal Research*, 92(1-2): 169-179.
- Hampton, C.M. and Bailey, D.K., 1985. Sublimates obtained during fusion of volcanic glasses. *Journal of Volcanology and Geothermal Research*, 25: 145-155.
- Ilyinskaya, E., Oppenheimer, C., Mather, T.A., Martin, R.S. and Kyle, P.R., 2010. Size-resolved chemical composition of aerosol emitted by Erebus volcano, Antarctica. *Geochemistry, Geophysics, Geosystems*, 11(3): 14.
- Jones, L.M. and Faure, G., 1967. Origin of the salts in Lake Vanda, Wright Valley, southern Victoria Land, Antarctica. *Earth and Planetary Science Letters*, 3(5): 142-144.
- Jones, L.M., Faure, G., Taylor, K.S. and Corbato, C.E., 1983. The origin of salts on Mount Erebus and along the coast of Ross Island, Antarctica. *Isotope Geoscience*, 1: 57-64.
- Kelly, P.J., Kyle, P., Dunbar, N. and Sims, K., 2008. Geochemistry and mineralogy of the phonolite lava lake, Erebus volcano, Antarctica: 1972-2004 and comparison with older lavas. *Journal of Volcanology and Geothermal Research*, 177(3): 589-605.
- Keys, J.R., 1980. *Salts and their distribution in the McMurdo Region, Antarctica*, Victoria University of Wellington, Wellington, 332 pp.
- Keys, J.R. and Williams, K., 1981. Origin of crystalline, cold desert salts in the McMurdo region, Antarctica. *Geochimica et Cosmochimica Acta*, 45: 2299-2309.
- Kodosky, L. and Keskinen, M., 1990. Fumarole distribution, morphology, and encrustation mineralogy associated with the 1986 eruptive deposits of Mount St. Augustine, Alaska. *Bulletin of Volcanology*, 52: 175-185.
- Krauskopf, K.B. and Bird, D.K., 1995. *Introduction to Geochemistry*. McGraw-Hill, New York, 647 pp.
- Leggo, P.J., Cocheme, J.-J., Demant, A. and Lee, W.T., 2001. The role of argillic alteration in the zeolitization of volcanic glass. *Mineralogical Magazine*, 65(5): 653-663.

- Margolin, J.B., 2006. Chemical and isotopic composition of snow in the summit area of Mount Erebus volcano, Antarctica. New Mexico Institute of Mining and Technology, Socorro, pp. 59.
- Meeker, K.A., Chuan, R.L., Kyle, P. and Palais, J., 1991. Emission of elemental gold particles from Mount Erebus, Ross Island, Antarctica. *Geophysical Research Letters*, 18(8): 1405-1408.
- Naughton, J.J., Greenberg, V.A. and Goguel, R., 1976. Incrustations and fumarolic condensates at Kilauea Volcano, Hawaii: field, drill-hole and laboratory observations. *Journal of Volcanology and Geothermal Research*, 1: 149-165.
- Naughton, J.J., Lewis, V.A., Hammond, D. and Nishimoto, D., 1974. The chemistry of sublimates collected directly from lava fountains at Kilauea Volcano, Hawaii. *Geochimica et Cosmochimica Acta*, 38: 1679-1690.
- Oppenheimer, C. and Kyle, P., 2008. Probing the magma plumbing of Erebus volcano, Antarctica, by open-path FTIR spectroscopy of gas emissions. *Journal of Volcanology and Geothermal Research*, 177(3): 743-754.
- Oppenheimer, C. et al., 2010. Atmospheric chemistry of an Antarctic volcanic plume. *Journal of Geophysical Research*, 115(D04303): 15.
- Óskarsson, N., 1981. The Chemistry of Icelandic lava incrustations and the latest stages of degassing. *Journal of Volcanology and Geothermal Research*, 10: 93-111.
- Rose, W.I., 1987. Active Pyroclastic Processes Studied with Scanning Electron Microscopy. In: J.R. Marshall (Editor), *Clastic Particles, Scanning Electron Microscopy and Shape Analysis of Sedimentary and Volcanic Clasts*. Van Nostrand Reinhold Co., New York, pp. 136-158.
- Rosenberg, P.E., 1988. Aluminum fluoride hydrates, volcanogenic salts from Mount Erebus, Antarctica. *American Mineralogist*, 73: 855-860.
- Stoiber, R.E. and Rose, W.I.J., 1974. Fumarole incrustations at active Central American volcanoes. *Geochimica et Cosmochimica Acta*, 38: 495-516.
- Sweeney, D., Kyle, P.R. and Oppenheimer, C., 2008. Sulfur dioxide emissions and degassing behavior of Erebus volcano, Antarctica. *Journal of Volcanology and Geothermal Research*, 177(3): 725-733.
- Turner, C.E. and Fishman, N.S., 1991. Jurassic Lake T'oo'dichi': A large alkaline, saline lake, Morrison Formation, eastern Colorado Plateau. *Geological Society of America Bulletin*, 103: 538-558.

Zreda-Gostynska, G., 1995. Characterization of gas and aerosol emissions from Mount Erebus Volcano, Antarctica, New Mexico Institute of Mining and Technology, Socorro, 225 pp.

Zreda-Gostynska, G., Kyle, P., Finnegan, D. and Prestbo, K.M., 1997. Volcanic gas emissions from Mount Erebus and their impact on the Antarctic environment. *Journal of Geophysical Research*, 102(B7): 15039-15055.